RICE UNIVERSITY

Impact of Fe(II) and Fe(III) on scale inhibitor: application to scale control in oil and gas systems

by

Zhang Zhang

A THESIS SUBMITTED IN PARTIAL FULFILLMENT

OF THE REQUIREMENTS FOR THE DEGREE

Doctor of Philosophy

APPROVED, THESIS COMMITTEE

Mason B. Tomson, Chair, Professor

Civil & Environmental Engineering

Philip B. Bedient, Professor

Civil & Environmental Engineering

Walter G. Chapman, Professor

Chemical Engineering

HOUSTON, TEXAS

April 2017

RICE UNIVERSITY

Impact of Fe(II) and Fe(III) on scale inhibitor: application to scale control in oil and gas systems

by

Zhang Zhang

A THESIS SUBMITTED IN PARTIAL FULFILLMENT

OF THE REQUIREMENTS FOR THE DEGREE

Doctor of Philosophy

APPROVED, THESIS COMMITTEE

Mason B. Tomson, Chair, Professor

Civil & Environmental Engineering

Philip B. Bedient, Professor

Civil & Environmental Engineering

Walter G. Chapman, Professor

Chemical Engineering

HOUSTON, TEXAS

April 2017

ABSTRACT

Impact of Fe(II) and Fe(III) on scale inhibitor: application to scale control in oil and gas systems

by

Zhang Zhang

The effect of Fe(II) on the performance of barite scale inhibitors was tested using an improved anoxic testing apparatus. Inhibitors were tested with from 1 to 50 mg/L Fe(II) at 70ºC and near neutral pH conditions. Most scale inhibitors show good Fe(II) tolerance at experimental conditions, while some phosphonates based scale inhibitors were significantly impaired by Fe(II). The formation of insoluble precipitates between Fe(II) and phosphonate is very likely the reason behind this detrimental effect. Fe(III) can significantly impair the performance of all scale inhibitors even at extremely low concentrations. However, the mechanism of this detrimental effect has not been studied. In this research, an analytical ultracentrifuge was utilized to separate ferric hydroxide nanoparticles from the aqueous phase. Scale inhibitor concentration in the aqueous and particle phases were measured and compared with barite induction time data. The mechanism of Fe(III) effect on scale inhibitor was experimentally shown a result of adsorption of scale inhibitor onto ferric hydroxide nanoparticles in solution. If inhibitors are added in excess of the adsorption ability of the ferric hydroxide particles, the remaining scale inhibitors in the aqueous phase can still provide inhibition. EDTA and citric acid, two of the most common organic chelating agents used in oilfield, were tested for their ability to reverse the detrimental effect of Fe(III) on scale despite the fact the EDTA is a much stronger chelating agent. The mechanistic difference between EDTA and citrate is discussed.

ACKNOWLEDGMENTS

This thesis could not have been accomplished without the support of many people who guided me and loved me along the way. First, I wish to express my profound gratitude to my advisor, Dr. Mason Tomson, who is a real inspiring, enthusiastic and exemplary scholar. From him, I've learnt not only the way of scientific thinking, the importance of academic integrity, but also his deep love for science and hardworking spirit. Thanks also goes to Dr. Bedient and Dr. Chapman, for their support to be on my PhD committee and offer guidance and technical insight into my research.

Special thanks goes to Dr. Amy Kan, who is one of the smartest and hardworking people I've ever had the privilege to know. Same gratitude extends to all my group members with whom I've shared many happy and frustrating moments: Dr. Fei Yan, Dr. Fangfu Zhang, Dr. Narayan Bhandari, Dr. Gordon Ruan, Ya Liu, Zhaoyi Dai, Guannan Deng, Alex Lv.

Finally, I would like to express my deep love and gratitude for my family and close friends. Although my parents are in China, they have always been my anchor through difficult times. To my fiancé ,Dr Lin Dong, who has given me huge support and love. Special thanks to Sherry Kao, a very good friend of mine, who has been by my side listening to my struggle and never judged me. Thanks also goes to Jialu Xu, Pingfeng Yu and other good friends of mine. The warmth of their friendship means so much to me.

Thanks also goes to Rice Brine Chemistry Consortium and China scholarship council for providing financial support.

Contents

List of Tables

List of Figures

Chapter 1. Research objective

Inorganic mineral scaling problem in oilfield causes millions of dollar loss every year. Scale can form because of temperature and pressure change or when incompatible water are mixed downhole. Scale deposition can happen in reservoir, transport tubing all the way to surface equipment(Crabtree, Eslinger et al. 1999). To treat scaling problem, the most common method is to inject chemicals scale inhibitors downhole with water. Some inhibitors are called threshold scale inhibitors. They can prevent large amount of scale from formation at extremely low concentration, usually a few mg/l, which is very cost-effective therefore widely used in production. However, their compatibility with common inorganic cations has not been thoroughly investigated. Incompatibility with cations could result in precipitation of scale inhibitors downhole and cause treatment failure. To prevent such failure, research regarding the interaction between common cations in brine and scale inhibitors is very important.

Ferrous iron (Fe(II)) is one of the most common cations existing in oil and gas production water. Depending on the geochemistry on the producing formation, the type of hydrocarbon produced and the characteristics of the producing well, the concentration of Fe can vary from several mg/L to hundreds of mg/L. Typically, during production process the produced water remains anaerobic in the oil wells, Fe should remain as Fe(II). However, oxidation of Fe(II) could still happen due to pump leakage and when produced waters flow close to the surface. Also, magnetite has been found in oil wells, suggesting that Fe(III) can be formed even in strictly anoxic conditions.

Fe in produced water have two major sources. One is from the prolonged contact with iron

containing mineral such as siderite ($FeCO_3$), chlorite ($(AlSi_3O_{10})Mg_5(Al,Fe)_3(OH)_3$), pyrite ($FeS_2$) and Ankerite ($Ca(Mg,Fe)(CO_3)_2$) in formation(PAYKANI and MARDAN). The other source is from corrosion of the pipelines. Under anaerobic condition, iron is oxidized to Fe(II) through reduction of water molecule which generates hydrogen.

The presence of iron ions in solution can have multiple effects on produced water chemistry. Fe(III) is extremely insoluble in water and forms various iron oxide precipitates which causes asphaltic sludging formation damage and adsorption of production chemicals. Fe(II) is much more soluble than Fe(III) and does not form precipitates easily at common oilfield pH condition. Compared to other common cations e.g. Ca^{2+} and Mg^{2+}, Fe(II) has a higher complex stability constant with some common inhibitor function groups like phosphonate and carboxyl due to its transition metal nature. However, few publications in the literature have investigated the effect of Fe(III) and Fe(II) on mineral scale inhibitors and no systematic research has been done to investigate the mechanism of this effect and how to overcome this effect.

This research utilizes laser light scattering nucleation detection apparatus to study the effect of Fe(II) and Fe(III) on scale inhibitor performance. The mechanism behind the detrimental effect of Fe(II) and Fe(III) on scale inhibitor performance is investigated and organic chelates are utilized in attempt to revere this detrimental effect. This thesis is organized as follows: Chapter 2 introduces research background. Chapter 3 gives a detailed description of the laser nucleation detection apparatus. Experiments involving Fe(II) is done by remodeled laser apparatus to adapt to the anoxic condition. Chapter 4 and Chapter 5 gives experimental results of Fe(III) and Fe(II) effect on scale inhibitor performance respectively. Chapter 6 is summary and future work. Chapter 7 is

reference.

Chapter 2. Background and literature review

2.1 Scale problem in oil and gas production

Few production problems strike fear into the hearts of engineering the way scale can(Crabtree, Eslinger et al. 1999). Scale, like those found in tea kettles and home plumbing, can result in millions of dollars - loss in oilfield production processes. Scale precipitation is caused by the super-saturation of excessive amount of cations, such as Ca^{2+}, Ba^{2+}, Mg^{2+} combining with anions like CO_3^{2-}, SO_4^{2-}. While the solubility product of a certain solid is above its K_{sp} value under a certain condition, precipitation will happen. Scale can deposit from injection, through reservoir all the way to surface equipment. Table 1 lists some of the most common mineral scales found in oilfield. When there is pressure and temperature change and incompatible water mixing, scale could precipitate from the water that occurs naturally in reservoir or produced water injected downhole for enhanced recovery.

Brine composition from different zones of the formation might be quite different and form precipitation when mixed in pipes. Also, wastewater from other industry is usually utilized as fracturing fluid to crash the rocks containing oil and gas. For example, acid mine draining wastewater is used for shale gas exploitation. Once the wastewater having extremely high SO_4^{2-} concentration meets downhole brine, barite precipitation could happen in a very fast rate and block pipes. Scaling can also happen due to the pressure and temperature change along the transport process, large amount of scale could accumulate onto the inner surface of a pipe. For example, the solubility of $CaCO_3$ dropped drastically with increasing temperature, as shown in the graph below. When pipes go further down into formation, previously unsaturated solution might become supersaturated with calcium carbonate. With the exploitation of oil and gas going deeper down the

formation, people are facing the challenge of high temperature and pressure. Typical temperature, pressure and TDS in the working depth of the formation might reach 150-200℃, 1,000-1,500 bar and 300,000 mg/l.Scale forms in different rates. Some pipes can remain unblocked for several months, but some might be blocked in one day.

Table 1. Common types of mineral scale

Mineral	Formula
Calcite	$CaCO_3$
Anhydrite	$CaSO_4$
Gypsum	$CaSO_4 \cdot 2H_2O$
Barite	$BaSO_4$
Celestite	$SrSO_4$
Mackinawite	FeS
Pyrite	FeS_2
Halite	NaCl
Fluorite	CaF_2
Sphaerlite	ZnS
Galena	PbS
Siderite	$FeCO_3$

Scale can develop in formation pores near wellbore resulting in a loss of permeability (as shown in Figure 1) or develop in transportation tubing (see Figure 2 and Figure 3). Moreover, scale build-up can also result in injection-well and production-well damage (see Figure 4 and Figure 5(Crabtree, Eslinger et al. 1999)).

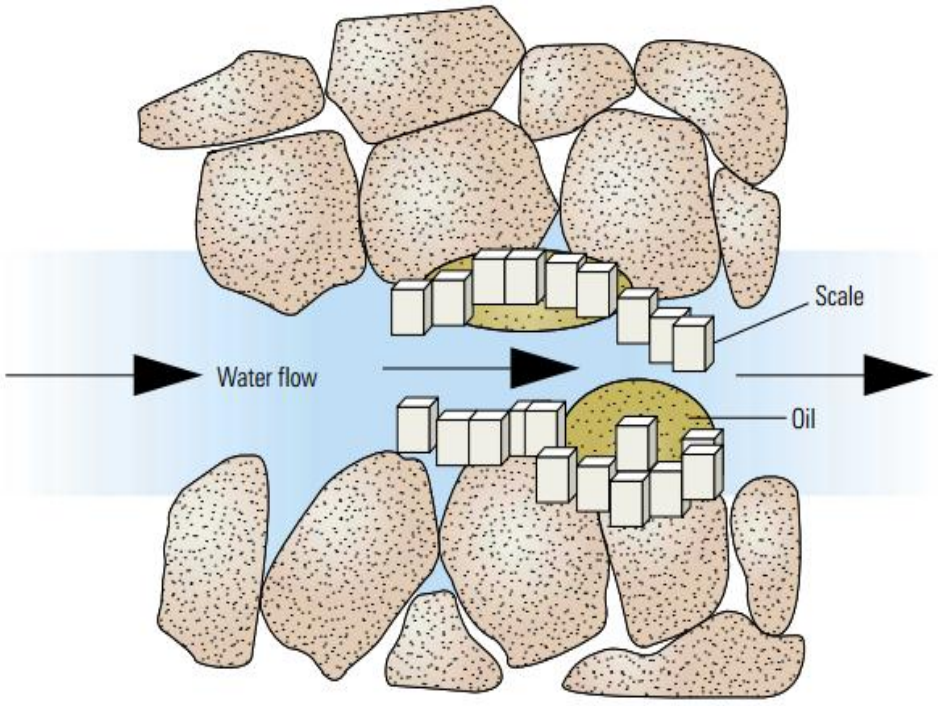

Figure 1. Matrix damage resulting from scale deposition in formation(Crabtree, Eslinger et al. 1999)

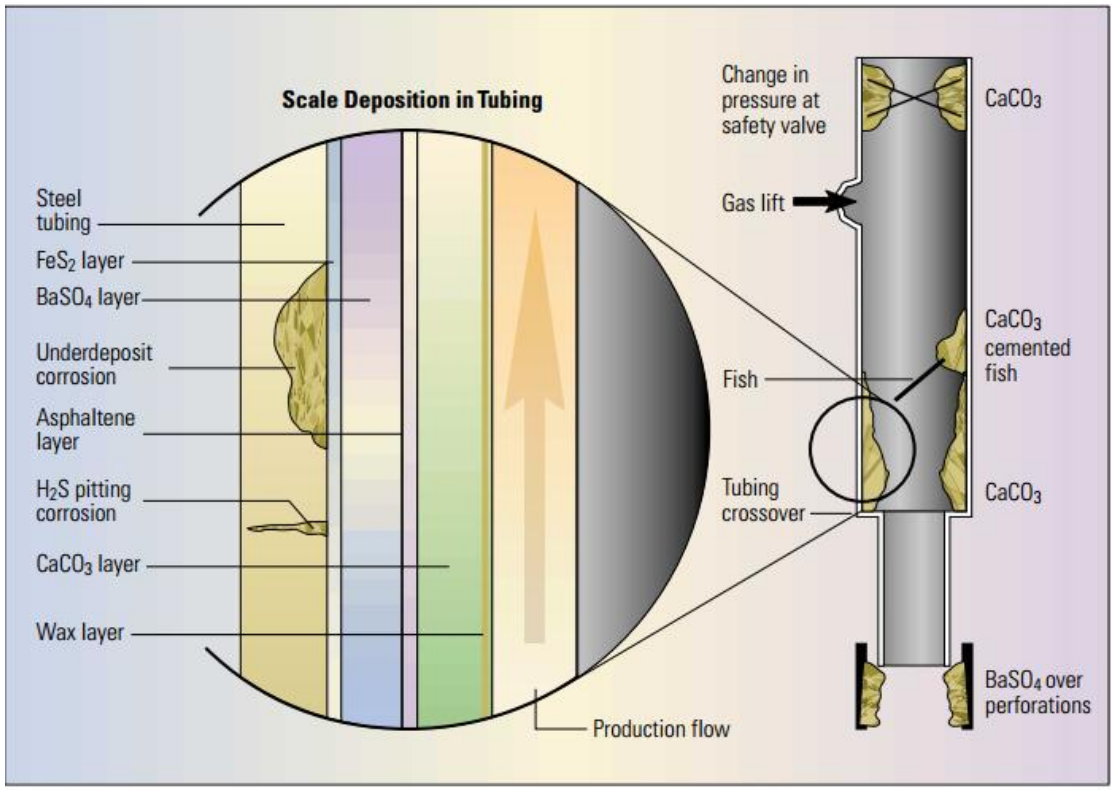

Figure 2. Scale in tubing(Crabtree, Eslinger et al. 1999)

Figure 3. Oilfield tubing blocked by scale

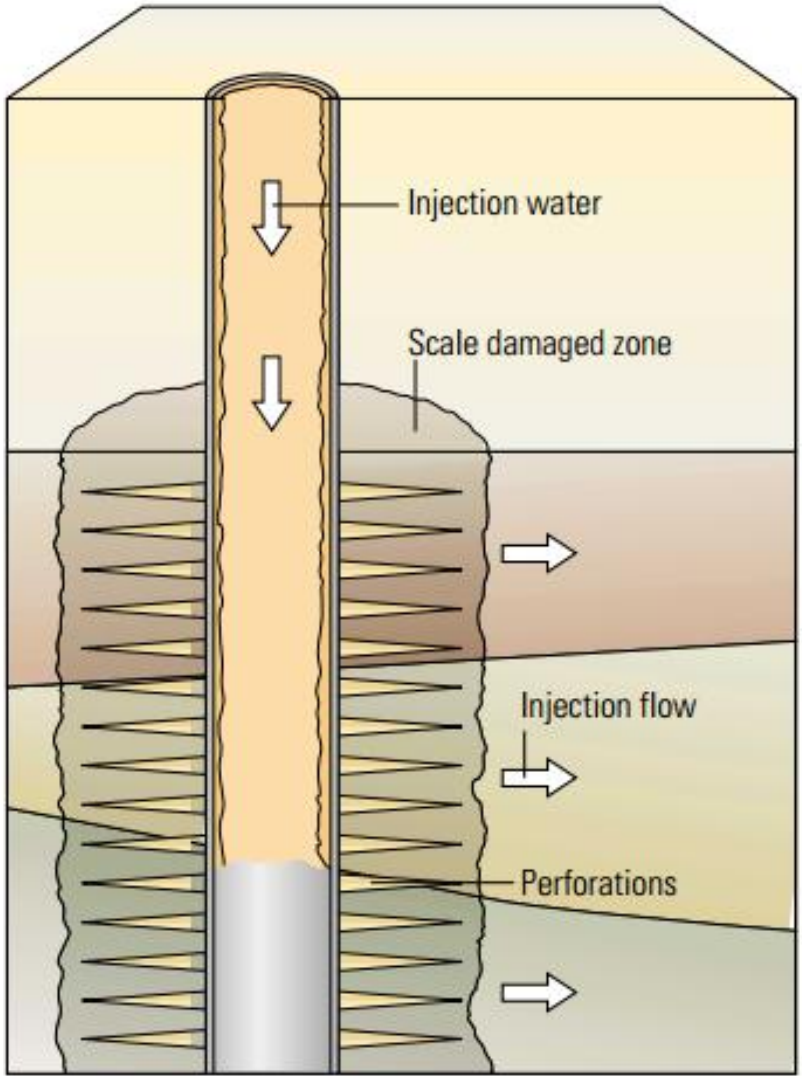

Figure 4. Injection-well damage caused by scaling(Crabtree, Eslinger et al. 1999)

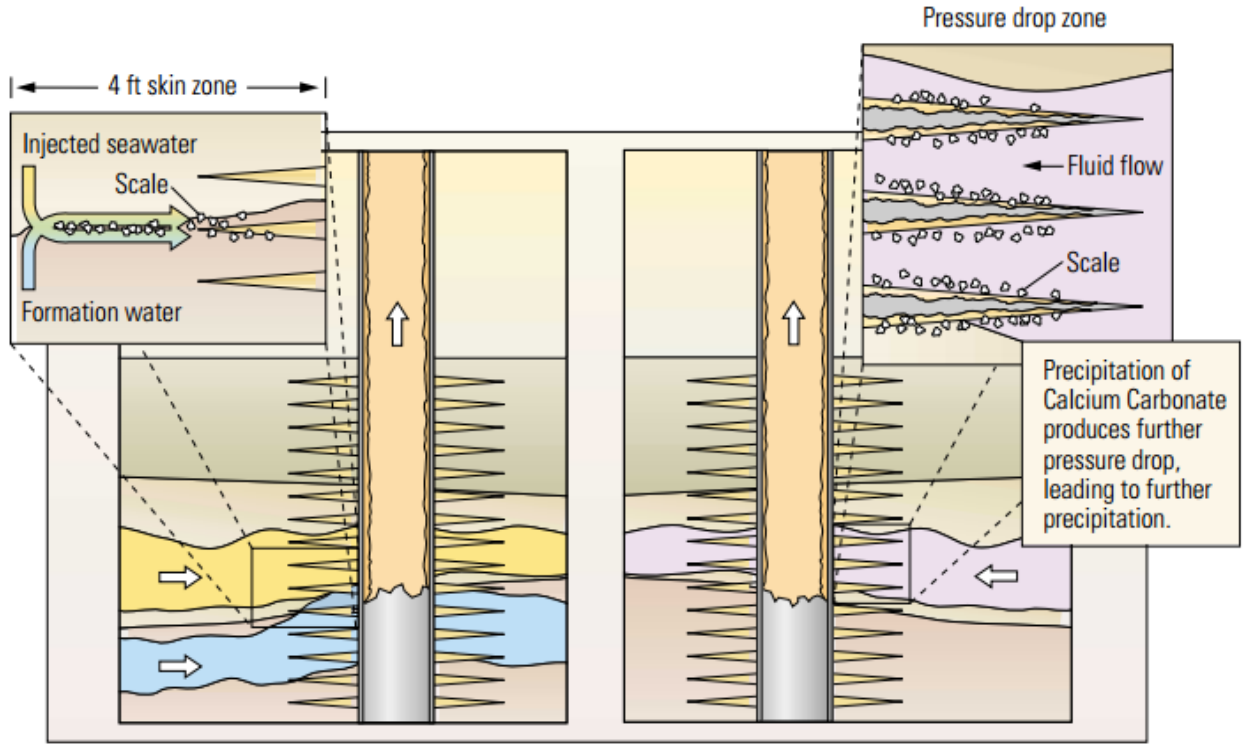

Figure 5. Production well damage caused by scaling(Crabtree, Eslinger et al. 1999)

It is expected that the oilfield scaling problem will become worse and more expensive. The reasons are as follows:(http://petrowiki.org/Scale_problems_in_production)

1. Tendency to longer tiebacks
2. Use of smart wells (integrity more critical)
3. More gas production (gas well formations tend to be more delicate)
4. Need to use greener chemicals
5. Increasing amounts of produced water

2.2 Common scales

Common scales contain carbonate, sulfate and sulfide scales. Sodium chloride (halite) is also important. The solubility of some scale, like carbonate and sulfide scale, is pH-sensitive. But some scale, like sulfate and sodium chloride, is insensitive to pH. The following sessions will give a brief introduction to the properties of these kinds of scale.

2.2.1 Carbonate scale

2.2.1.1 Calcium carbonate

Calcium carbonate consists of three crystal phases---calcite, aragonite and vaterite, shown in Figure 6.Calcite is one of the most ubiquitous mineral and is the stable form of calcium carbonate. A large number of organism make their shells and skeletons by calcite or aragonite. Calcite normally exists in igneous mineral, sedimentary rocks and fossils. Earth contains about 12% by weight of calcite and related carbonate minerals(Kan and Tomson 2012).

Calcite belongs to trigonal-rhombohedral crystal system. Most calcite is relatively pure (Deer), Many divalent ions can partition into the calcite crystals, but in relatively small amount. Mn can be up to 42 or 50 mol percent. Also, in natural samples, Fe is found to exist up to 5 to 10 mol percent (Deer). Hamad et al. has investigated the stoichiometry of $FeCO_3/CaCO_3$ solid solution(Alsaiari, Yean et al. 2008).

Precipitation of calcite happens when there is a pressure drop or temperature raise. When pressure drops below bubble point of carbon dioxide, CO_2 will escape from the solution, increases the pH

value and causes precipitation. When temperature raises, the solubility of calcite drops and results in precipitation. In oilfield production, pure calcite scale is rare. 20% of Fe and Mgalways corperate into calcite (Kan and Tomson 2012). Strontium (Sr^{2+}), Lead (Pb^{2+}) and Manganese (Mn^{2+}) are other kinds of ions that usually integrated into calcite. Dolomite ($CaMg(CO_3)_2$) is very difficult to form under standard temperature and pressure and has never been synthesized in laboratory condition.

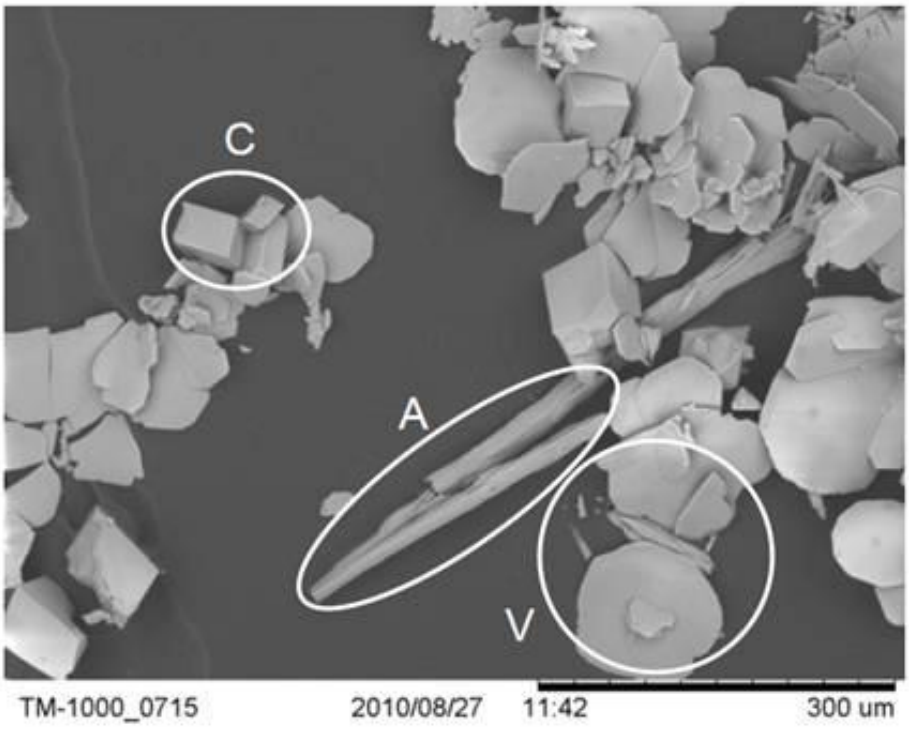

Figure 6. SEM picture of calcite, aragonite and vaterite (Tang, Thompson et al. 2009)

2.2.1.2. Iron carbonate

Ferrous carbonate occurs as natural siterite and a major source of iron in groundwater. $FeCO_3$ often serves as a corrosion-protective layer on carbon steel tubing to prevent further corrosion. In some wells, there is a high partial pressure of CO_2, which can cause severe corrosion. A deposit of thin $FeCO_3$ layer always protect the tubing wall from further corrosion. Especially in downhole

condition, the environment is very reductive. The possibility of forming $FeCO_3$ in the presence of dissolved Fe(II) from tubing becomes significant. At low temperatures $FeCO_3$ is slow to form, but so is corrosion. As the temperaure increases to about 100°C, the rate of $FeCO_3$ formation accelerates. Somewhere between 90° and 110°C, $FeCO_3$ will begin to decompose and form magnetite, Fe_3O_4, which is a better corrosion-prevention film.Greenberg et al. studied the precipitation and dissolution kinetics of iron carbonate(Greenberg and Tomson 1992).

2.2.2 Sulfate scale

2.2.2.1 Barium sulfate

Barite is the mineral name for barium sulfate ($BaSO_4$). Barite is one of the least soluble sulphate mineral. Sulfate scale are usually formed when formation water and injected seawater mix. And the mixing occurs in the near-wellbore region of the producing wells, it causes precipitation of sulfate scales as formation damage. Unlike calcium carbonate scale, the precitation of varite is easier to control since it is not influenced by changing pH or gas phase composition. The removal of barite in oilfield is notoriously hard (Kelland 2014). In sereve scaling cases, it has to be removed by mechanical means such as milling or jet blasing(Kelland 2014). There is only one chemical class capable that has been consistently used in the feld for dissolving barium sulfate scale at an appreciable rate and that is the salts of diethylenetriamine pentaacetic acid (DTPA) at pH higher than 12(Kelland 2014). It is widely applied due to its efficiency and relatively lower cost than other dissolvers e.g. ionic liquids. The reaction of barium sulfate with DTPA dissolvers (in Figure 7) is slow at room temperature, but can be improved at downhole temperatures and under good agitation.

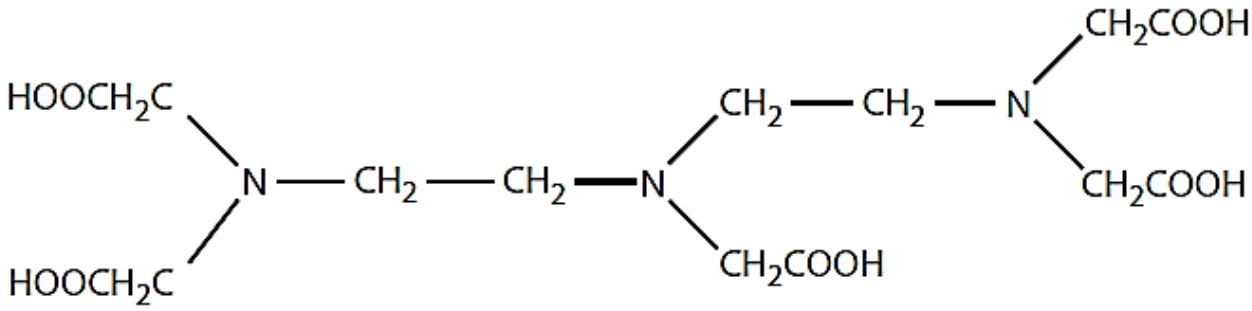

Figure 7. Structure of DTPA (Kelland 2014)

Due to its severe damage to oilfield and an easy-to-control precipitation process, barite is chosen to be the scale to study for this research.

2.2.2.2 Calcium sulfate

Calcium sulfate is easier to deal with compared to other sulfate scale. It has three major phases, anhydrite ($CaSO_4$) and gypsum ($CaSO_4 \cdot 2H_2O$) and hemihydrate ($CaSO_4 \cdot 1/2\ H_2O$). These three phases could transform between each other depending on temperature, water activity, pressure and supersaturation state. Calcium sulfate usually occurs when injection water (e.g. seawater) containg high concentration of sulfate mix with formation water with a high Ca^{2+} concentration, or when temperature and pressure change from downhole to surface. There is a large pressure effect on anhydrite solubility at lower temperature and less pressure effect at high temperature. Therefore, pressure drop can be a major cause of $CaSO_4$ scale in producing wells. Also, calcium sulfate precipitation can result from an increase in temperature during the processing of the brine on the surface (e.g., heater), membrane filtration, steam flood, or when large quantities of thermodynamic hydrate inhibitors are used for hydrate control ((Kan, Fu et al. 2002, Kan, Fu et al. 2003, Lu, Kan et al. 2010)). In the presence of methanol or MEG, as hydrate inhibitors, anhydrite was observed at much lower temperatures than expected due to the lowering water activity in the presence of

methanol or MEG. Also, many of the inhibitors that are effective against barite and calcite do not prevent calcium sulfate nucleation and growth, probably because Ca-Inhibitor solids form pseudo-scale before inhibition occurs, but more research is needed.

2.2.2.3 Strontium sulfate

Celestite is the mineral name for strontium sulfate ($SrSO_4$) and belongs to the orthorhombic crystal system (SEM picture of celestite shown in Figure 8). Celestite can be precipitated by migrating strontium-bearing ground water or basinal brines in carbonate rocks, concretions and modules; in hydrothermal veins and mafic volcanic rocks. Strontium sulfate is considerably more soluble than barium sulfate, but it is typically less soluble than calcium sulfates. Strontium sulfate solubility decreases with temperature. Until the advent of seawater injection in the Middle East, pure $SrSO_4$ was seldom observed and was not considered a major problem in water injection operation. However, serious $SrSO_4$ scale problems have occurred in the producing wells in a number of Middle East fields after breakthrough of seawater, due to mixing of the sulfate bearing seawater and the strontium in the formation waters in the producing wellbores.

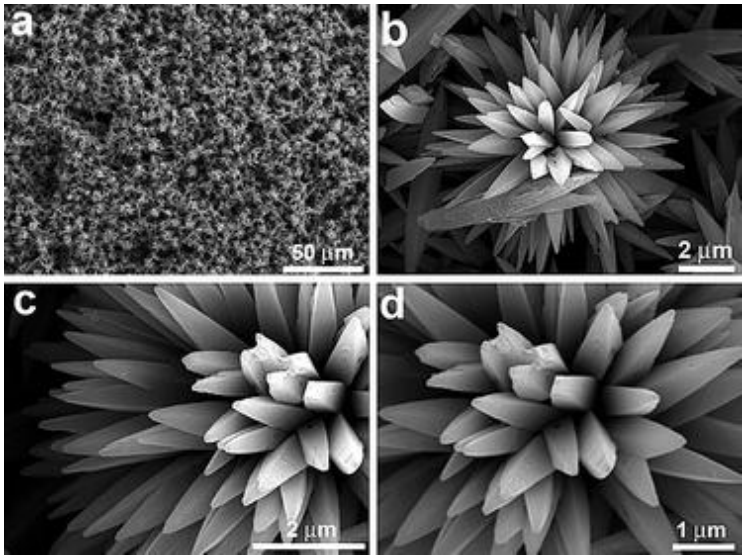

Figure 8. SEM picture of Celestite (Wang, Zhen et al. 2011)

2.2.2.4 Sulfide scale

Although sulfide scales are less common than carbonate and sulfate scales but still they can cause serious problem. Some formation water naturally contain some hydrogen sulfide, but for oil wells, most hydrogen sulfide comes from the reduction of sulfate in injected water by sulfate-reducing bacteria. Many of the deeper and hotter gas fields contain 25 percent by volume, or more. FeS is the most common sulfide scale which forms mainly from the corroded Fe(II) from steel tubing combining with sulfide. Other two sulfide scale are even more sparingly soluble sulfide, ZnS and PbS. Mixed Zn/Pb sulfide scale appears to be quite common in high pressure, high temperature wells in North Sea. Considering the importance of these materials to production, surprisingly little is known about the prediction and control of metal sulfide deposits. A good threshold inhibitor for sulfide scale has not been discovered as those for Calcium Carbonate or Barium Sulfate scale (Kelland 2014).

2.2.2.5 Halite

Sodium chloride is much more soluble than scales described above. Halite does not typically form in less than about 320,000 mg/L TDS brine in oilfield condition. Its solubility increases with increasing temperature. The salt is common particularly in high pressure high temperature wells. Therefore, as temperature decreases, the salt could become saturated and start to precipitate. Also, the other major source of NaCl scale is from water evaporation and pressure. Halite solubility is reduced in the presence of methanol. In the presence of methanol, halite scale can become a problem at much lower TDS values, circa and above 180,000 mg/L(Kelland 2014).

2.3 Crystallization

Crystallization of minerals undergoes two stages, nucleation and crystal growth. This section will introduce classic nucleation and crystal growth theory.

2.3.1 Nucleation mechanism

Nucleation is composed of primary nucleation and secondary nucleation. Primary nucleation refers to nucleation systems that do not contain exising crystals. While secondary nucleation refers to nucleation happening in supersaturated solution while crystals are present. The crystals act as seeds to induce nucleation to happen.

Primary nucleation include homogeneous nucleation and heterogeneous nucleation. Heterogeneous nucleation is induced by foreign particles like dust, colloids, aerosols. While homogeneous nucleation happens spontaneously, caused by molecular collision as shown in Figure 9. The formation of crystal nuclei is usually a series of bimolecular collision. The nuclei has to reach a critical size in order to resist the tendency to redissolve. Once the nuclei exceeds the critical size, it will become stable and continues to grow.

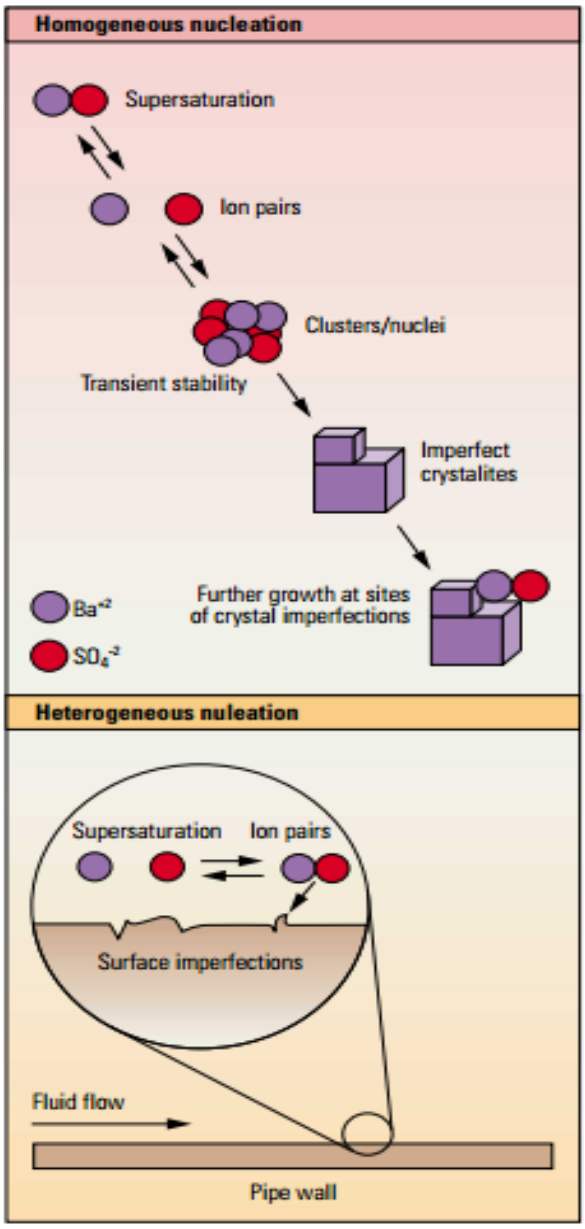

Figure 9. Homogeneous and Heterogeneous nucleation(Crabtree, Eslinger et al. 1999)

2.3.1.1 Homogeneous nucleation

The overall excess free energy of a particle forming from a solution can be expressed as

$$\Delta G = \Delta G_S + \Delta G_V = 4\pi r^2\gamma + \frac{4}{3}\pi r^3 \Delta G v$$

ΔG_S ----the surface excess free energy, which is the free energy between the surface of particle and bulk of the particle

ΔG_V ----volume excess free energy, which is the free energy between a partcle and the solute in the solution.

γ----interfacial tension between the crystalline surface and the saturated solution

ΔG_v ----the free energy change of the transformation per unit volume

$$\frac{d\Delta G}{dr} = 8\pi r\gamma + 4\pi r^2 \Delta G_v = 0$$

we have

$r_c = \frac{-2\gamma}{\Delta G_v}$, plug into the equation, we get $\Delta G_{crit} = \frac{16\pi\gamma^3}{3(\Delta G_v)^2} = \frac{4\pi\gamma r_c^2}{3}$

When $r=r_c$, the crystal has the largest value of free energy. The behavior of the crystal, whether it will grow or dissolve, should lower the value of free energy. Therefore, the particles smaller than the critical size tend to dissolve while those bigger than the critical size will continue to grow.

Classic nucleation rate is expressed as

$$J = Ae^{-\frac{\Delta G}{kT}}$$

where k is the Boltzmann constant,

R is gas constant, 8.314 J/K mol

N is the Avogadro number, $6.023*10^{23}$/mol

Gibbs-Thomson relationship gives

$$lnS = \frac{2\gamma v}{kTr}$$

$$S = \frac{c}{c^*}$$

c----the solution concentration

c^*----the equlibrium saturation at the given temperature

γ ----interfacial tension

From above equations, we get $-\Delta G_v = \frac{2\gamma}{r} = \frac{kTlnS}{v}$, put into nucleation rate equation

$$J = Ae^{\frac{-16\pi\gamma^3 v^2}{3k^3T^3(lnS)^2}}$$

The nucleation rate is related to interfacial tension , supersaturation S and temperature. A is a factor that is related to the collision frequency (Mullin 2001).

.

2.3.1.2 Heterogeneous nucleation

Heterogeneous nucleation is induced by foreign particles or surfaces, as shown in Figure 9. It is common in atmospheric process like condensation. Foreign solids can catalyze nucleation process, reduce the energy barrier. So the critical energy barrier of heterogeneous nucleation is typically smaller than that of homogeneous nucleation. The relationship between interfacial tension and contact angle is shown inFigure 10(Mullin 2001).

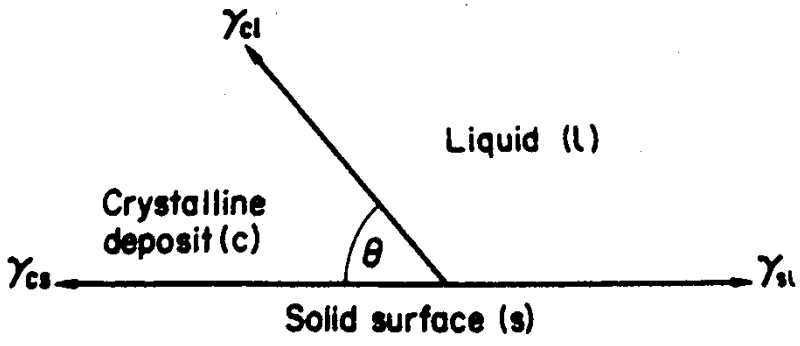

Figure 10. The relationship of interfacial tension(Mullin 2001)

$\gamma_{sl} = \gamma_{cs} + \gamma_{cl}cos\theta$

γ_{sl} ----interfacial tension between solid and liquid phase

γ_{cs} ----interfacial tension between crystal and solid phase

γ_{cl} ----interfacial tension between crystal and liquid phase

θ ----the angle of contact between the crystalline deposit and the foreign solid surface

θ depends on the affinity between the crystalline and solid surface. If equals to 180°, there is completely no affinity between the crystalline phase and solid phase. If equals 0°, it is a complete wetting situation, which is seeding a supersaturated solution with the desired product crystals. indicates partial affinity (Mullin 2001).

The surface energy differs for homogeneous and heterogeneous nucleation, because in heterogeneous nucleation, the crystal is also in contact with solid surface.The surface energy for homogeneous is $\overline{\gamma_{CW}}A$, for heterogeneous is $\overline{\gamma_{CW}}A_{CW} + (\overline{\gamma_{CS}} - \overline{\gamma_{SW}})A_{CS}$. CW refers to crystal-water, *CS* refers to crystal-solid and SW refers to solid-water(Mullin 2001).

Therefore, interfacial tension is important for predicting the thermodynamicas and kinetics of the nucleation process. And interfacial tension is related to the solubility. An empirical relationship between interfacial tension and solubility is as follows.

$$\frac{4r^2\gamma}{kT} = 4.7 - 0.272lnC_{sat}$$

r----the mean ionic radius (m)

γ----the interfacial mineral-aqueous solution free energy

C_{sat} ----solubility of the mineral (~$K_{sp}^{1/2}$)

which indicates the higher solubility a crystal has, the lower the interfacial tension it gets and easier to form(Mullin 2001).

2.3.2 Ostwald step rule

As indicated above, the solid form with the highest solubility will precipitate first because they have the lowest interfacial tension between the solid and solution. In other words, the least stable form is likely to precipitate first. As Ostwald describes “an unstable system does not necessarily transform directly into the most stable state, but into one which most closely resembles its own” . It indicates that the direction of reaction might not necessariliy proceed towards the thermodynamically most stable one, but the kinetically fastest one. This rule is important for solid solution formation since it is almost always in metastable form and cannot always reach thermodynamics equilibrium (Mullin 2001).

2.3.3 Crystal growth

In 1939, Volmer first proposed that crystal growth is actually a discontinuing process, starting by atoms and molecules absorbing onto the face of crystals. These atoms and molecules migrate over the surface and are attracted to “active centers” and integrated into crystal lattice until one layer is completed. Kossel (1934) proposed that instead of a smooth surface, crystal face is composed of steps and kinks which accelerates crystal growth rate as shown in Figure 11. Frank (1949) proposed that few crystals actually grows in the perfect layer by layer manner. Most crystal surface are covered by screw dislocation and grows spirally. Now, people realize that there are several complex steps going on in the growth process. Stumm and Morgan describes the basic steps of

crystal growth as following steps (Lasaga 2014).

(1) Transport of atoms and molecules through the solution

(2) Attachment of atoms to the surface

(3) Movement of atoms on the surface

(4) Attachment of atoms to edges or kinks

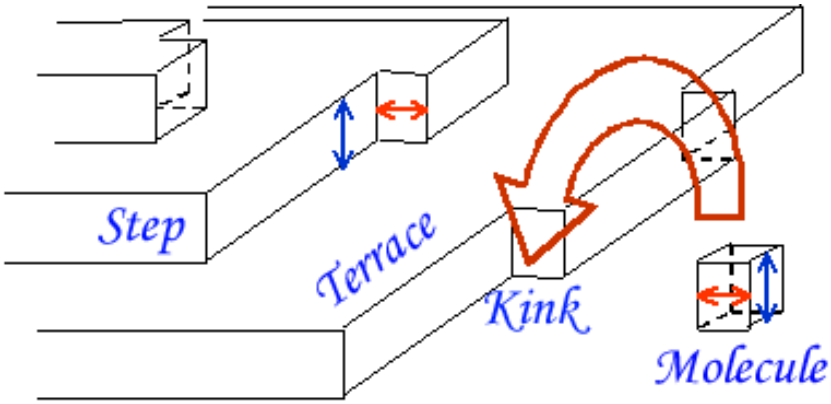

Figure 11. Steps and kinks in the surface of crystal (Lasaga 2014)

2.3.3.1 The diffusion-reaction theories

The basic steps of nucleation contain two major parts: the transport of ions to the surface of crystal (transport process) and the movement of ions on the surface, integration into the crystal lattice (surface process).

The model proposed by Berthoud (1912) and Valeton (1924) proposed that the overall crystal growth process as a combination of both diffusion and surface reaction process. And the driving force for both process is the concentration difference(Mullin 2001).

$\frac{dm}{dt} = k_d A(c - c_i)$ for the diffusion process

$\frac{dm}{dt} = k_r A(c_i - c^*)$ for the surface reaction process

m----mass of solid deposited in time t

k_d----a coefficient of mass transfer by diffusion

k_r----a rate constant for the surface reaction process

c_i---solute concentration in the solution at the crystal-solution inerface(Mullin 2001)

Assume the overall crystal growth process as a first-order reaction, use k_G as the overall crystal growth reaction coefficient, we get

$$\frac{dm}{dt} = k_G A(c - c^*)$$

By canceling C_i term from the above two equations, we can get

$$\frac{dm}{dt} = \frac{A(c - c^*)}{\frac{1}{k_d} + \frac{1}{k_r}}$$

$$\frac{1}{k_G} = \frac{1}{k_d} + \frac{1}{k_r}$$

when k_d is much higher than k_r, $k_G = k_d$ the process is surface reaction limited

when k_r is much higher than k_d, $k_G = k_r$ the process is diffusion limited

Lasaga also gives some criteria to decide which of the above process is the dominant one (Lasaga 2014).

(1) if the rate of growth is surface controlled, there should be very small concentration gradients in the reactants within the medium surrounding the growing phase

(2) The activation energy can also indicate which process is dominant. If the activation energy is higher than 5 Kcal/mol, then the process is surface control.

2.3.4 Saturation index

K_{sp} is the activity product when a solid is at equilibrium with aqueous phase.

Take $CaCO_3$ for example, at equilibirum in a certain temperature

$$K_{sp} = \{Ca^{2+}\}\{CO_3^2\ \}$$

$$K_{sp} = [Ca^{2+}]\gamma_{Ca^{2+}}[CO_3^{2-}]\gamma_{CO_3^{2-}}$$

$\{Ca^{2+}\}$ is the activity of Ca^{2+}

$[Ca^{2+}]$ is the concentration of Ca^{2+}

$\gamma_{Ca^{2+}}$ is the activity coefficient of Ca^{2+}

$$SI = \log\frac{IAP}{K_{sp}(T,P)}$$

2.3.5 Activity coefficient

There are several equations available to calculate activity coefficients, which should be applied at different ionic strength. Figure 12shows the applicability of different equations.

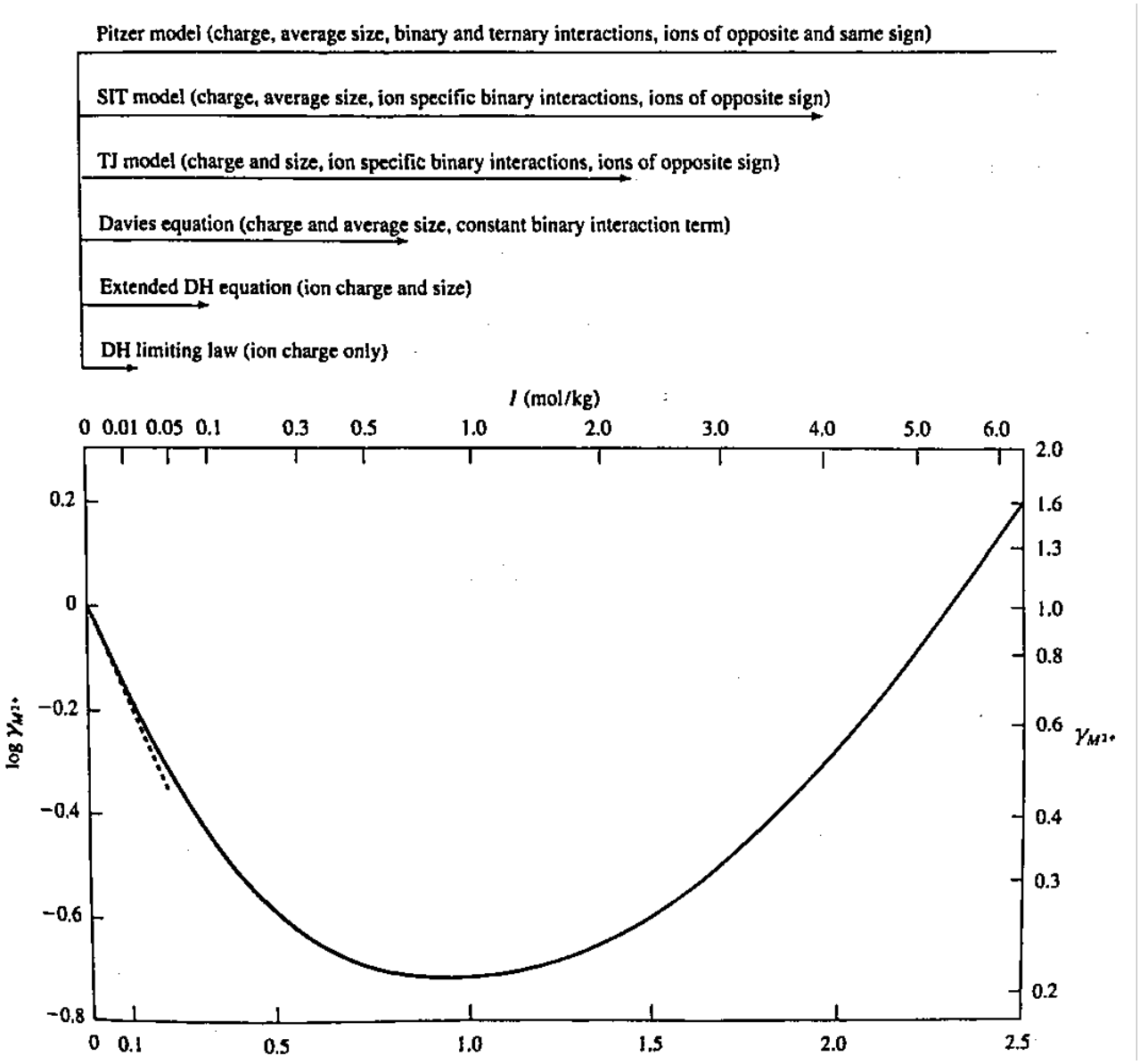

Figure 12. The applicability of different activity coefficient equations (Langmuir 1997)

Davies equation is one of the most used equations for activity coefficient calculation.

$$\log \gamma = -AZ^2 \left(\frac{\sqrt{\mu}}{1+\sqrt{\mu}} - 0.3\mu\right)$$

μ is the ionic strength of the solution

$$A = 1.82 \times 10^6 (\epsilon T)^{-\frac{2}{3}}$$

$\in$: dielectric constant of the medium

Z: the charge of ion

μ: ionic strength

$$\mu = \frac{1}{2}\sum_i C_i Z_i^2$$

where

C_i: the concentration of ion I, in mol/l

Z_i: the charge of ion

2.3.6 Induction time

There is usually a period of time elapsed between supersaturation and the appearance of the crystals. This amount of time elapsed is called induction time. Induction time might contain several different parts as shown in Figure 13 (Mullin 2001). For example, t_{ind} can be written as $t_r + t_n + t_g$. t_r or "relaxation time" is the time for the system to achieve a quasi-steady-state distribution of molecular clusters. t_n is the time required for the formation of a stable nucleus. t_g is the time for the nucleus to grow to a detectable size. To calculate the exact value of each part is very difficult. Induction time can be influenced by a lot of factors including temperature, speed of agitation, the existence of seed etc. Induction time are usually measured by visual method, laser light scattering or electric zone sensing methods (Mullin 2001). Different results might be generated by different detection methods. In this research, laser scattering method is used for induction time detection. Measured light intensity data is outputed to a software developped by Rice Brine Chemistry Consortium. The software is written by Visual Basic in Microsoft Excel. The induction time selection principle can be simply put as follows: Light intensity data is rounded to 3 digits, then

the mode of the rounded dataset is identified. Average value of the data that is within the range of mode±0.001 mA is calculated. Induction time is identified as the first time when the laser signal is lower than "average - 0.0005", and all data afterwards are always lower than "average value - 0.0005".

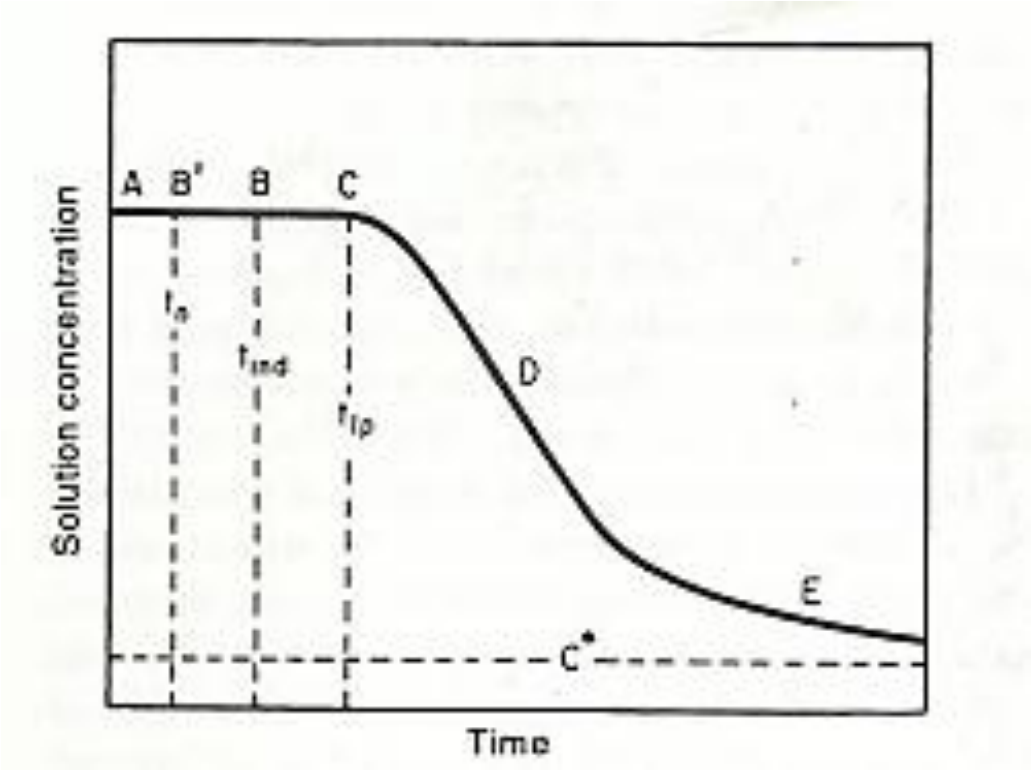

Figure 13 Desupersaturation curve (Mullin 2001)

The induction time selection software is developped by Rice University Brine Chemistry Consortium. Laser intensity signal data is first rounded from 5 digits to 3 digits or 3 digits plus 0.0005. Then the mode of the rounded dataset is identified and average of the data that are within the range of mode ± 0.001mv. Then induction time is identified as the first time when the laser signal is lower than “average – 0.0005” and all data afterwards are always lower than “average value – 0.0005”.

2.4 Scale inhibition

2.4.1 Introduction

Scale formation and inhibition are intimately related to each other. After the basic theory of crystallization is reviewed, some of the mechanism studies and theories proposed regarding scale inhibition, mostly on chemical scale control using scale inhibitors, will be discussed in this section.

Because of the tremendous financial loss caused by scaling, scale inhibition has been widely investigated. Scale control is needed primarily in the production facilities, but seawater injection and produced water reinjection may also need scale control. Some of the nonchemical scale control include desulfation of injected water to prevent sulfate and sulfide scales (Kelland 2014), using electric field to prevent scale form in the produced fluid instead of on the walls and surfaces(Kelland 2014), scale control using acoustic waves (Kelland 2014), magnetic fields or coated surfaces (Kelland 2014). Another option is to let scale form and then remove it using chemical dissolver or mechanical methods. More commonly, scale control chemicals are used. Therefore, the focus of this research is on scale inhibition chemicals, a.k.a. scale inhibitors. These are chemicals which delay, reduce or prevent scale formation when added in small amount to normally scaling water. Since 1936, threshold inhibitors have been widely applied rather than sequestering agents which has to be added in stoichiometric amounts to inhibit precipitation (Kelland 2014). Chemical threshold scale inhibitors generally require the addition of only a few milligrams per liter to inhibit scale. Most of the scale inhibitors function by either preventing the very tiny crystal precipitate from the water or preventing the precipitated scale crystals from adhering to solid surface. The mechanism by which scale inhibitors work is still not fully understood. Inhibitors have to be present in supersaturated solution in order to react with crystals

for scale inhibition. Therefore, inhibitors need to be applied in upstream of the problem area. Inhibitors have to be present in continuous basis which is usually realized by continuous injection or “squeeze treatment”. In squeeze treatment, inhibitors are adsorbed onto the reservoirs or tubing. Then during flow-back process, the adhered inhibitors are released back into the water phase at low concentrations.

There are two classes of scale inhibitors, thermodynamic and kinetic inhibitors. Thermodynamic inhibitors are normally complexing and chelating agents like EDTA and nitrilotriacetic acid. HCl is also a great thermodynamic scale inhibitor for carbonates and sulfides. These inhibitors work by chelating the cation composition ion of scale and lower the saturation index of that scale. While kinetics inhibitors prolong scale induction time and retard scale formation. Following are some of the standards of scale inhibitors in oil industry(Fink 2011, Kelland 2014).

1. Effective inhibition effect even at low inhibitor concentration;
2. Compatibility with produced water;
3. Balance of adsorption on the rock first and then slow desorption into produced water;
4. Tolerance of high temperature;
5. Low toxicity and high biodegradability;
6. Low cost.

Among these standards, #3 is related to the squeeze treatment mentioned above. If inhibitors fail to adsorb onto rock first, it will be flushed out from the well and fail to protect the well. However, if scale inhibitor adsorbed to rock too strongly with little desorption, there will be little scale inhibitor in produced water to prevent scaling. Considering thermodynamic inhibitors are overall

much more expensive than kinetic inhibitors and kinetic inhibitors have same good performance on scale control, kinetic inhibitors are more popular in the industry. Therefore, the scale inhibitors studied in this research are all kinetics scale inhibitors.

2.4.2 Inhibition mechanism

As introduced in section 2.3, the process of nucleation and crystal growth is well understood with numerous equations and thermodynamic theories proposed. However, no equivalent set of fundamental principles that can be used to predict scale inhibition. The nature, amount, or type of these interactions of the inhibitor with the crystal/nucleus surface cannot now be predicted from any set of fundamental principles of thermodynamics or kinetics. There is only empirical observations as of a specific kind of inhibitor is better for scale A than scale B. There is little agreement on how to model inhibition at the molecular or process level. This dearth of guiding theoretical laws is common to all forms of scale formation, not just in the oil-field produced fluids.

Brine Chemistry Consortium researchers at Rice University have modeled the influence of inhibitors on the nucleation time, semi-empirically by assuming a separation of the effect of the inhibitor from that of the uninhibited mineral, for example for barite(Liu, Kan et al. 2014):

$$\log_{10}\left(t_{ind}^{inh}, sec\right) = log_{10}(t_{ind}^{0}, sec) + b_{inh}\left(\frac{L}{mg}\right) * C_{inh}(\frac{mg}{L})$$

where C_{inh} is the concentration of inhibitor added and b_{inh} is an inhibitor effectiveness term. This empirical equation works quite well for a large range of inhibitors and minerals, but is not mechanistic in origin. Furthermore, the empirical b_{inh} term can become complicated over the whole range of pH, T, P, and compositions encountered in oil and gas wells. The advantage of the equation is that the effect of the inhibitor is separate from the basic nucleation of the scale forming

mineral, but the disadvantage is that there is no fundamental understanding of the b_{inh} term to aid in estimating its value for a new inhibitor or for additional conditions(Liu, Kan et al. 2014).

There are some intuitive speculations that scale inhibitors must interact with the forming nuclei or the growing crystal in some manner(Tomson, Fu et al. 2002). Burton-Caberrara-Frank (BCF) spiral growth mechanism theory is always used to interpret inhibition mechanism. In this theory, kink sites grow in a spiral. Inhibitors are speculated to work through the adsorption onto the active sties and blocking spiral growth. Since only active sites have to be blocked to prevent the spiral growth, crystal surface can be covered by less than monolayer of inhibitors. And many equations based on this theory will describe the reduction of growth rate proportional to the fraction of the crystal surface covered by inhibitor, or by the fraction of the critical coverage. However, it does not apply to the critical nature of inhibition. In experimental observation, a few percentages of inhibitor concentration change can cause the induction time to increase by 1 or 2 orders of magnitude(Tomson, Fu et al. 2002).

It was generally observed that calcium in solution significantly enhances the scale inhibition efficiency. Tomson et al. investigated the adsorption mechanism of inhibitor onto crystals and concluded that the primary driving force of inhibitor adsorption is hydrophobic repulsion of macro neutral inhibitor molecules from liquid solution, instead of the generally presumed specific inhibitor-surface interaction(Tomson, Fu et al. 2002). Inhibitor molecules are mostly macro molecules and become dissociated in water solution. Inhibitors are often dissociated in solution and can form large neutral molecules with existing cations in brine such as Ca^{2+}. Some research has similar findings that PPCA scale inhibitor is only effective when dissociated or metal

complexed while the un-dissociated PPCA cannot(Liu, Kan et al. 2014).

Except adsorption, lattice substitution is also a possible inhibition mechanism. Inhibitor could complex foreign ions which can insert into crystal lattice and distort the lattice structure of target scale. Once inserted, foreign ions can distort the lattice and connected inhibitor molecules can form a complex surface or crystalline nets(Mullin 2001).

2.4.3 Common scale inhibitors

There is a board range of scale inhibitors in the industry. Different scales need different inhibitors for better control. Some scale inhibitors, such as SPCA, PPCA, DTPMP and PVS can inhibit several kinds of scale especially sulfate and carbonate scale. But they do not work very well for halite and sulfide scales probably due to different precipitation mechanism. Hexacyanoferrate salts and nitrilotrialkanamides and quaternary salts are two kinds of typical halite inhibitors. Recently, a breakthrough discovery of FeS scale inhibitor was announced by Clariant. It is claimed that this newly discovered scale inhibitor (SCALETREAT®FeS iron sulfide scale inhibitor) is a truly threshold scale inhibitor which prevents FeS scale at much lower dosage than existing chemicals such as THPS (tetrakishydroxymethylphosphonium sulfate) and acrolein.

Common scale inhibitors can be divided by functional groups they contain: polysulfonates, polycarboxylates and phosphorus (P) containing inhibitors. Non polymers with only sulfonate or carboxylate groups are fairly poor inhibitors. Inhibitors with sulfonate or carboxylate groups are generally polymers. However, P-containing inhibitors can be divided into several subtypes: polyphosphates, phosphate esters, non-polymeric phosphonates, polyphosphonates and polyphoninates(Kelland 2014). Also, some inhibitors could contain more than 1 kinds of above

function groups. Here in the following secions, one or several representative inhibitor will be listed for each category and their application will be discussed briefly.

2.4.3.1 Polysulfonates.

SPCA and PVS are representative chemicals of polysulfonate scale inhibitors. Polysulfonates have many advantages. First, they have high thermal stability, which makes them applicable at high temperature oil wells(Kelland 2014). Second, they can be applied in high Ca^{2+} and Mg^{2+} concentration brine due to lower stability constants with these two ions (Fink 2011). Third, sulfonic acid is a strong acid with low pKa value, which enable polysulfonates to work well in low pH solution. Furthermore, polymer with vinyl sulfonic acid group has been found to be a great killer of barite scale(Fink 2011).

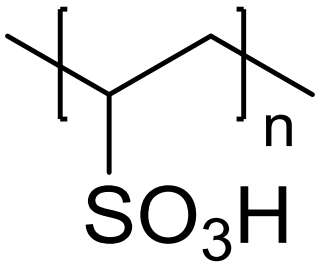

Figure 14. Structure of polyvinyl sulfonate

2.4.3.2 Polycarboxylates.

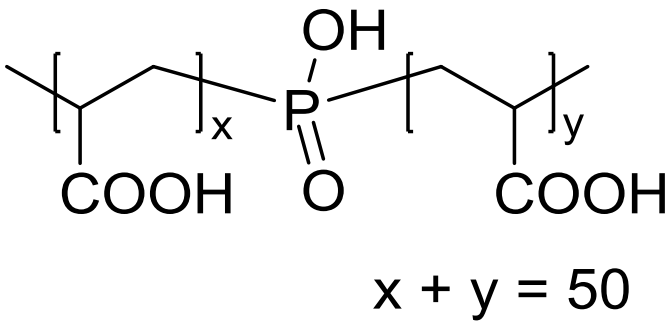

Figure 15. Structure of phosphino polycarboxylic acid (PPCA)

Three kinds of polycarboxylic acids are commonly used: polyacrylic acid, polymethacrylic acid and polymaleic acid. Polycarboxylates are of low cost and widely applied in oil industry. In the molecule structure, polycarboxylates with some percentage of amide, hydroxyl, quantenary amine, phosphonate or phosphinate groups could increase their inhibition performance. One good example is PPCA (phosphino polycarboxylic acid) which has longer squeeze lifetime, higher calcium compatibility and better Barite scale inhibition than polycarboxylic acid.

The disadvantage of polycarboxylate scale inhibitor is its low biodegradability. Recently, some more environmental friendly scale inhibitors have been invented such as Carboxy Methyl Inulins (CMI).

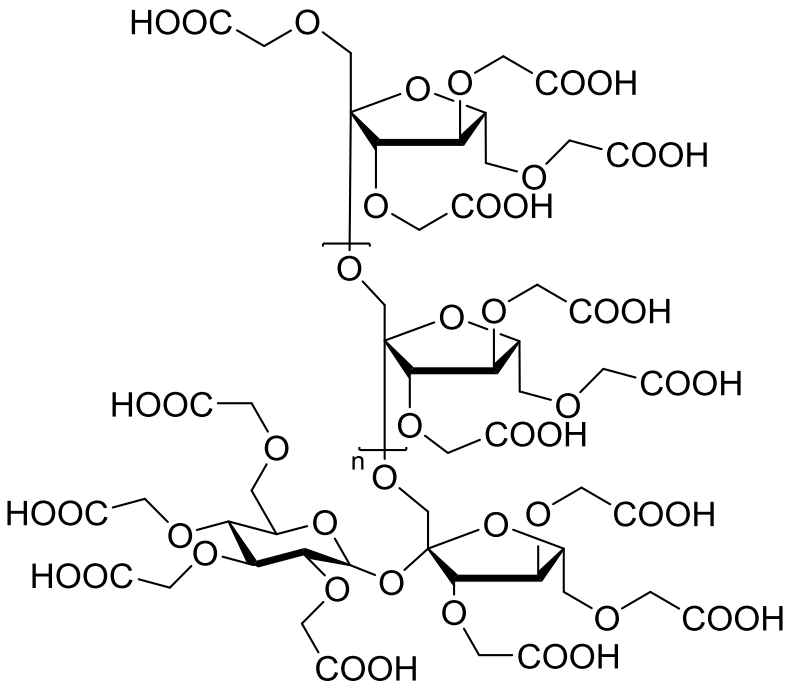

Figure 16. Structure of CMI

2.4.3.3. Polyphosphates and phosphate esters

Polyphosphates (Figure 18) are common carbonate scale inhibition with high thermal stability. They are often used in boiler waters for scale control. Phosphate esters are good inhibitors for $CaCO_3$, $CaSO_4$ and $BaSO_4$ scales in neutral and alkaline solution.

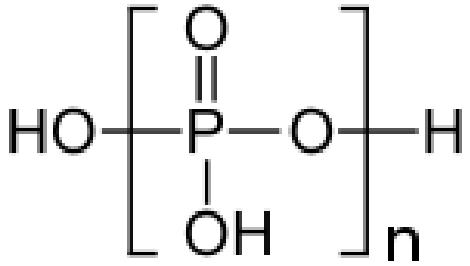

Figure 17. Structure of polyphosphoric acid

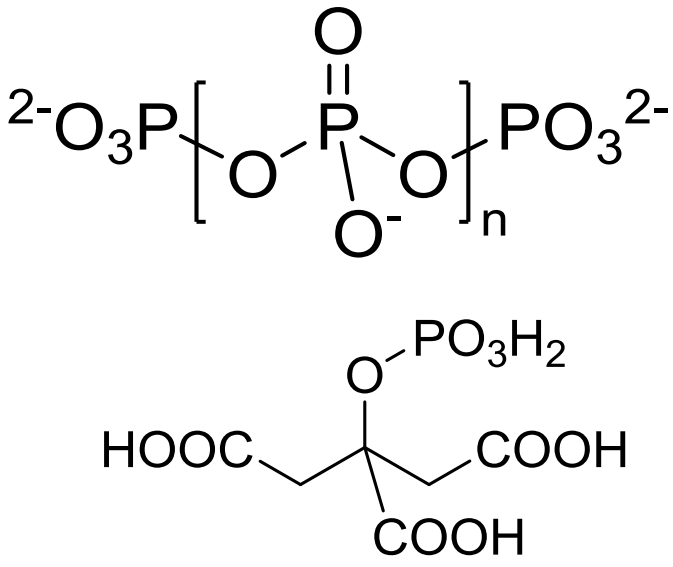

Figure 18. Structure of polyphosphate (top) and citric acid phosphate (bottom)

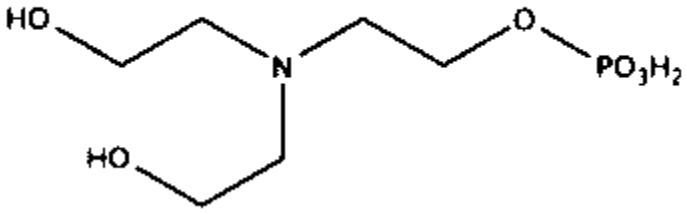

Figure 19. Structure of Triethanolamine phosphate ester

2.4.3.4 Polyphosphonates

There are two main classes of polyphosphonates, those with a polyamine backbone and those with a polyvinyl backbone. They are particularly useful for Barite scale inhibition and for squeeze applications.

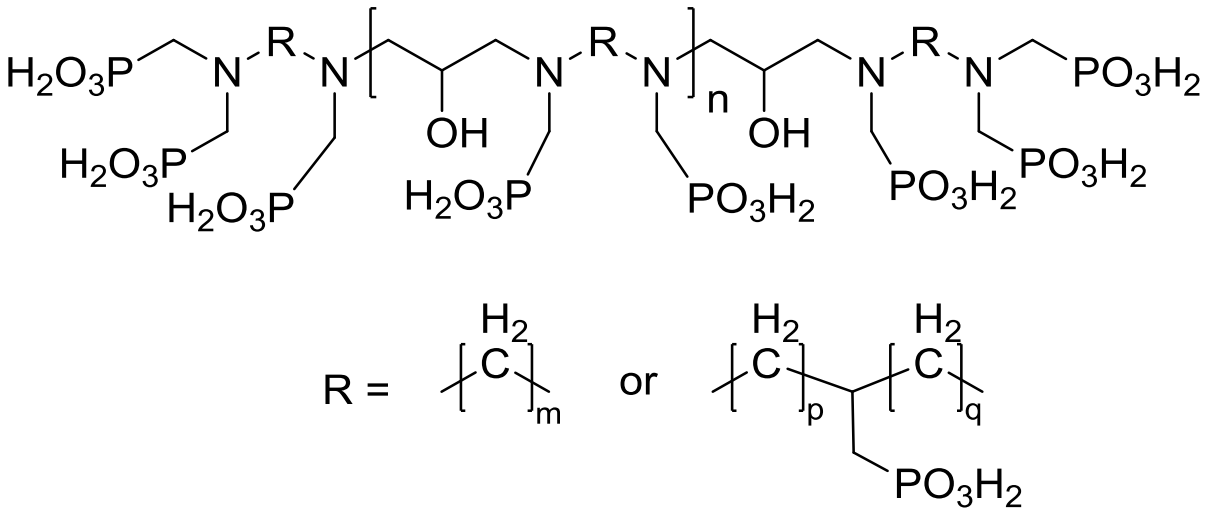

Figure 20. N-phosphonomethylated amino-2-hydroxypropylene polymers

2.5 Fe in aqueous solution

Iron is a metal in the first transition series. It is, by mass, the most common element on Earth, forming much of Earth's outer and inner core. It is the fourth most common element in the Earth's crust.

Iron exists in a wide range of oxidation states, -2 to +6, with +2 and +3 as the most common states. Examples of iron in different oxidation state is listed in Table 2.

Table 2. Representative compound structures of various iron oxidation states

Oxidation state	Representative compound
-2	Disodium tetracarbonylferrate (Collman's reagent)
0	Iron metal
1	Cyclopentadienylirondicarbonyl dimer
2	Ferrous sulfate
3	Ferric chloride
6	Potassium ferrate

2.5.1 Speciation and solubility of Fe(II) and Fe(III) in water

In solution, most of the iron exists either in Fe(II) or Fe(III) states. In water, ferrous iron can be oxidized to ferric iron. The oxidation kinetics is dependent on temperature, O_2 level and pH

(Stumm and Morgan 2012).

$$-\frac{d[Fe^{2+}]}{dt} = k[Fe^{2+}][OH^{-}]^2 P_{O_2}$$

Where k= 8.0 (±2.5) * 10^{13} min^{-1} atm^{-1} mol^{-2} $liter^2$ at 20°C. For a given pH, the rate increases about tenfold for a 15°C temperature increase. Fe(II) tend to display a greater solubility than do Fe(III) constituents.

Fe(II) exists in solution in three forms based on different pH condition. They are $Fe(H_2O)_6^{2+}$, $Fe(H_2O)_5(OH)^{+}$ and $Fe(H_2O)(OH)_3^{-}$. The water ligand is always omitted so they are always written as Fe(II), $FeOH^{+}$ and $FeOH^{-}$. Below is in a 0.001M NaCl solution, total Fe concentration = 5.6 mg/l (0.1mmol/l), temperature=25°C condition, the speciation of these three Ferrous iron compounds concentration change with pH. Calculation is done by Visual MINTEQ ver. 3.1. The assumption is no precipitation happens in solution.

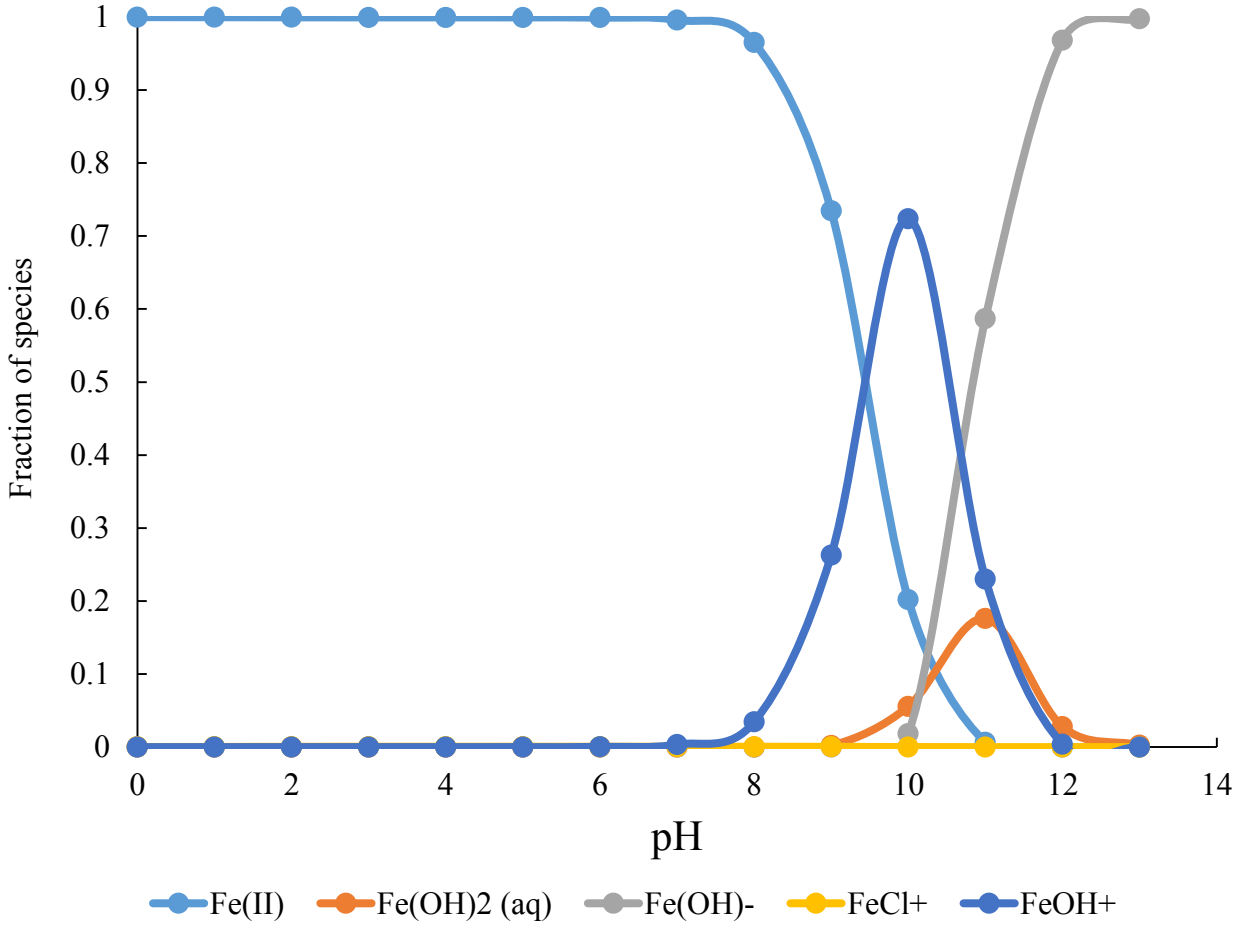

Figure 21. Speciation of Fe(II) species

From Figure 21, we know at low pH range, the dominant species in solution is Fe(II) while at high pH range, $Fe(OH)_3^-$ becomes more significant. The flip point is between pH 9 and 11. However, in Figure 21, precipitation of ferrous hydroxide is not considered. In fact, from pH 10 to pH 13, the solution is already supersaturated with amorphous ferrous hydroxide. In Figure 22, the solubility of Fe(II) in above solution at different temperature and ionic strength is plotted for comparison.

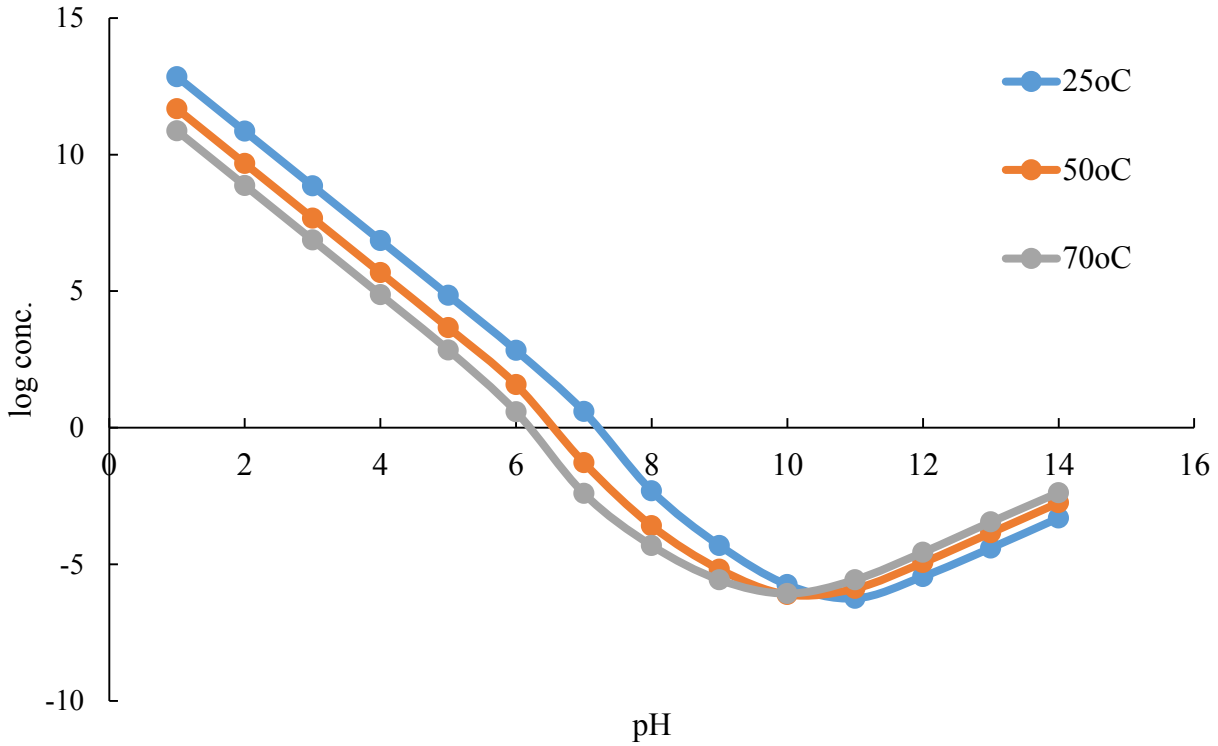

Figure 22. Logarithm of solubility (unit: mol/l) of ferrous hydroxide change with temperature

We can see from the above graphs that, at acidic condition (pH from 1 to 6), the solubility concentration of Fe(II) in this solution is very large.

Besides hydroxide, Fe(II) solubility in water is also determined by carbonate and sulfide concentration. In most natural waters, the solubility of ferrous iron is controlled by the solubility of $FeCO_3$ (s), In an alkalinity containing water, the CO_3^{2-}, even at low pH, is sufficient to limit the iron solubility. The solubility product of $FeCO_3$ is about 200 times smaller than the solubility of $CaCO_3$. Thus, for a water which is in equilibrium with $CaCO_3$, its maximum soluble iron is about 200 times smaller than its calcium content. However, when pH goes beyond 8~9, ferrous hydroxide is again controlling the solubility of ferrous iron. Also, the presence of a small amount

of sulfide can influence Fe(II) solubility.

There are several aqueous species of Fe(III) in solution. Figure 23 shows the aqueous species included in Visual MINTEQ software. The calculation assumes there is no precipitation.

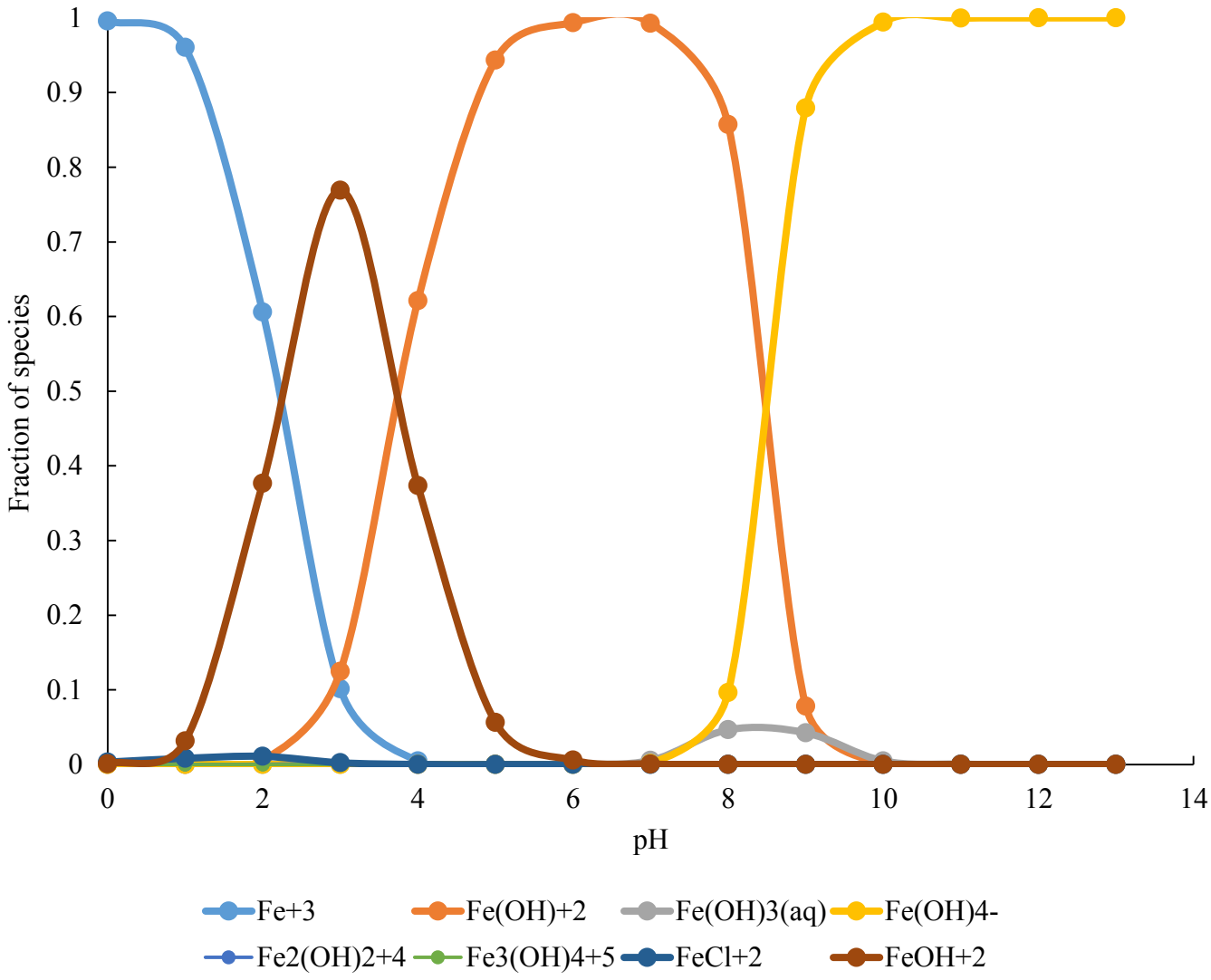

Figure 23. Fe(III) aqueous species in solution change with pH

From Figure 23 we can see, the dominant species of Fe(III)in solution changes with pH. At low pH, the dominant species is Fe(III) while at higher pH, it is $Fe(OH)_4^-$.

Compared to Fe(II), Fe(III) is orders of magnitudes less insoluble than Fe(II), it is only sparingly soluble in aqueous solution at pH above 2. The solubility of Fe(III)is controlled in natural waters by the solubility of ferric hydroxide. Visual MINTEQ ver. 3.1 is used to calculate Fe(III) solubility in equilibrium with one of the iron oxide species---ferrihydrite. The solubility is plotted in Figure 24 and compared with Fe(II) solubility in Table 3.

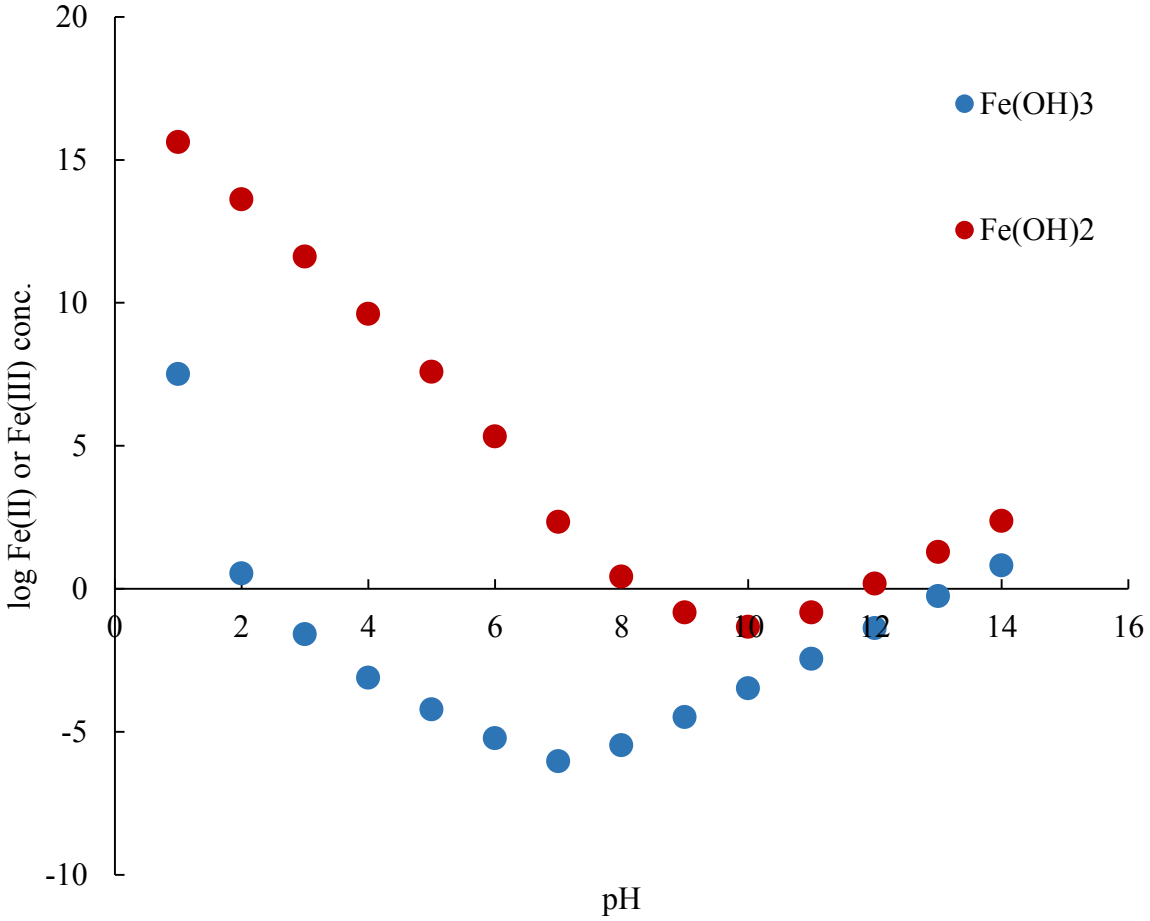

Figure 24. Ferrous hydroxide and ferric hydroxide solubility at 70°C, 0.001M NaCl solution

Table 3. Solubility of ferrous and ferric hydroxide at different pH, 70°C, 0.001M NaCl (Calculated by Visual MINTEQ ver. 3.1)

pH	Fe(III) solubility (mg/l)	Fe(II) solubility (mg/l)
1	3.21E+07	4.15E+15
2	3.44E+00	4.15E+13
3	2.58E-02	4.15E+11
4	7.82E-04	4.13E+09
5	6.14E-05	3.91E+07
6	6.03E-06	2.14E+05
7	9.46E-07	2.17E+02
8	3.36E-06	2.71E+00
9	3.28E-05	1.50E-01
10	3.32E-04	4.73E-02
11	3.55E-03	1.51E-01
12	4.25E-02	1.53E+00
13	5.54E-01	1.96E+01
14	6.63E+00	2.35E+02

2.5.2 Iron oxides

There are fifteen iron oxides, oxide hydroxides and hydroxides known to date (Cornel and Shwertmann 1991). Most common iron oxide minerals include Goethite, Akaganeite, Lepidocrocite, Feroxyhyte, Ferrihydrite, Hematite, Maghemite, Magnetite. In addition to above compounds, $Fe(OH)_2$, FeO (wustite), a β-Fe_2O_3, a ε-Fe_2O_3, a high pressure FeOOH, a ferromagnetic δ-FeOOH and a crystalline $Fe(OH)_3$ (bernalite) exist(Cornel and Shwertmann 1991). The solubility products of the different structural forms of iron oxides are not accurately known. Feitknecht assumes for Geothite, Lepidocrokite and Hematite, Maghaematite Ksp value

of 10^{-44}, $10\text{-}^{42.5}$, $10^{-42.5}$ and 10^{-41} respectively(Cornel and Shwertmann 1991). And a solubility product of 10^{-36} for amorphous ferric oxide was assumed (Stumm and Morgan 2012).

Iron oxide surface is generally covered with hydroxyl groups. Atoms, molecules, polymers, ligands can react with surface groups by following mechanisms (Stumm 1992). 1) Surface complexation, including surface hydrolysis, surface coordination with metal and ligands. Surface coordination includes formation of inner-sphere or outer-sphere complexes between surface and metal ions, or surface precipitates. Metal, ligand and surface can also form ternary complexes. Ligand always get adsorbed onto surface through ligand exchange. 2) Electric interactions at surfaces. 3) Hydrophobic expulsion. This includes non-polar organic solutes which are usually sparingly soluble in water, trying to reduce their contact with water by adsorbing onto solid surfaces. 4) Adsorption of surfactants. 5) Adsorption of polymers and of polyelectrolytes, e.g. humic substances and proteins(Stumm 1992).

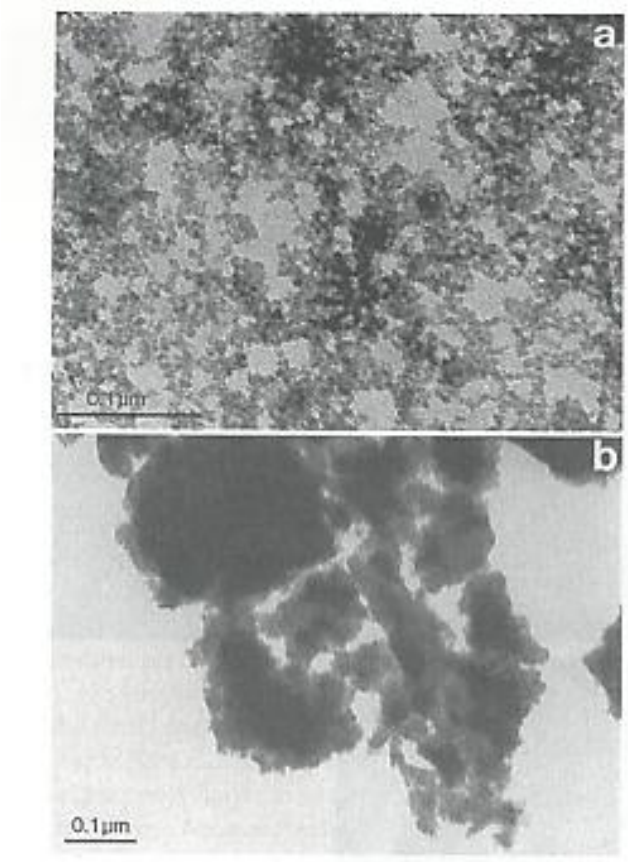

Figure 25. TEM image of 2-line ferrihydrite (a) and 6-line ferrihydrite (b) (Cornell and Schwertmann 2003)

The iron oxide mineral formed in this research is likely to be ferrihydrite. Both synthetic and natural formed ferrihydrite are poorly ordered (Cornell and Schwertmann 2003). The degree of ordering is variable and a range of XRD patterns can be achieved. Two extremes of crystal order are referred to as 2-line and 6-line ferrihydrite, as shown in the TEM image in Figure 25. The main difference between the 2-line and 6-line ferrihydrite is their crystal domains (Cornell and Schwertmann 2003). Exact formula for ferrihydrite is not established due to the lack of precise separation of structural OH and H_2O from adsorbed water.

Surface area of ferrihydrite have been determined by a wide range of methods and are reported as

varying between 100 and 700 m^2/g, as shown in Table 4 (Cornell and Schwertmann 2003).

Table 4. Surface areas of ferrihydrite measured by different methods (Cornell and Schwertmann 2003).

Tab. 5.1. Surface areas of ferrihydrites by different methods.

Method		*Surface area* (m^2g^{-1})	*Comment*[a)]
BET	Ar	215–270	
	H_2O	300 (±50)	
P ads.		720	
Neg. ads. Na^+ pH 4		270–335	
Neg. ads. Mg^{2+} pH 5		700	
BET-N_2		340	synthetic 2-line
		176; 313	
EGME		390	
BET-N_2		269	
BET-N_2		230	
BET-N_2		225	synthetic 6-line
		203	
		204	
EGME		390	
BET-N_2		205	
TEM		250	
Fitting parameter for Triple-layer model		600–700	
BET-Ar		68–425	natural
EGME		221–560	2–6-line with 1.3–5.5% C org.

2.5.3 pe-pH diagram of iron

In oxygenated water, Fe(II) can be oxidized to Fe(III). The speciation of Fe(II) and Fe(III) is determined by both pH and pe value. The term pe is defined as,,$pe=-\log_{10}\{e^-\}$, where $\{e^-\}$ is the effective activity of the electron, in molal units, similar to pH. Note: pe=16.9 E (V). A pe-pH diagram is the best way to describe iron speciation in water.

Table 5. Reactions to construct pe-pH diagram (Stumm and Morgan 2012)

Table 8.5. Equations Used for the Construction of Figure 8.8

Equations Used for the Construction of the pε-pH Diagram	Functions pε	
$Fe^{3+} + e^- = Fe^{2+}$	$p\varepsilon = 13 + \log [Fe^{3+}]/[Fe^{2+}]$	①
$Fe^{2+} + 2e^- = Fe(s)$	$p\varepsilon = -6.9 + \frac{1}{2}\log [Fe^{2+}]$	②
$Fe(OH)_3(amorph, s) + 3H^+ + e^- = Fe^{2+} + 3H_2O$	$p\varepsilon = 16 - \log [Fe^{2+}] - 3\ pH$	③
$Fe(OH)_3(amorph, s) + 2H^+ + HCO_3^- + e^- = FeCO_3(s) + 3\ H_2O$	$p\varepsilon = 16 - 2\ pH + \log [HCO_3^-]$	④
	$[HCO_3^-] = C_T\alpha_1$	
$FeCO_3(s) + H^+ + 2e^- = Fe(s) + HCO_3^-$	$p\varepsilon = -7.0 - \frac{1}{2}\ pH - \frac{1}{2}\log [HCO_3^-]$	⑤
$Fe(OH)_2(s) + 2H^+ + 2e^- = Fe(s) + 2H_2O$	$p\varepsilon = -1.1 - pH$	⑥
$Fe(OH)_3(s) + H^+ + e^- = Fe(OH)_2(s) + H_2O$	$p\varepsilon = 4.3 - pH$	⑦
$FeOH^{2+} + H^+ + e^- = Fe^{2+} + H_2O$	$p\varepsilon = 15.2 - pH - \log ([Fe^{2+}]/[FeOH^{2+}])$	⑧
	Functions pH	
$FeCO_3(s) + 2H_2O = Fe(OH)_2(s) + H^+ + HCO_3^-$	$pH = 11.9 + \log [HCO_3^-]$	ⓐ
$FeCO_3(s) + H^+ = Fe^{2+} + HCO_3^-$	$pH = 0.2 - \log [Fe^{2+}] - \log [HCO_3^-]$	ⓑ
$FeOH^{2+} + 2H_2O = Fe(OH)_3(s) + 2H^+$	$pH = 0.4 - \frac{1}{2}\log [FeOH^{2+}]$	ⓒ
$Fe^{3+} + H_2O = FeOH^{2+} + H^+$	$pH = 2.2 - \log ([Fe^{3+}]/[FeOH^{2+}])$	ⓓ
$Fe(OH)_3(s) + H_2O = Fe(OH)_4^- + H^+$	$pH = 19.2 + \log [Fe(OH)_4^-]$	ⓔ

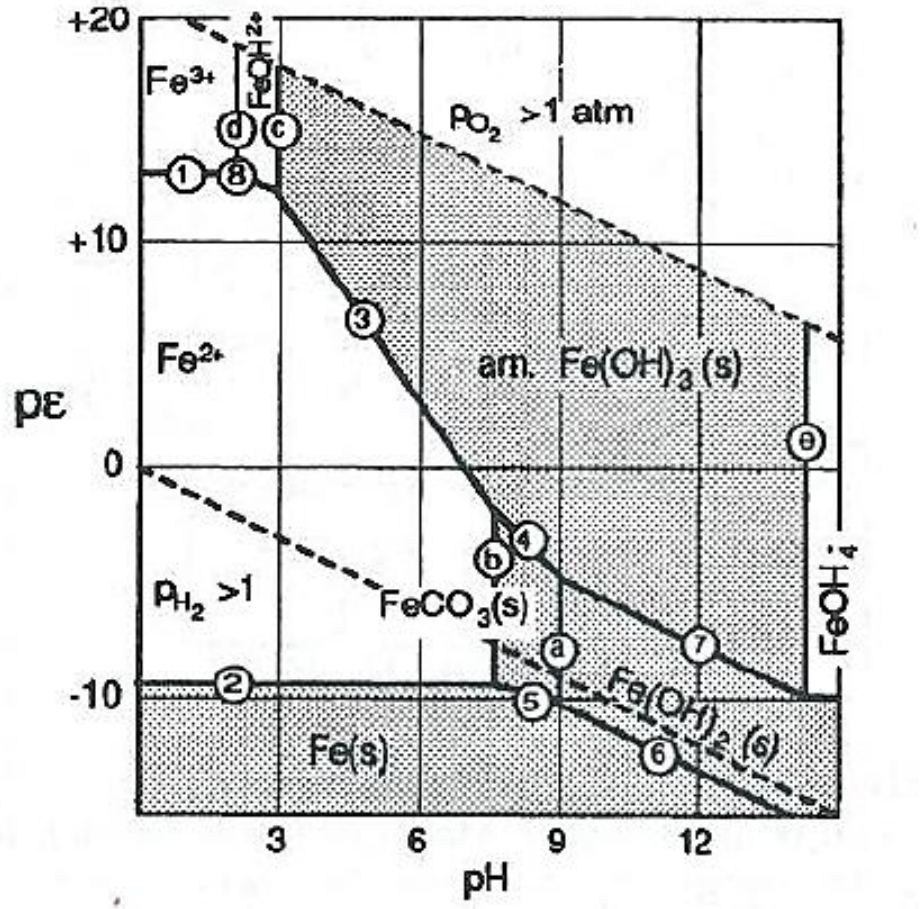

Figure 26. pe-pH diagram of 10^{-5} M total Fe and 10^{-3}M total carbonate at 25°C (Stumm and Morgan 2012)

2.5.4 Iron in produced water

Iron ions exist extensively in oilfield produced water. Depending on the geochemistry on the producing formation, the type of hydrocarbon produced and the characteristics of the producing well, the concentration of Fe(II) can vary from several mg/l to hundreds of mg/l. Guerra et al. reported a concentration of 0-1100 mg/l for conventional produced water and 0.001-258 mg/l for unconventional produced water from the summarization of numerous studies and USGS produced water database(Guerra, Dahm et al. 2011). King et al. reported a concentration of iron from 25 to

2000 mg/l for shale gas produced water. Typically during production process, in the oil wells, production flow lines, the produced water remains anaerobic, so Fe should remain as Fe(II). However, oxidation of Fe(II) could still happen due to pump leakage and when produced waters flow close to the surface, and when magnetite (Fe_3O_4) is produced in anoxic waters by reaction of Fe(II) with H^+ to form H_2 plus Fe(III).

Fe(II) in produced water have two major sources. One is from the prolonged contact with iron containing mineral such as siderite ($FeCO_3$), chlorite ($Mg_5(Al,Fe)_3(AlSi_3O_{10})(OH)_3$), pyrite ($FeS_2$) and Ankerite ($Ca(Fe, Mg)(CO_3)_2$) in formation (PAYKANI and MARDAN). Especially during acid stimulation and CO_2 flooding process, reservoir condition become acidic and accelerate the dissolution of $FeCO_3$, rust on tubing, and siderite, resulting in elevated concentrations of Fe(II) in produced water. The other source is from corrosion of the pipelines. Under anaerobic condition, iron is oxidized to Fe(II) through reduction of water molecule which generates hydrogen.

The presence of iron ions in solution can have multiple effects on produced water chemistry. Fe(III) is extremely insoluble in water. When pH rises at downhole conditions, such as when acid in the treatment fluid becomes spent, it will precipitate and cause formation damage and reduce the effectiveness of acidizing operation (PAYKANI and MARDAN , Fink 2011). The release of Fe(III) can cause asphaltic sludging formation damage. Sludging is formed by reaction of the iron ions with polar groups in asphaltenes in the reservoir oil (Fink 2011). Though Fe(II) is more soluble than Fe(III) in brine, it can form iron sulfide and iron carbonate scales which are extremely difficult to inhibit. In the production process, there are two classes of iron control chemicals. One is to use reducing agents to reduce Fe(III) to Fe(II), such as erythorbic acid or ascorbic acid; the

other is using complexing agents a.k.a. sequestering agents or chelates, such as citric acid, EDTA and nitrilotriacetic acid (Fink 2011).

2.5.5 Iron-inhibitor interaction

Only a few publications in the literature have investigated the effect of iron on mineral scale inhibitors. The literature can be divided into two categories by the precipitation system studied---$BaSO_4$ and $CaCO_3$. In $CaCO_3$ system, researchers found Fe(II) has a detrimental effect on scale inhibitor performance, especially phosphonates. Cushner et al. found for calcium carbonate system, phosphonates inhibitors are significantly impacted but polymer (PAA) and phosphate ester (TEAPE) are less affected by Fe(II)(Cushner, Melchior et al. 1990). Shen et al. made similar observation in calcium carbonate system that commercial inhibitor chemicals including polycarboxylic acid, aminotri (methylene phosphonic) acid and carboxymethyl inulin performance dropped sharply at the presence of Fe(II) as low as 5 mg/l (Shen, Shcolnik et al. 2011). Although these researchers have not come up with a mechanism of the Fe(II) impact, it could be a combined impact of the interaction between Fe(II) with both scale inhibitor and $CaCO_3$. Besides the strong binding of Fe(II) with scale inhibitor function groups, Fe(II) itself can serve as a calcite precipitation inhibitor(Herzog, Shi et al. 1989). Also, Fe(II) and $CaCO_3$ could form Fe-Ca-CO_3 solid solution with different stoichiometry which changes $CaCO_3$ precipitation kinetics(Alsaiari, Yean et al. 2008), probably also inhibition kinetics. Also the observation is consistent with the rule that inhibitors are generally the insoluble salts of one of the lattice ions. Fe(II) could serve as a $CaCO_3$ inhibitor since $FeCO_3$ is insoluble.

In $BaSO_4$ precipitation systems, the impact of Fe(II) on scale inhibitors is still under debate.

Gaffney et al. found that Fe(II) can severely impact DTPMP performance, however the experiments were done under aerated conditions, it is not sure whether the detrimental effect is due to Fe(II) alone (Gaffney, Jackson et al. 1988). Coleman et al. degassed the brine for 4 hours and used tube-blocking test to study the effect of Fe(II) on $BaSO_4$ scale inhibitors(Coleman, Graham et al. 1999). They found that polymeric phosphonates and polymeric phosphonate and poly-phosphino-carboxylic acid were impaired while polyvinyl sulphonate and sulphonated co-polymer were unaffected. However, Stoppelenburg et al. investigated the Fe effect on $BaSO_4$ inhibitor DTPMP under anaerobic and aerobic conditions and found that DTPMP performance is severely impaired by Fe(III), but enhanced by the existence of Fe(II) (Stoppelenburg and Yuan 2000). The reason for the disagreement of results could be accidental oxidation of Fe(II) during reaction or that different solution condition used in different studies lead to different interaction between Fe(II) and scale inhibitors. Therefore, more systematic research is needed to study the Fe(II) effect on inhibitors at different solution conditions using strictly anoxic apparatus.

Friedfield et al. investigated ferrous phosphonate speciation and solubility(Friedfeld, He et al. 1998). They used phosphonate nitrilotris (methylene phosphonic acid) (NTMP), which is a commonly used commercial scale inhibitor. The stoichiometry is found to be $Fe_{2.5}$HNTMP. The dependence of pK_{sp} on temperature and ionic strength is found to be: $\mathrm{pK_{sp}} = 39.54 - 6.14\, I^{0.5} + 2.181 - 1315/T$. The speciation and stability constants of each ferrous NTMP species can be calculated. The pK_{sp} change with ionic strength and temperature is shown in Figure 27.

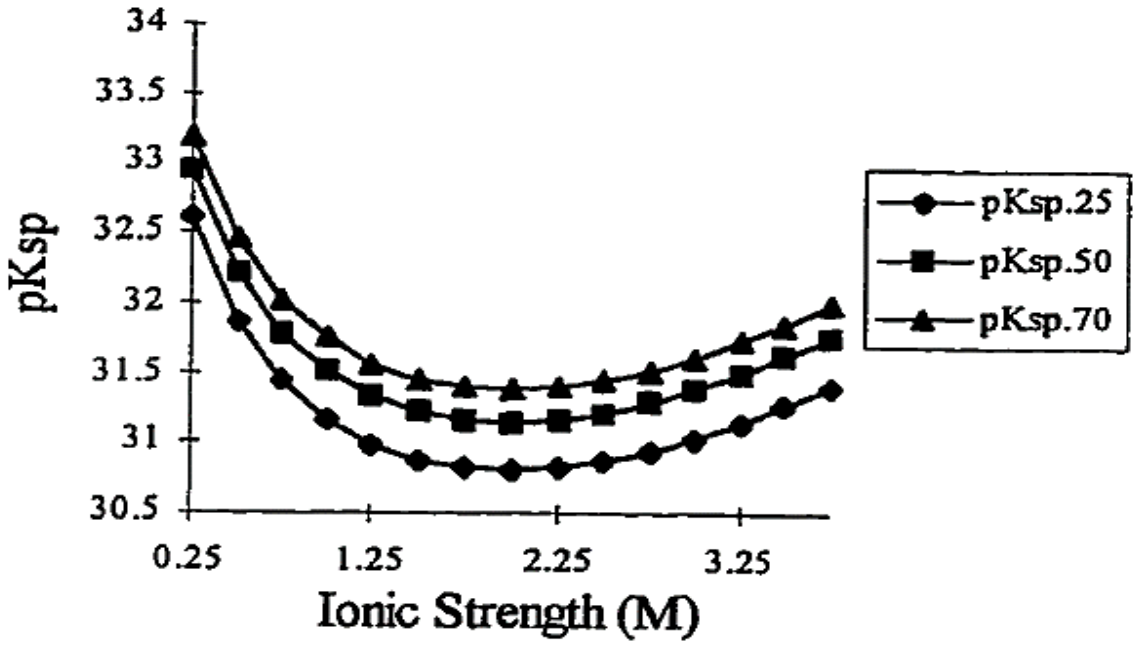

Figure 27. pK_{sp} of Fe-NTMP as a function of ionic strength at 25°C, 50°C and 70°C (Friedfeld, He et al. 1998)

2.5.6 The application of chelating agents for iron control

In oilfields one of the most common iron control methods is to use complexing agents. Ethylenediaminetetraacetic acid (EDTA), citric acid, nitrilotriacetic acid (NTA) are the most commonly used complexing agents for iron (Kelland 2014). They are all strong chelates for iron and relatively cost-effective. Several paper have been reported using EDTA, NTA, citric acid or their blend for iron control in acid stimulation condition (Ewing, Pabley et al. 1983, Hall and Dill 1988, Taylor and Nasr-El-Din 1999, Taylor, Nasr-El-Din et al. 1999). EDTA has a much higher stability constant with iron than NTA or citric acid, but has low solubility in acidic conditions. Another problem with EDTA is that it is not readily biodegradable. NTA is acid soluble and biodegradable, but with a lower stability constant than EDTA. Citric acid is acid-soluble and environmentally friendly, but it might form Ca-citrate precipitate at high Ca^{2+} concentration.

Shenet al. used citrate to sequestrate iron and found that inhibitor performance wassignificantly improved. They attributed the reason to prevention of iron carbonate seed crystals by citrate.(Shen, Shcolnik et al. 2011)

Chapter 3. Experimental Methods

In this study, a strictly anoxic bottle-test apparatus is used to investigate the Fe(II) effect on $BaSO_4$ scale inhibitors at dissolved oxygen level below 5ppb. This bottle test apparatus enables tests above room temperature and features a constant Argon purge to prevent oxygen diffusion.

3.1 Experimental Apparatus.

3.1.1 Fe(III) testing apparatus

The Fe(III) testing apparatus is based on laser nucleation detection method developed by Yan et al. and has been applied to test inhibition efficiency of several scale inhibitors at different pH, temperature, and Saturation Index values(Yan, Kan et al. 2014). Setup of the laser apparatus is shown in Figure 28. Temperature and mixing of solution are carefully controlled by a digital water bath and magnetic stir plate. A photodetector is used to detect laser signal and is connected to a multi-meter which transforms laser signal to electronic current in mA. When scale forms, the laser light will be scattered by the scale particles suspended in solution which causes decrease of the current intensity. Typical data is shown in Figure 29. In this study, induction time is taken as the time for the photocurrent to drop indicating particles starting to form and scatter the beam. Electronic current is recorded by MeterView software. Electronic current data is imported into a software developed by Brine Chemistry Consortium to calculate the induction time. Reagents are added by glass syringes. Error of the amount of solution taken by syringe every time does not exceed 2%.

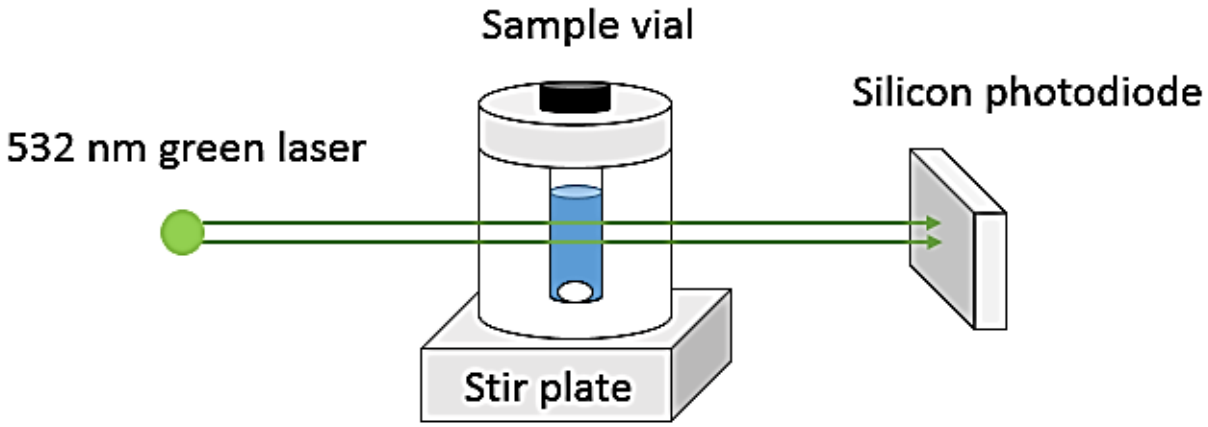

Figure 28. Setup of the laser apparatus

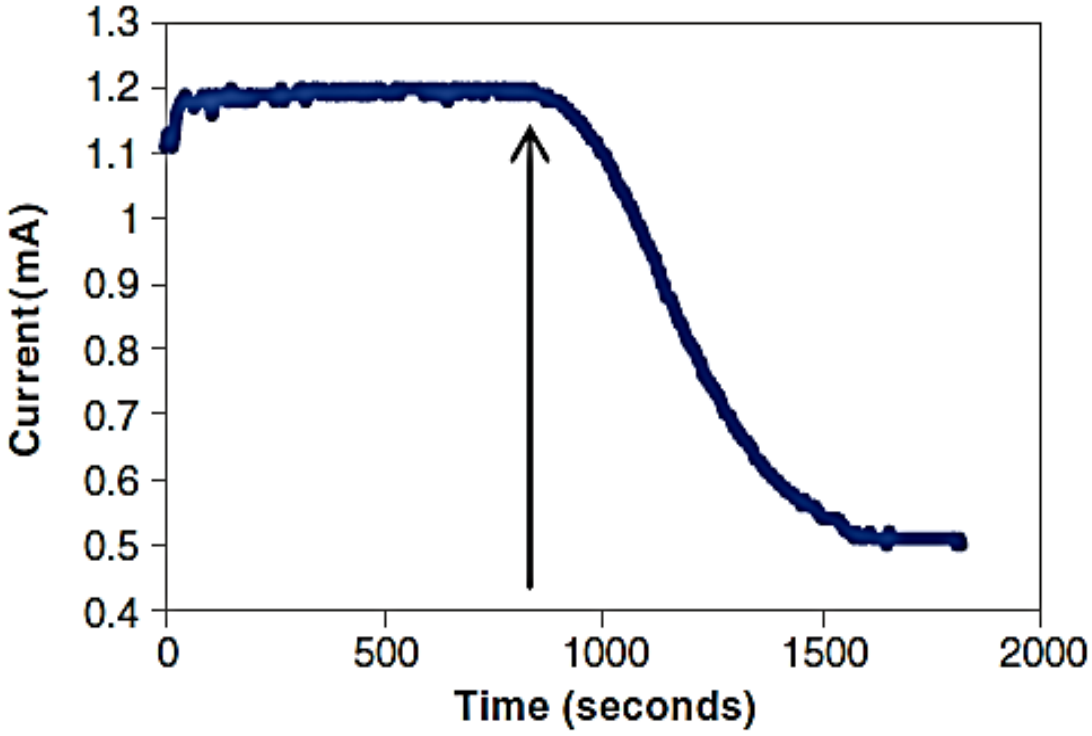

Figure 29. Typical data acquired using the laser apparatus (condition: barite nucleation at T=70°C, 1M NaCl, SI of barite=2.00, pH=6.73, inhibitor=0.3mg/L SPCA) (Yan et al., 2014)

3.1.2 Fe(II) testing apparatus

In this study, the above laser apparatus is remodeled to adapt to anoxic condition and Figure 30 is a diagram of the anoxic laser apparatus. As shown in Figure 30, high purity Argon gas is flowed through the oxygen trap (Supelpure®-O Oxygen Trap, Sigma-Aldrich) and used to purge four bottles of stock solutions. Solution volume of each bottle is about 90ml. Metering valves installed in the flow line are used to control Argon flow. A 30ml glass vial is used as reaction vessel. Inner wall of the glass vial is carefully washed by potassium permanganate before use. A silicone septum is installed in the vial lid, allowing needle and tubing to go through.

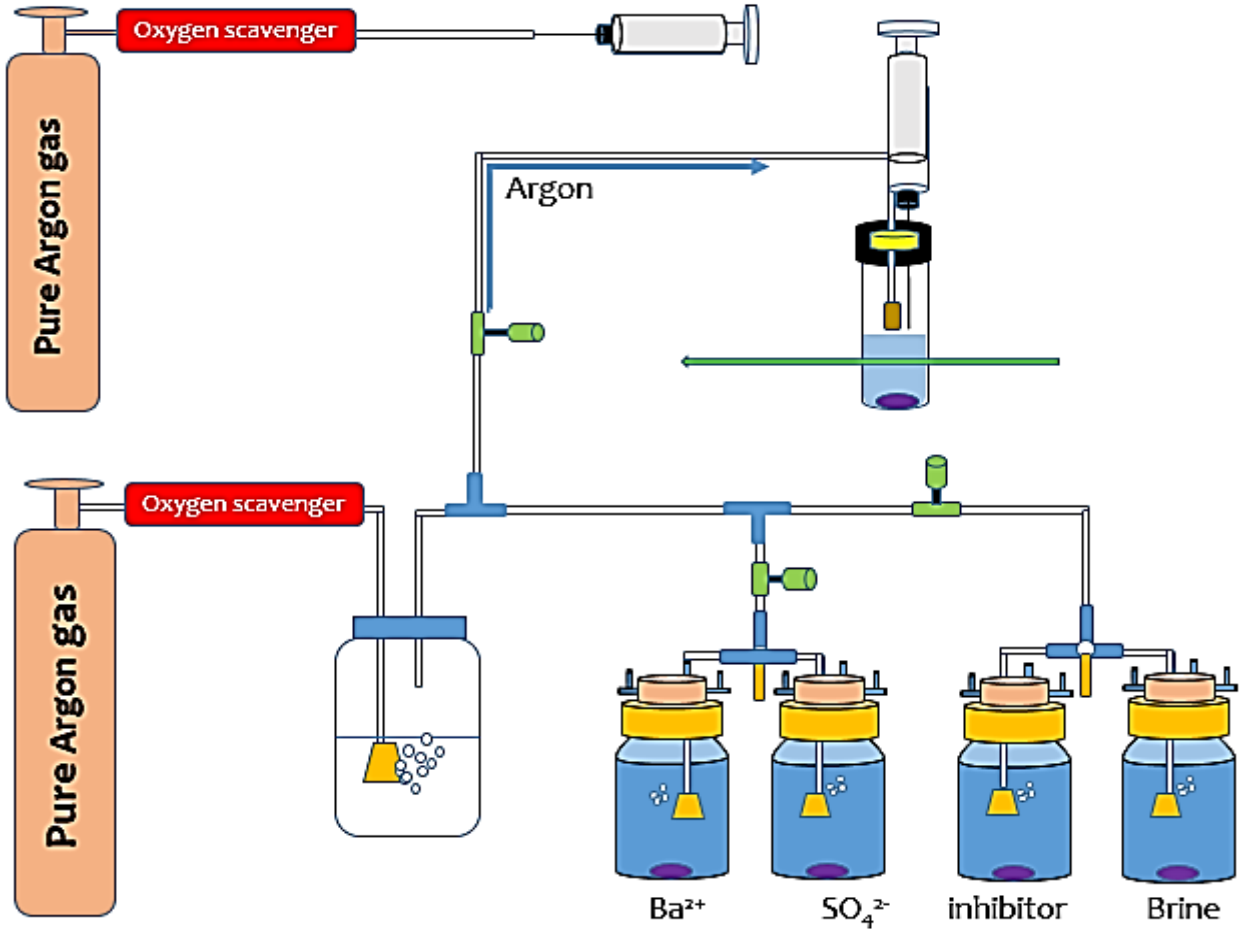

Figure 30. Anoxic laser nucleation detection apparatus

Before an experiment starts, 4 bottles of solutions containing $BaCl_2$, Na_2SO_4, inhibitor and background brine, are sparged vigorously for 15 minutes. CHEMetrics K-7513 ampoules measure the dissolved oxygen concentration to be below 5ppb (shown in Figure 31). After background brine is purged to anoxic level, pre-weighed amount of hydroxylamine hydrochloride reducing agent is put into the solution followed by iron chloride solid. The sparging stones in all four bottles are lifted to just above the solution to keep a constant Argon cover. A washed 30ml glass vial is purged by Argon for 15 minutes, then the sparging stone is lifted to avoid interfering with reaction. Hamilton Gastight® syringes (shown in Figure 31) are used to transfer anoxic solutions from the bottles to glass vial. The syringes are connected to needles shown below. Before use, syringes are connected to another Argon gas tank as shown in Figure 30. The plunger is pulled back and forth for over 20 times to change the air inside to Argon. Then the needle is inserted into the solution bottle through a port on the bottle lid, pulled up the solution then quickly inserted to the glass vial through the septum to inject solutions. The solutions are injected in the order of Na_2SO_4, scale inhibitor, $FeCl_2$, and then $BaCl_2$. Airtight syringes and the ampoules used in the experiments are shown in Figure 31.

Figure 31. Left: CHEMetrics K-7513 ampoules used to measure the dissolved oxygen concentration. Right: Hamilton Gastight syringes used to transfer anoxic solutions

Hydroxylamine hydrochloride ($HONH_3^+Cl^-$) is used as reducing agent in this study. Hydroxylamine hydrochloride is used to keep iron ions in ferrous state. The reduction reaction is expressed in equation (1) and (2) (Bengtsson et al., 2002).

$$4Fe^{3+} + 2NH_2OH \rightarrow 4Fe^{2+} + N_2O + 6H^+ + H_2O \quad (1)$$

$$2Fe^{3+} + 2NH_2OH + 2OH^- \rightarrow 2Fe^{2+} + N_2 + H_2O \quad (2)$$

In this study, $HONH_3^+Cl^-$ is added with a molar ratio of $HONH_3^+Cl^-$/ Fe(II)=2:1. The reduction reaction products do not interfere with reaction and $HONH_3^+Cl^-$ is found to have little interference with $BaSO_4$ precipitation or inhibitor performance.

The anoxic condition of the reactor was tested under 80°C for a 3-hour period. Ferrous iron and total iron concentrations are measured by HACH 1,10-Phenanthroline Method and USEPA FerroVer® Method. The test is done following the experiment procedures described above. Initial total Fe concentration is measured as 0.63mg/l. Fe(II) concentration remains stable within 3 hours as shown in Table 6. . Since all experiments in this study are done at 70°C within the period of 3 hours, Fe should be kept in the ferrous state.

Table 6. Fe(II) concentration in the reactor at 80°C.

Time (hour)	Fe(II) concentration (mg/l)
0	0.62
1	0.60
3	0.65

Later, the apparatus was further improved by using switching valve instead of syringe to transfer anoxic solutions since small amount of Fe(II) oxidation was found probably due to the exposure of syringe needle to atmosphere during solution transfer. Figure 32 shows the improved Fe (II) testing apparatus. Reducing agent used in experiments is switched from hydroxylamine hydrochloride to ascorbic acid.

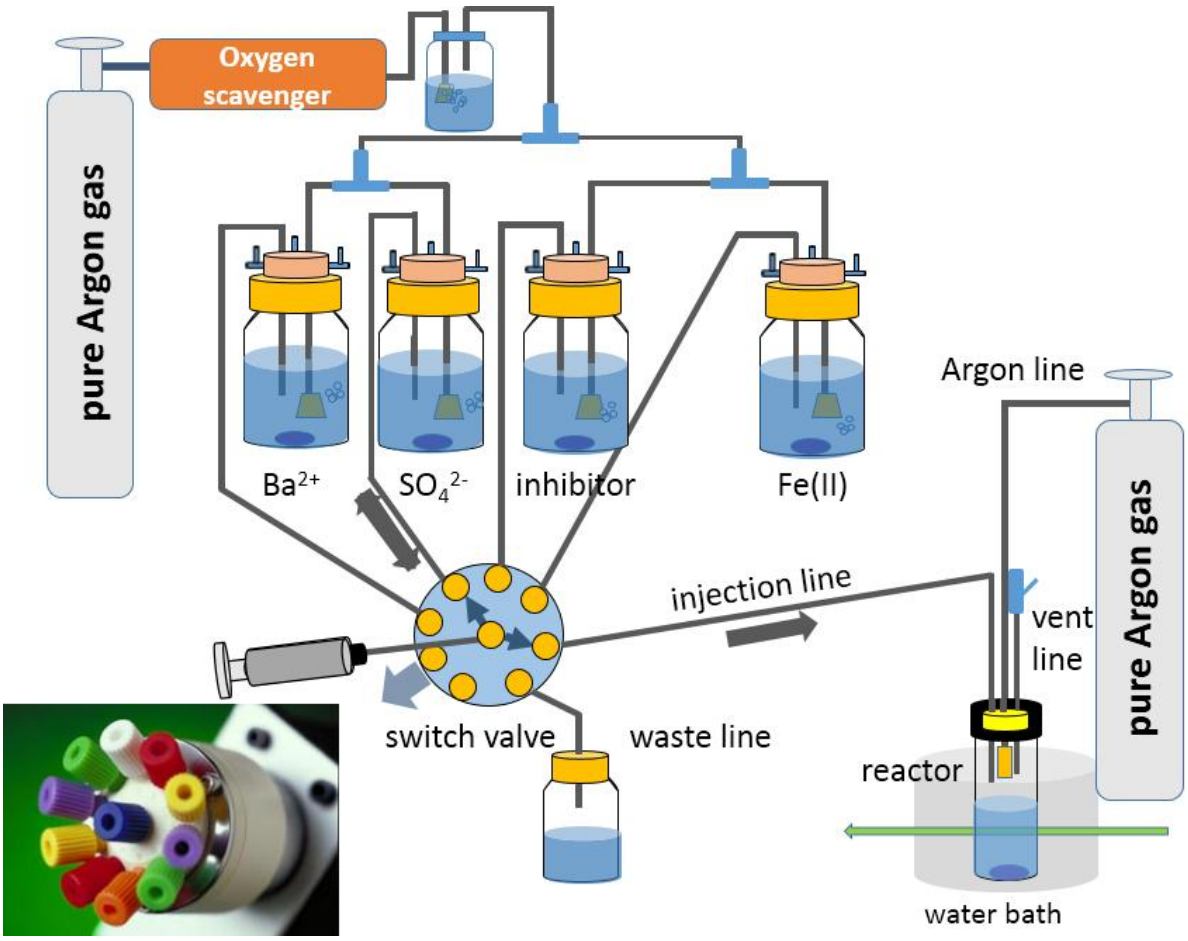

Figure 32. Experimental apparatus

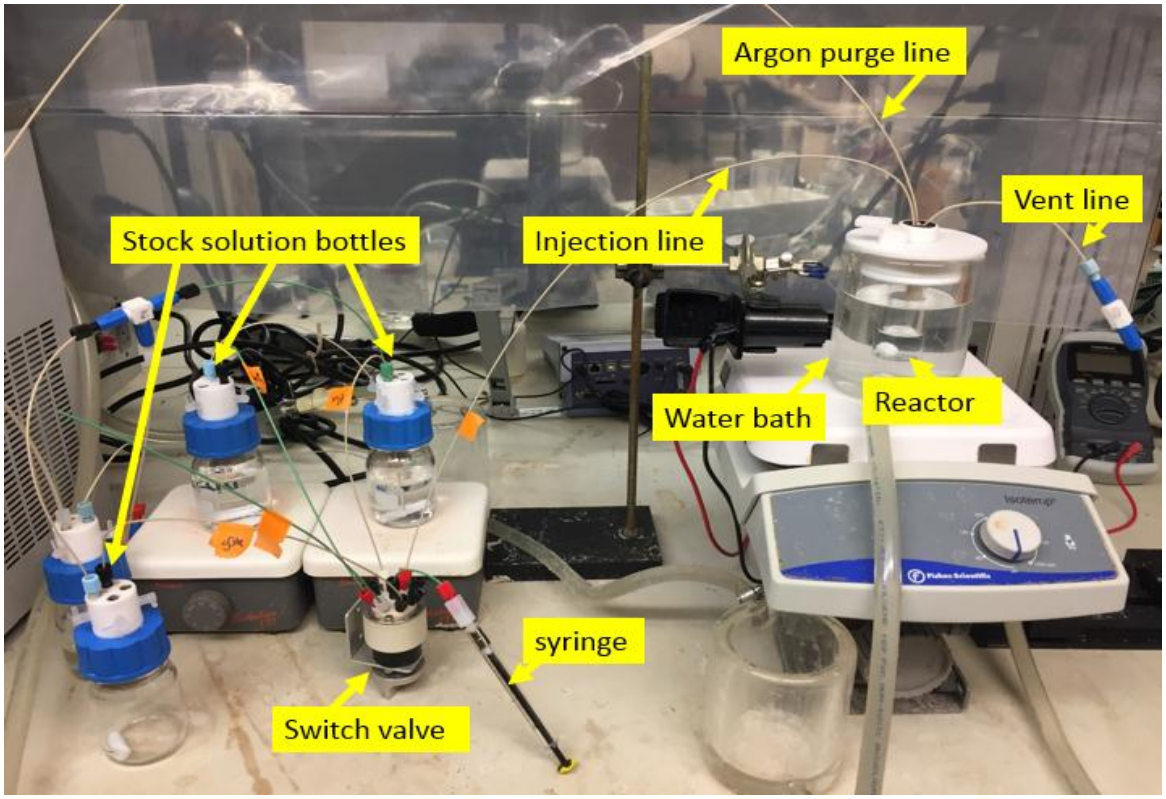

Figure 33. Picture of experimental apparatus

The experimental procedures are as follows: High purity Argon gas is flowed through the oxygen trap (Supelpure®-O Oxygen Trap, Sigma-Aldrich) and used to purge four bottles of stock solutions: $BaCl_2$, Na_2SO_4, inhibitor and background brine. Solution volume of each bottle is about 90ml. These 4 bottles of solutions are sparged vigorously for 15 minutes. CHEMetrics K-7513 ampoules measure the dissolved oxygen concentration to be below 5ppb. After background brine is purged to anoxic level, pre-weighed amount of ascorbic acid reducing agent is put into the brine solution followed by weighed iron ammonium sulfate solid. The sparging stones in all four bottles are lifted to just above the solution to keep a constant Argon cover. A washed 30ml glass vial is purged by Argon for 15 minutes, then the sparging stone is lifted to avoid interfering with reaction. It should be noted that in experiments with low Fe(II) concentration (<10 mg/L), Fe(II) stock solution is in a separate bottle like shown in Figure 32. When Fe(II) concentration is higher than

10 mg/L, iron ammonium sulfate solid is added into the SO_4^{2-} solution bottle. The reason is to lower oxidation risk. 6mL Ba^{2+} and 6mL SO_4^{2-} were taken from for the experiment. To avoid dilution thus lowering barite SI, combined volume of inhibitor and Fe(II) taken for experiment is around 1mL. Therefore, when Fe(II) testing concentration is beyond 10 mg/L, we need a very high concentration of Fe(II) stock solution which can be prone to oxidation. In this case, merging Fe(II) and SO_4^{2-} stock solution will solve the problem.

Figure 34. Switch valve used in this research

A switch valve is used to transfer solution from stock solution bottle to reactor. The switch valve used in this research is made from PEEK material, purchased from Valco Instrument, as shown in Figure 34. The switch valve has several ports surrounding a central port. A gastight glass syringe is connected to the central port through PEEK tubing. The central port can be connected to any of the surrounding ports by turning the switch on the valve. Take the transfer of SO_4^{2-} solution for example: To transfer SO_4^{2-} solution, turn the switch on the switching valve to connect SO_4^{2-} stock solution bottle to gastight syringe. The valves on the SO_4^{2-} solution bottle are closed. Argon pressure inside the SO_4^{2-} stock solution bottle will build up (but below the pressure tolerance of the glass bottle) and push solution from the bottle into the gastight syringe Solution in the gastight

syringe will be pushed back into the stock solution bottle and sparged by Argon. Then the above procedure will be repeated for 6~7 times. The purpose of repeating the procedure is to eliminate the oxygen in the solution as much as possible. After completing this procedure, the switch on the valve will be turned to connect the gastight syringe to the injection line. Then the $SO4^{2-}$ solution in the syringe will be pushed into the reactor. The same procedures are applied to other three bottles of stock solutions. A 30ml glass vial is used as reaction vessel. Inner wall of the glass vial is carefully washed by potassium permanganate before use. A rubber septum is installed in the vial lid, allowing tubing to go through. Reducing agent ascorbic acid is used to help keep Fe(II) in reduced state. The advantage of this improved apparatus is that during transfer, the anoxic solution was not exposing to atmosphere. Also, Argon gas was used to push solution into syringe rather than pulling solution into syringe, which might cause O_2 contamination.

The reducing agent used in this research, ascorbic acid, was found not to influence barite nucleation or inhibitor performance. Tests were run for 1 hour (all the experiments duration were below 1 hour) up to 50 mg/L Fe(II) at experimental condition (1M NaCl, pH 6.74, 400 mg/L Ca^{2+} and 70^{o}C) to observe if Fe(II) got oxidized. There is no yellow color or ferric hydroxide particles appearing in solution, which are two visible signs of Fe(II) oxidation. Yellow color and particles start to appear after exposing the solution for a while in the air. Therefore, it is assumed that there is no Fe(II) oxidation during experiments and any effect to scale inhibitor performance is attributed to Fe(II) alone.

Results achieved by these two apparatus is different. These two sets of results will both be shown in following chapters respectively.

Chapter 4. Fe(III) effect on scale inhibitor performance

4.1. Experimental results of Fe(III) effect on scale inhibitors

Experimental results on Fe(III) impact on scale inhibitors is presented in this section. In order to simulate oilfield produced water condition, the experiments are conducted at the following solution condition: 1M NaCl, 400 mg/l Ca^{2+}, pH 6.74 and 70°C. All the experiments have 400 mg/l Ca^{2+} in the solution to simulate oilfield produced water condition. The stock solution of Fe(III) was made by adding known amount of $FeCl_3$. $6H_2O$ solid into 1% HNO_3 solution. pH of the Fe(III) stock solution is at about 2.0. Fe(III) solution is added into the system by injecting a calculated volume (usually below 1 mL) of the Fe(III) concentrated stock solution by glass syringe. Total volume of reaction solution is about 13mL. After injecting, Fe(III) stock solution is diluted to the desired concentration level. Reaction solution is buffered by 10mM of PIPEs buffer, therefore pH is not significantly influenced by the injection of acidic Fe(III) stock solution. Ba^{2+}, SO_4^{2-} and inhibitor stock solution are also delivered by glass syringe.

DTPMP, PPCA and PVS are three scale inhibitors with different function groups---phosphonate, carboxylate and sulfonate. The structures of inhibitors are shown below in Figure 35.

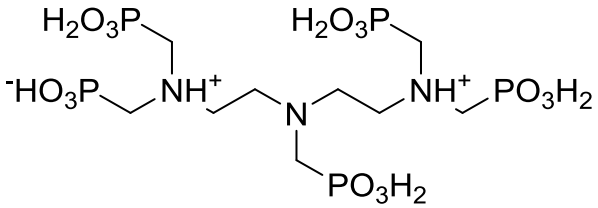

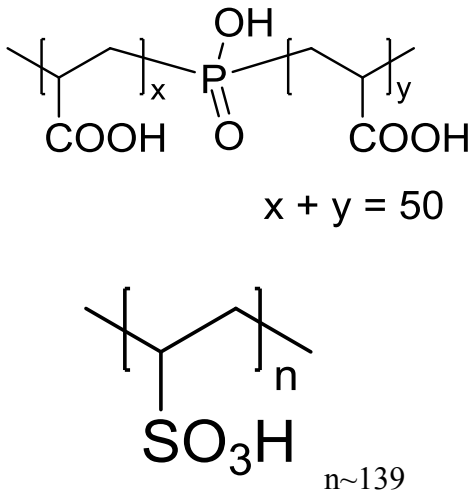

Figure 35. The structure of DTPMP (top), PPCA (middle) and PVS (bottom)

Table 7. Barite nucleation kinetics under different scale inhibitors at 1M NaCl, pH 6.74, 70°C and 400 mg/L Ca^{2+} ,barite SI=2.00 condition. The reagents were added in the following order. 1) $SO4^{2-}$ stock solution 2) scale inhibitor stock solution 3) Fe(III) stock solution. 4) Ba^{2+} stock solution. If duplicates were performed, the standard deviations are listed.

Experiment#	DTPMP (mg/L)	PPCA (mg/L)	PVS (mg/L)	Fe(III) (mg/L)	t_{ind} (s)
1	0	0	0	0	20±3
2	1.22	0	0	0	2,180±335
3	1.22	0	0	0.40	241
4	1.22	0	0	1.00	64±4
5	1.22	0	0	2.00	22±3
4	1.92	0	0	0	23,698±933
5	1.92	0	0	1.00	403
6	0	1.22	0	0	987
7	0	1.22	0	1.00	42
8	0	0	1.22	0	600
9	0	0	1.22	1.00	67

From Table 7, we can see barite nucleation takes an average of 20s when there is no Fe(III) or scale inhibitor (exp #1). With 1.22 mg/L DTPMP (exp #2) barite nucleation induction time increased to 2,062s. When 1 mg/L Fe(III) was added to exp #2 solution (exp #4), barite nucleation time shortened from 2,062s to 41s. Barite induction time increased to about 23,039s with 1.92 mg/L of DTPMP (exp #4). With 1 mg/L Fe(III) present, barite inhibition time reduces to 403s (exp #5) indicating there is some inhibition ability left. Similar impairment of inhibitor performance is observed for PPCA and PVS from exp #6-9. From above results, we can see that Fe(III) have detrimental effect on the inhibition performance of DTPMP, PPCA and PVS.

4.2 Discussion

Ferric hydroxide is a sparingly insoluble precipitate in solution. Based on the calculation of Visual MINTEQ ver. 3.1 (using SIT theory for activity coefficient calculation), the solubility of ferrihydrite at 6.74 pH, 70ºC, 1M NaCl, Barite SI=2.00, 400 mg/L Ca^{2+} is only $3.73*10^{-11}$ mol/L and the solution is highly supersaturated with respect to various ferric hydroxide minerals, as shown in Table 8. Therefore, Fe(III) exists in the form of ferric hydroxide particle at this experimental condition.

Table 8. Saturation index of various iron oxide minerals at 6.74 pH, 70°C, 1M NaCl, Barite SI=2.00, 400 mg/L Ca^{2+}, 1 mg/L Fe(III) condition

Mineral name	Ion activity product	log K_{sp}	Saturation Index
$Fe(OH)_{2.7}Cl_{0.3}$	$a_{Fe^{3+}} a_{OH^-}^{2.7} a_{Cl^-}^{0.3}$	-40.84	7.54
Ferrihydrite	$a_{Fe^{3+}} a_{OH^-}^{3}$	-38.80	5.68
Ferrihydrite (aged)	$a_{Fe^{3+}} a_{OH^-}^{3}$	-39.31	6.19
Goethite	$a_{Fe^{3+}} a_{OH^-}^{3}$	-41.51	7.48
Hematite	$a_{Fe^{3+}} a_{OH^-}^{3}$	-42.71	8.77
Lepidocrocite	$a_{Fe^{3+}} a_{OH^-}^{3}$	-40.63	5.20
Maghemite	$a_{Fe^{3+}} a_{OH^-}^{3}$	-38.81	3.38

The rate of nucleation of a solution can be affected by the presence of traces of impurities in the system (Mullin 2001). In some cases, the impurities can be inhibitors. In other cases, they can be accelerators. No general rule applies (Mullin 2001). In the presence of a suitable foreign body or surface, nucleation can be induced (Mullin 2001). Therefore, one hypothesis for the mechanism of Fe(III) effect on scale inhibitors is that precipitated ferric hydroxide particles might provide surface nucleation sites in the solution and accelerate barite nucleation. Experiments were conducted to test this possibility at a condition of barite SI=1.50, 400 mg/L Ca^{2+}, 1M NaCl, pH 6.74 condition with 0, 0.4, 1.6 and 2 mg/L Fe(III). Experiment temperature was also maintained at 70°C, but SI is lowered from 2.00 to 1.50 to give sufficient long barite induction time to observe any difference. Table 9 shows the experimental results.

Table 9. Barite nucleation induction time in the presence of different Fe(III) concentration level

Fe(III) concentration (mg/L)	0	0.4	1.6	2
Induction time	246s, 316s	302s, 276s	256s, 291s	261s, 275s

Single factor ANOVA with duplication statistical analysis (Excel 2013) shows that the barite nucleation induction time with 0, 0.4, 1.6 and 2 mg/L Fe(III) are not significantly different, P = 0.8485. Therefore, acceleration of barite nucleation by ferric hydroxide particles might not be responsible for the reduction of barite inhibition time at this experimental condition.

Ferric hydroxide particles are known to strongly adsorb anions (Dzombeck and Morel, 1990). The surface of ferric hydroxide is covered with active hydroxyls function groups (freshly precipitated ferric hydroxide is typically assumed to have a surface area of about 600 m^2/g with about 2 active sites per nm^2, Visual Minteq 3.1). Therefore ferric hydroxide particles could adsorb inhibitor molecules and reduce their barite inhibition ability. Phosphonates are known to strongly adsorb to hydroxides (Nowack and Stone, 1999). Ferric hydroxide also strongly adsorbs various organic anions such as carboxylic, oxalate, sulfonate, lactate etc (Cornell and Schwertmann, 2003). Therefore, another possible explanation for Fe(III) detrimental effect on scale inhibitors is the adsorption of scale inhibitors onto the surface of ferric hydroxide particles. When Fe(III) stock solution is added into the solution at pH 6.74, Fe(III) immediately precipitates as ferric hydroxide colloidal particles. If scale inhibitors were absorbed onto the ferric hydroxide surfaces, the inhibition would be reduced. Any remaining unabsorbed scale inhibitor would still inhibit barite precipitation.

To test the hypothesis that the Fe(III) effect is due to precipitation and subsequent adsorption of inhibitor from solution, three conditions must be met:

1. There is inhibitor loss from the aqueous phase after the addition of Fe (III) stock solution;
2. The amount of inhibitor that disappears from the aqueous phase is in the solid ferric hydroxide phase; and
3. The concentration of inhibitor remaining in the aqueous phase matches the barite induction time observed at the same concentration of the free inhibitor.

Figure 36. The analytical ultracentrifuge machine, tube and rotor used in this research

To test these three criteria, we needed to completely separate the ferric hydroxide particles from the solution and measure the scale inhibitor concentration remaining in the aqueous phase and adsorbed to the particles. DTPMP was chosen as a representative scale inhibitor because it is

commonly used (refs). Also, the concentration of DTPMP can be readily measured (refs).

The ferric hydroxide particles were so fine that they passed through a 0.02 nm membrane filter. After centrifugation at 5000, 10000 and 20000 rpm, supernatant still contained more than 50% of initial Fe(III) concentration. Therefore, an analytical ultracentrifuge (BC Optima L-80XP ultracentrifuge was run at 45000 rpm for 40 min. The ferric hydroxide particles appeared to have been separated from the solution. Using ICP-OES after the ultracentrifuge the concentration of Fe(III) in the supernatant was 0.169 ± 0.01 mg/L, probably suggesting that still some of the ferric hydroxide fines remained in solution. Experiments were conducted at room temperature because the ultracentrifuge machine could only be operated below 40^{o}C, and the adsorption of DTPMP onto ferric hydroxide particles might shift during the ultracentrifugation. Background brine (1M NaCl, pH 6.74, 400 mg/L Ca^{2+}) Fe(III) and DTPMP stock solutions were mixed at room temperature. 10mM PIPEs was used as buffer to keep solution pH at 6.74. The mixture was then put into analytical ultracentrifuge to separate particles from aqueous solution. After successfully completing the particle-solution separation, a known mass of the supernatant was removed by plastic pipette. Concentrations of DTPMP and Fe(III) in the supernatant were measured by ICP-OES. Remaining mass in the ultracentrifuge tube was acidified by adding 0.1ml of 8N HCl to dissolve any existing ferric hydroxide particles. Immediately after adding the 8N HCl a white precipitate was observed, which was probably the acidified PIPEs buffer .The acidified solution with the white precipitate was filtered through 0.45um filter paper. The retentate was collected and put into 0.1mM NaOH, after which it slowly dissolved. No significant amount of Fe(III) and DTPMP was found in the retentate. DTPMP and Fe(III) concentration in the filtrate was also measured. Experiments following above procedures were conducted at two conditions as shown

in Table 10. For each experimental condition, two experiments were conducted.

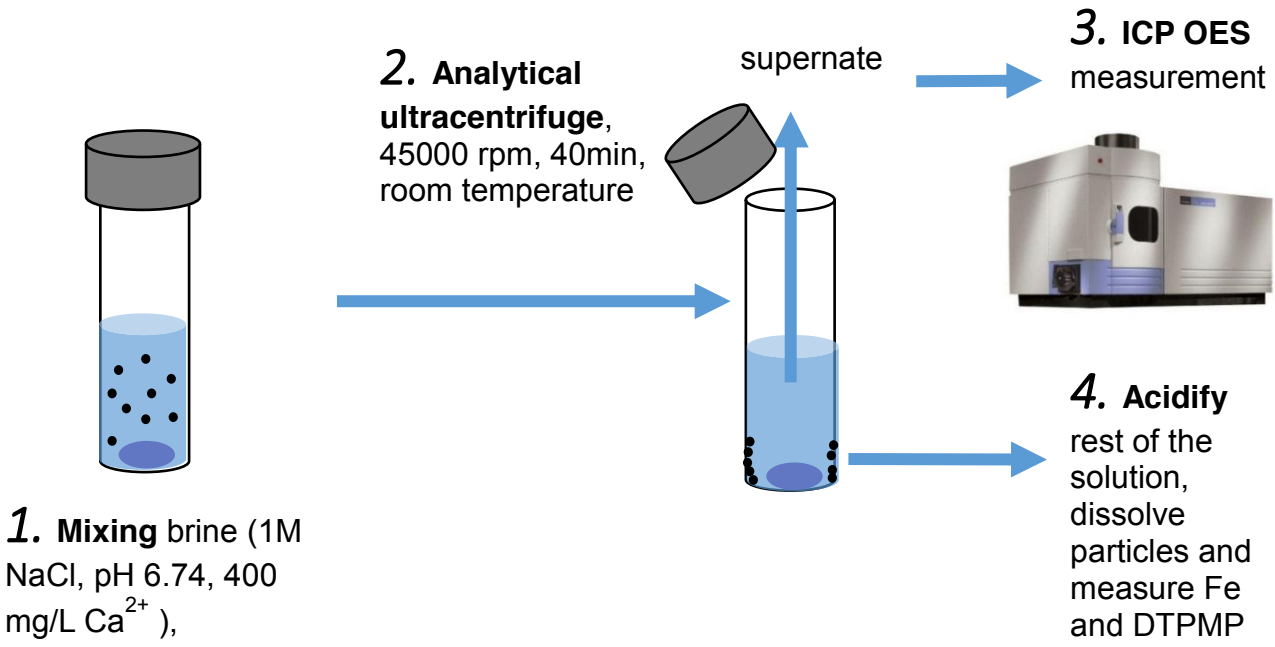

Figure 37. Schematic procedure of adsorption experiment

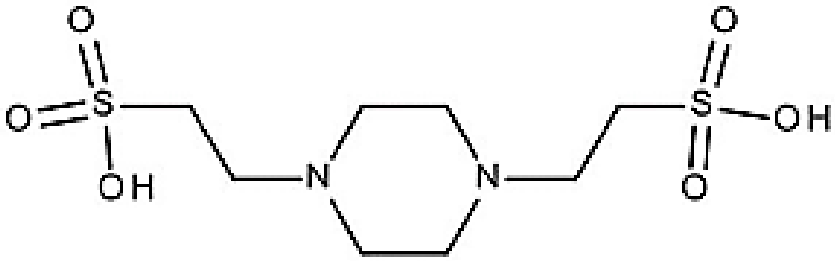

Figure 38. Structure of PIPEs buffer

Table 10. Experimental condition at 25°C, pH 6.74, 400 mg/L Ca^{2+}

Experiment #	Initial DTPMP (mg/L)	Initial Fe(III) (mg/L)
1&2	2.29	1
3&4	3	1

Table 11. Measurement of DTPMP and Fe in the supernatant after ultracentrifuge

Experiment #	P (mg/L)	DTPMP (mg/L)
1	0.344	1.27
2	0.340	1.26
3	0.561	2.07
4	0.535	1.98

The measurement of P was done by ICP-OES. Since P concentration in both cases are very low for ICP-OES, they were both measured at axial mode and good linear standard curve were achieved. Standard curve of P and Fe is shown in Figure 39. ICP-OES was adopted to do P measurement instead of using HACH method in this case. HACH method is a very accurate method for detection of low concentration organic Phosphorous as introduced previously. However, a relatively high concentration of organic buffer in the solution exerts some difficulty to UV digestion process.

From the data in Table 10 and Table 11, it is possible to confirm our hypothesis that the effect of Fe(III) on inhibition is by removing inhibitor from solution. By combining data from Table 10 and Table 11, the concentration of DTPMP for experiments 1 and 2 dropped from 2.29 mg/L (initial) to 1.26 and 1.27 mg/L (after ultracentrifugation). In experiments 3 and 4, DTPMP concentration dropped from 3 mg/L (initial) to 2.07 and 1.98 mg/L (after ultracentrifugation). In both cases, there

was about 1 mg/L DTPMP lost from the aqueous phase. Assuming ferrihydrite is the initial Fe(III) precipitate with a reported surface area of 600 m2/g and molecular wt. of 106.86 g/mole, (Liu and Mallero, 1999), 1 mg/L Fe(III) corresponds to 1.91 mg/L of ferrihydrite with a surface area of 1.15 m2. It has been reported that 1 mg of DTPMP covers about 1 m2 of surface area (Tomson et al. 2004). In this experimental condition, we find 1mg/L Fe(III) corresponds to ~1 mg/L DTPMP adsorbed. Therefore, we would expect the ferrihydrite to adsorb a maximum of about 1.15 mg of DTPMP per liter, as was observed. Similar was found in the mass balance experiments reported next.

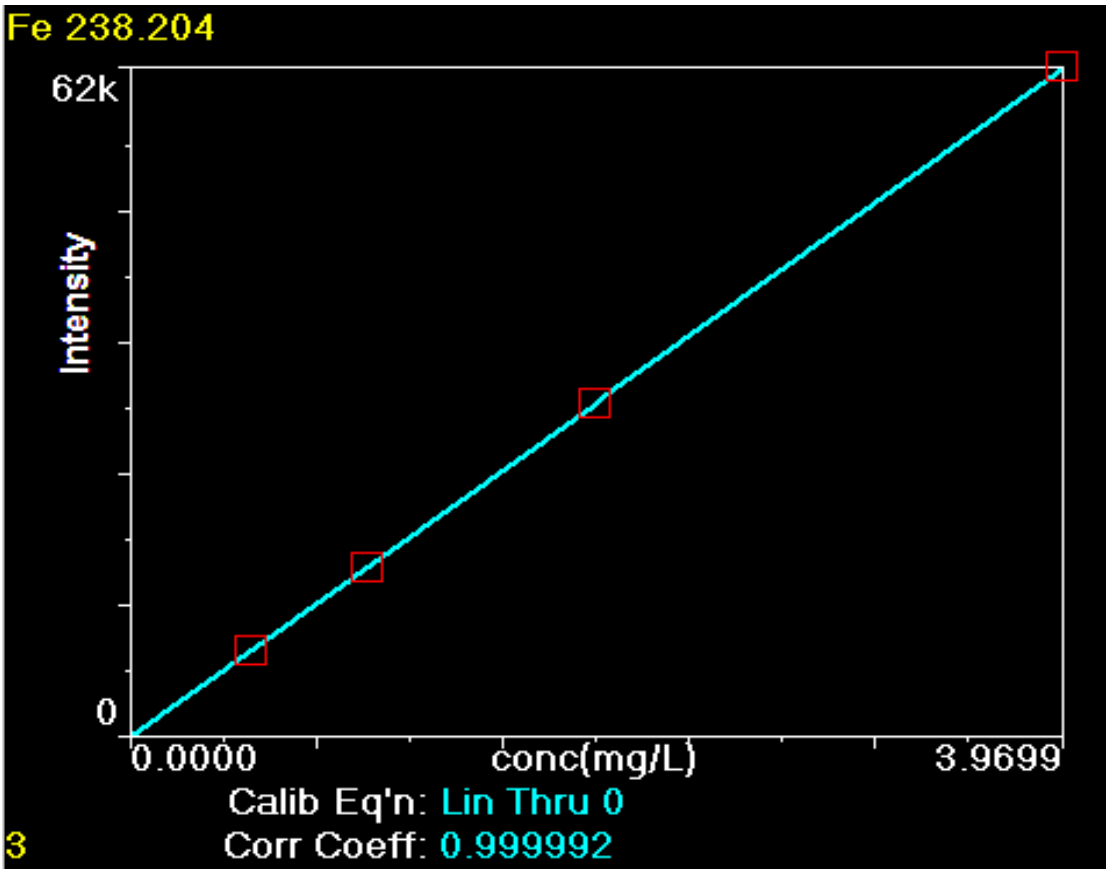

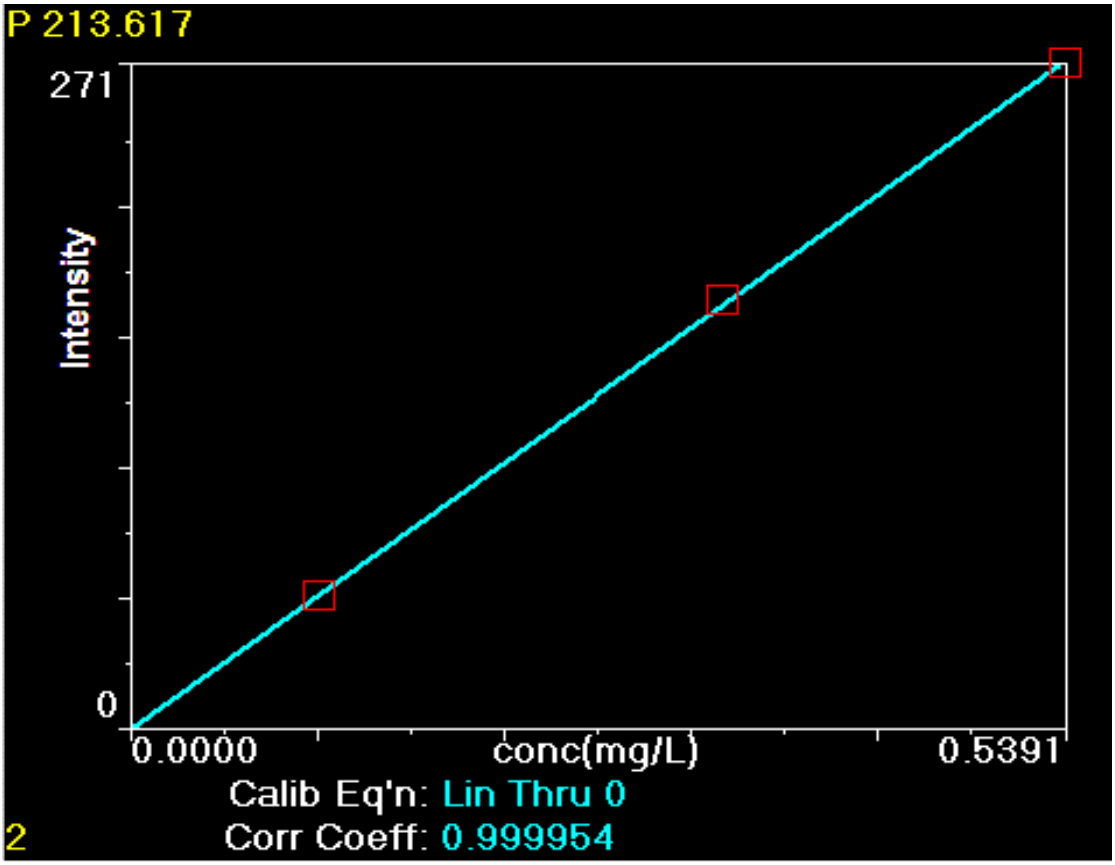

Figure 39. ICP-OES standard curves for P and Fe

Mass balance was confirmed to within experimental error using the first experimental conditions in Table 10 for both Fe(III) and DTPMP. Three mass balance experiments were conducted. The measurement results and mass calculation are shown in Table 12.

Table 12. Mass balance calculation of DTPMP and Fe(III)

12a. Mass balance calculation of DTPMP

#	Mass of DTPMP in supernate*	Mass of DTPMP in filtrate	Mass of DTPMP combined	Total mass of DTPMP added	Recovery rate
5	0.0079mg	0.0166mg	0.0245mg		82%
6	0.0095mg	0.0152mg	0.0248mg		83%
7	0.0094mg	0.0141mg	0.0235mg	0.030mg	78%

12b. Mass balance calculation of Fe(III)

#	Mass of Fe in supernate	Mass of Fe in filtrate	Mass of Fe combined	Total mass of Fe added	Recovery rate
5	0.0009mg	0.0098mg	0.0107mg		82%
6	0.0011mg	0.0095mg	0.0105mg		81%
7	0.0011mg	0.0089mg	0.0101mg	0.013mg	78%

*Data in this column was calculated by DTPMP concentration in the supernatant multiplied by the mass of supernatant taken for ICP-OES measurement. The mass of supernatant taken is varied every time.

The recovery rate of Fe and DTPMP are both between 78% and 83%. The reason for the systematic difference is not known, but might have been due to some unknown loss in the analytical ultracentrifuge or incomplete solid dissolution and measurement. At the end of the mass balance

experiments under the conditions of experiments 1 and 2, the average Fe(III) in solution was 0.169 mg/L and DTPMP was 1.476 mg/L and if it is assumed that the residual Fe(III) in solution was ferrihydrite this would correspond to removing 0.195 mg/L of DTPMP, thereby again leaving 1.281 mg/L of DTPMP free in solution, similar to that observed in Table 11.

Finally, the following demonstrates that the remaining scale inhibitors in the aqueous phase matches the barite induction time observed at the same experimental condition. An empirical log-linear relationship between inhibitor concentration and $\log_{10}(t_{ind}^{inh}/t_{ind}^{0})$ has been reported (Liu et al. 2014, more refs). Furthermore, it has recently been shown that this functional form can be shown to be a consequence of classical nucleation theory (Joey, personal communications)

$$\log_{10}\left(\frac{t_{ind}^{inh}}{t_{ind}^{0}}\right) = b_{inh}\left(\frac{L}{mg}\right) \times C_{inh}\left(\frac{mg}{L}\right)$$

t_{ind}^{inh} is induction time of barite nucleation at inhibitor concentration C_{inh}

t_{ind}^{0} is induction time of barite nucleation without any inhibitor

C_{inh} is inhibitor concentration

b_{inh} is inhibition efficiency

Using this log-linear relationship, the observed induction times at 25°C in the absence of Fe(III) can be correlated to the DTPMP concentrations in Table 13. With this correlation, the amount of scale inhibitor that should remain in solution to correspond to the observed induction time data can be calculated (Table 14).

Table 13. DTPMP concentration and corresponding barite nucleation induction time

DTPMP concentration (mg/L)	Induction time (s)
0	31
0.82	169
1.22	230
2	1183

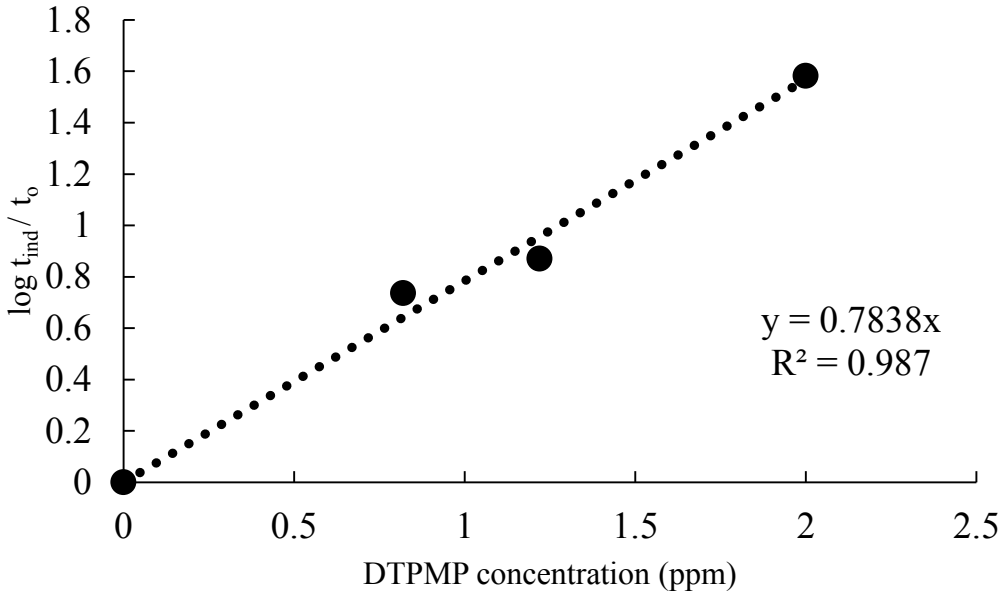

Figure 40. Linear relationship between inhibitor concentration and log t/t_o without Fe (III)

The measured barite induction time corresponding to condition 1, Table 10, would be 278s. We can back-calculate C_{inh} to be 1.22 mg/L. The same method can be used to calculate how much inhibitor is remained in experiment 3&4. Calculation results are listed in Table 14.

Table 14. Comparison of measured remaining DTPMP concentration and measured barite nucleation induction time

#	Averaged measured induction time	Calculated DTPMP remaining in solution (mg/L)	Measured remaining DTPMP in solution (mg/L)
1&2	255，301	1.21±0.06	1.27&1.26
3&4	1521，1037	2.05±0.15	2.07&1.98

The calculation results in Table 14 shows that with experimental conditions of 1&2 and of 3&4, the calculated remaining DTPMP concentration in solution matches well with the measured remaining DTPMP concentration in solution.

In summary, the data strongly supports the hypothesis about the mechanism of Fe(III) effect on scale inhibitor, that is a portion of the inhibitor adsorbs onto the ferric hydroxide particle surfaces and the remaining inhibitor inhibits nucleation independently.

4.3 The application of organic chelating agents on reversing Fe(III) effect on scale inhibitor

To prevent the negative impact of iron, chelating agents such as EDTA and citric acid are commonly used in oil and gas production for iron control. Therefore, EDTA and citric acid are tested in this study to reverse Fe(III) impairment on scale inhibitors. The results are plotted in Figure 41

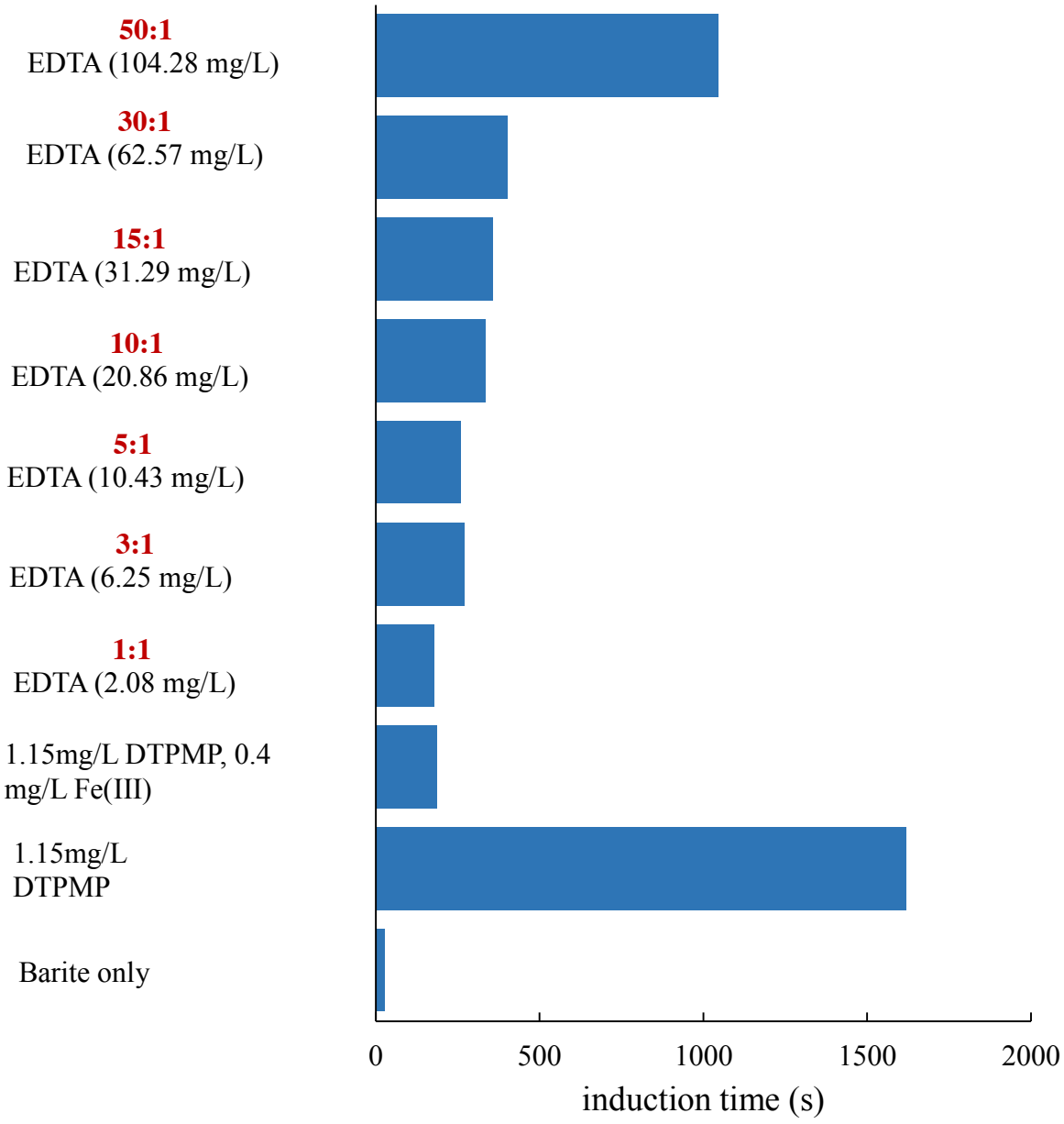
50:1
EDTA (104.28 mg/L)
30:1
EDTA (62.57 mg/L)
15:1
EDTA (31.29 mg/L)
10:1
EDTA (20.86 mg/L)
5:1
EDTA (10.43 mg/L)
3:1
EDTA (6.25 mg/L)
1:1
EDTA (2.08 mg/L)
1.15mg/L DTPMP, 0.4 mg/L Fe(III)
1.15mg/L DTPMP
Barite only
0
500
1000
1500
2000
induction time (s)

42a.

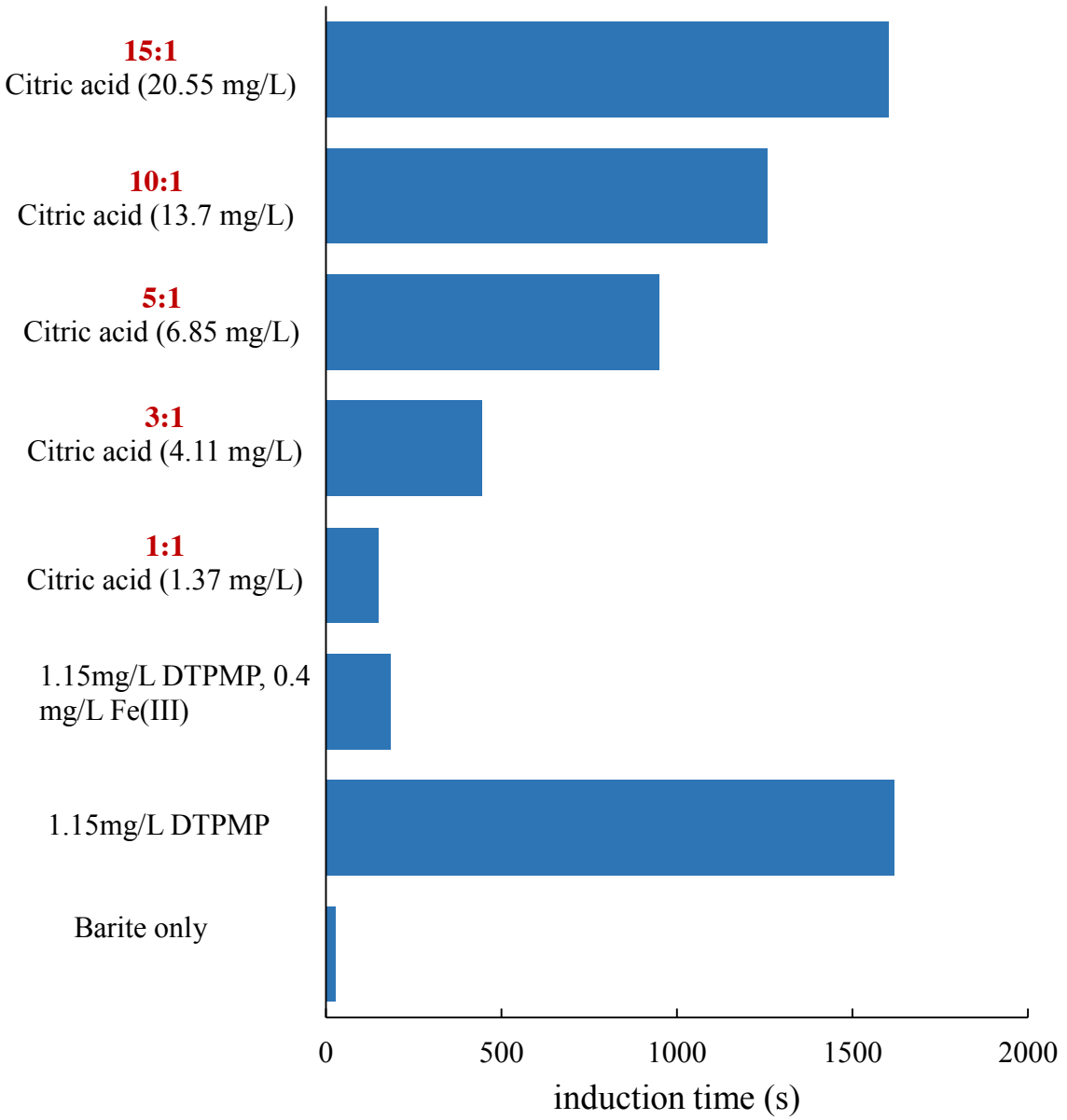

42b

Figure 41. Use different amounts of EDTA (Figure 42a) and citric acid (Figure 42b) versus time to reverse the effect of Fe(III) on DTPMP inhibition of barite nucleation. All experiments contained 1.15ppm DTPMP plus 0.4 mg/L Fe(III) and were conducted at 6.74 pH (10 mM PIPES buffer), 1 M NaCl, 400 mg/L Ca^{2+}, barite SI = 2.00 and 70°C. The numbers above each citric acid concentration is the molar ratio of citric acid to Fe(III). Solutions were added in the order: 1. Na_2SO_4 (in 1M NaCl solution containing 400 mg/l Ca^{2+}); 2. DTPMP; 3. EDTA or citric acid; 4. $BaCl_2$; and 5. $FeCl_3$ –both #4 and 5 were in 1M NaCl solution containing 400 mg/l Ca^{2+}.

Table 15. Induction time data at 70°C, pH 6.74, 400 mg/L Ca^{2+}

Exp #	DTPMP (mg/l)	Fe(III) (mg/L)	EDTA (mg/L)	Citrate (mg/L)	Ligand:Fe(III) Molar Ratio	t_{ind} (s)
1	0	0	0	0	0	20
2	1.15	0	0	0	0	1751
3	1.15	0.4	0	0	0	241
4	1.15	0.4	0	1.37	1:1	154
5	1.15	0.4	0	4.11	3:1	357
6	1.15	0.4	0	6.85	5:1	504
7	1.15	0.4	0	13.7	10:1	1019
8	1.15	0.4	0	20.55	15:1	1625
Exp #	**DTPMP (mg/l)**	**Fe(III) (mg/L)**	**EDTA (mg/L)**	**Citrate (mg/L)**	**Ligand to Fe(III) Molar Ratio**	**t_{ind} (s)**
9	0	0	0	0	0	20
10	1.15	0	0	0	0	1751
11	1.15	0.4	0	0	0	241
12	1.15	0.4	2.08	0	1:1	315
13	1.15	0.4	6.25	0	3:1	308
14	1.15	0.4	10.43	0	5:1	311
15	1.15	0.4	20.86	0	10:1	399
16	1.15	0.4	31.29	0	15:1	428
17	1.15	0.4	62.57	0	30:1	502
18	1.15	0.4	104.28	0	50:1	1172

The experimental condition was maintained at 70°C, pH 6.74, 1M NaCl and 400 mg/L Ca^{2+}. In Table 15, exp # 1-8, we can see barite nucleation has an induction time of 20s without any scale inhibitor (exp #1). When 1.15 mg/L DTPMP is in solution, barite nucleation induction time increases to 1751s (exp #2). In exp #4-8, five concentration levels of citric acid, 1.37, 4.11, 6.85, 13.70 and 20.55 mg/L (molar ratio of citrate: Fe=1:1, 3:1, 5:1, 10:1, 15:1) are added to exp # 3 solution. Barite nucleation induction time are 154s, 357s, 504s, 1019s, 1625s. DTPMP inhibition ability in the presence of 0.4 mg/L Fe(III) is gradually reversed by adding increasing concentration of citric acid. When citric acid is added at a molar ratio of 15:1 to Fe(III), the detrimental effect of Fe(III) on citric acid is completely reversed.

EDTA is also tested for its ability to reverse Fe(III) impairment on DTPMP inhibition performance at the same experimental condition. Increasing concentration of EDTA was added into the system from molar ratio EDTA:Fe(III) 1:1 to 50:1 (from 2.08 mg/L to 104.28 mg/L) as shown in experiment #12 to #18. In Table 15, different from the results with citric acid, when we add increasing amount of EDTA, from molar ratio of EDTA:Fe(III) 1:1 to 30:1, the effect of Fe(III) was not significantly reversed. Barite nucleation induction time only changes from 315 to 502s. It is when EDTA:Fe(III) ratio equals 50:1 that the effect of Fe(III) is almost reversed (1172s).

4.4 Discussion

EDTA is known to be a stronger chelating agent for Fe(III) than citric acid. Table 16 lists the Logarithm of stability constants between Fe(III) and EDTA /citric acid. The stability constant for Fe(III)-EDTA is $10^{25.7}$, for Fe(III)-citrate is $10^{11.85}$. Fe(III)-EDTA complex is more than 10 orders of magnitudes more stable than Fe(III)-citrate complex. If Fe(III) is chelated by EDTA/citric acid

immediately when it is added, EDTA should chelate more Fe(III) than citric acid, form less ferric hydroxide particles and gradually revert Fe(III) impairment on DTPMP. Visual Minteq calculation shows that in exp #4-8, only less than 1% of Fe(III) is chelated. In exp # 12-18, almost 100% Fe(III) were chelated. However, experiment results suggest the weaker chelate, citric acid, works much better than EDTA in reverting Fe(III) impairment on DTPMP. It takes much higher amount of EDTA to reverse Fe(III) effect on scale inhibitor than citric acid.

Table 16. Logarithm of stability constants between Fe(II) and Fe(III) and EDTA and citric acid

	Fe(II)	Fe(III)
EDTA	14.3	25.7
Citric acid	3.2	11.85

Why citric acid works better than EDTA while EDTA is the stronger chelating agents? The reason is that they work by different mechanism. Data in Table 15 shows that EDTA needs to be added at 50:1 molar ratio (EDTA:Fe(III)) to almost reverse the effect. The reagents in the experiment was added in the order of Na_2SO_4 (in 1M NaCl solution containing 400 mg/l Ca^{2+}), DTPMP, Na_2H_2EDTA /citric acid, $BaCl_2$ (in 1M NaCl solution containing 400 mg/l Ca^{2+}) and $FeCl_3$. Fe(III) was introduced into the system by adding a calculated volume of concentrated Fe(III) stock solution. The stock solution was added into brine and dilute 50 times to reach desired concentration level of 0.4 mg/L. When the stock solution touches brine, it began to hydrolyze and form ferric hydroxide particles immediately before being diluted. EDTA works by direct chelation of Fe(III) at 1:1 molar ratio, therefore, EDTA need to be provided in the same molar concentration as Fe(III)

stock solution to complete prevent the formation of ferric hydroxide particles. That's why, we observed that at a 50:1 molar ratio (EDTA:desired Fe(III) concentration), the effect of Fe(III) was reversed.

Citric acid works by a different mechanism. Same as EDTA experiments, Fe(III) starts to hydrolyze and form ferric hydroxide particles as soon as it touches rest of the solution. However, instead of direct chelation, citric acid can adsorb on the surface of ferric hydroxide particles and cover the active adsorption sites. There are some publications studying the adsorption of citric acid onto ferric hydroxide particles. Schindler et al. studied adsorption mechanism of l-tartaric acid, meso-tartaric acid and citric acid on amorphous ferric hydroxide in 0.1M $NaNO_3$, pH 3 condition(Cornell and Schindler 1980). They find that citric acid has the strongest surface complex stability. They also give a maximum surface coverage density of 1 molecule / 100$Å^2$for citric acid on amorphous ferric hydroxide. Assume a citric acid surface coverage of 1 molecule / 100$Å^2$, 1.37 mg/L citric acid (exp # 4 in Table 15) should be able to cover a ferric hydroxide surface of 4.3 m^2/L (~30.71 mg/L Fe(III)). Exp #10 only has 0.4 mg/L Fe(III), but DTPMP performance is still impaired. An explanation for this conflicting results might be that exp # 10 has 1M NaCl, 400 mg/L Ca^{2+} and a pH of 6.74 as solution background. The literature describes a solution background of 0.1M $NaNO_3$ and pH 3. The difference in solution composition could result in different citric acid adsorption ability. 1 molecule / 100 $Å^2$ surface coverage might not apply in this case. Further research of citric acid adsorption onto ferric hydroxide in 1M NaCl, 400 mg/L Ca^{2+} and a pH of 6.74 solution is needed. The other possible explanation is that DTPMP and citric acid molecules might adsorb competitively onto ferric hydroxide particle surface. Citric acid might not be able to reach its maximum surface coverage because of the co-adsorption of DTPMP on ferric hydroxide

particle surface. The adsorption of DTPMP onto ferric hydroxide surface in the presence of different concentrations of citric acid should also be investigated in future research. The adsorption of citric acid onto ferric hydroxide particles might be the reason why citric acid can reverse the effect of Fe(III) when it chelates much less Fe(III) than EDTA.

In above discussion, we concluded that EDTA reverses Fe(III) by direct chelation at 1:1 molar ratio. Another experiment here is designed to test above conclusion. This set of experiments is conducted also at 70ºC, 1M NaCl, pH 6.74 condition. The difference is the order of reagent addition. As shown in Table 17 we can see barite has a nucleation induction time of 20s (exp #1). When there is 1.15 mg/L DTPMP, barite induction time is increased to 1153s (exp # 2). When 1 mg/L Fe(III) is added to exp #2 solution, barite induction time drops to 60s (exp #3). Exp #4 and 5 have the same solution composition. Their difference is the way in which Fe(III) and EDTA are added into the system. In exp #4, reagents are added in the following sequence: Na_2SO_4, DTPMP, Na_2H_2EDTA, $FeCl_3$, and $BaCl_2$. Barite nucleation induction time is 60s, same as exp #3. In exp #5, $FeCl_3$ and Na_2H_2EDTA stock solutions (2mmol/L) are mixed at equal volume at pH 2.0 condition. After mixing, all Fe(III)(1mmol/L) is chelated by EDTA (calculated by Visual MINTEQ ver. 3.1). In exp #5, the reagents are added in the following sequence: Na_2SO_4, DTPMP, Fe(III)- EDTA mixture and $BaCl_2$. Fe(III)-EDTA mixture has a pH of 2.0. The addition of the mixture into the system results in a drop of pH from 6.74 to 6.50 (the system is buffered by 5mM PIPEs). Exp #5 give result of 1156s. The results of exp # 2 and 5 are very close. Therefore, after Fe(III)-EDTA mixture is added into the system, the impairment of DTPMP performance by Fe(III) is not observed. This experimental result again proved that if EDTA is able to chelate 100% Fe(III) before Fe(III) starts to hydrolyze, it can reverse the detrimental effect of Fe(III) to scale inhibitors.

Table 17. Barite nucleation induction time at 1M NaCl, 6.74 pH, 70°C

Exp#	DTPMP (mg/L)	EDTA (mg/L)	Fe(III) (mg/L)	Induction time (s)
1	0	0	1	20
2	1.00	0	0	1153
3	1.00	0	1	60
4	1.00	5.22	1	60
5	1.00	5.22	1	1156

Chapter 5. Fe (II) impact on scale inhibitors

5.1 Experimental data of Fe(II) impact on scale inhibitors using apparatus before improvement

The following experiment results are collecting by the anoxic Fe(II) testing apparatus before improvement introduced in previous chapter. The impact of Fe(II) on scale inhibitors is investigated at different pH and temperature conditions. Also, the impact of Fe(II) on different scale inhibitors are tested. Experimental conditions are shown in Table 18.

Table 18. Chemical conditions of the solutions

Components	25°C experiment	70°C experiment
NaCl	1 mol/l	1 mol/l
Ca^{2+}	---------	4000 mg/l
Ba_{2+}	122.18 mg/l	223.76 mg/l
SO_4^{2-}	85.42 mg/l	156.43 mg/l
Barite Saturation Index (SI)	2.00	2.00
DTPMP	0-0.4 mg/L	1-3 mg/L
PPCA	---------	1-3mg/L
PVS	---------	1-3mg/L
PIPES	5 mmol/l if target pH is 6.74	5 mmol/l if target pH is 6.74
Sodium acetate	5 mmol/l then adjusted by adding 1mol/l HCl if target pH is 5.5	5 mmol/l then adjusted by adding 1mol/l HCl if target pH is 5.5
Fe(II)	1-20 mg/l	1-3 mg/l
Hydroxylamine hydrochloride	2.48-49.64 mg/l	2.48-7.45 mg/l

*All the saturation index and density related calculation is done by ScalesoftPizter 2013.

5.1.1 Influence of increasing Fe(II) concentration

Table 19. Influence of Fe(II) on DTPMP performance at 25°C, no Ca, 1M NaCl, pH=5.5, barite SI=2.00 condition

Exp #	DTPMP conc. (mg/L)	Fe(II) (mg/L)	t_{ind} (s)
1	0	0	120
2	0.1	0	435
3	0.3	0	9000
4	0.1	1	219
5	0.1	10	242
6	0.1	20	281
7	0.3	1	4000
8	0.3	10	1652
9	0.3	20	987
10	0.3	30	660

Table 19 shows barite nucleation induction time in the presence of 0.1 and 0.3 mg/L DTPMP and the influence of 1, 10, 20 and 30 mg/L Fe(II) to DTPMP performance at 25°C, no Ca, 1M NaCl, pH=5.5, barite SI=2.00 condition. From Table 19, we can see barite nucleation takes 120s. When 0.1 and 0.3 mg/L DTPMP are added, barite nucleation is prolonged to 435s and 9000s respectively. When there are 1, 10 and 20 mg/L Fe(II), barite nucleation time in the presence of 0.1 mg/L DTPMP drops to 219s, 242s and 281s from 435s. When there are 1, 10, 20 and 30 mg/L Fe(II) barite nucleation time in the presence 0.3 mg/L DTPMP also drops from 9000s to 4000s, 1652s, 987s and 660s respectively.

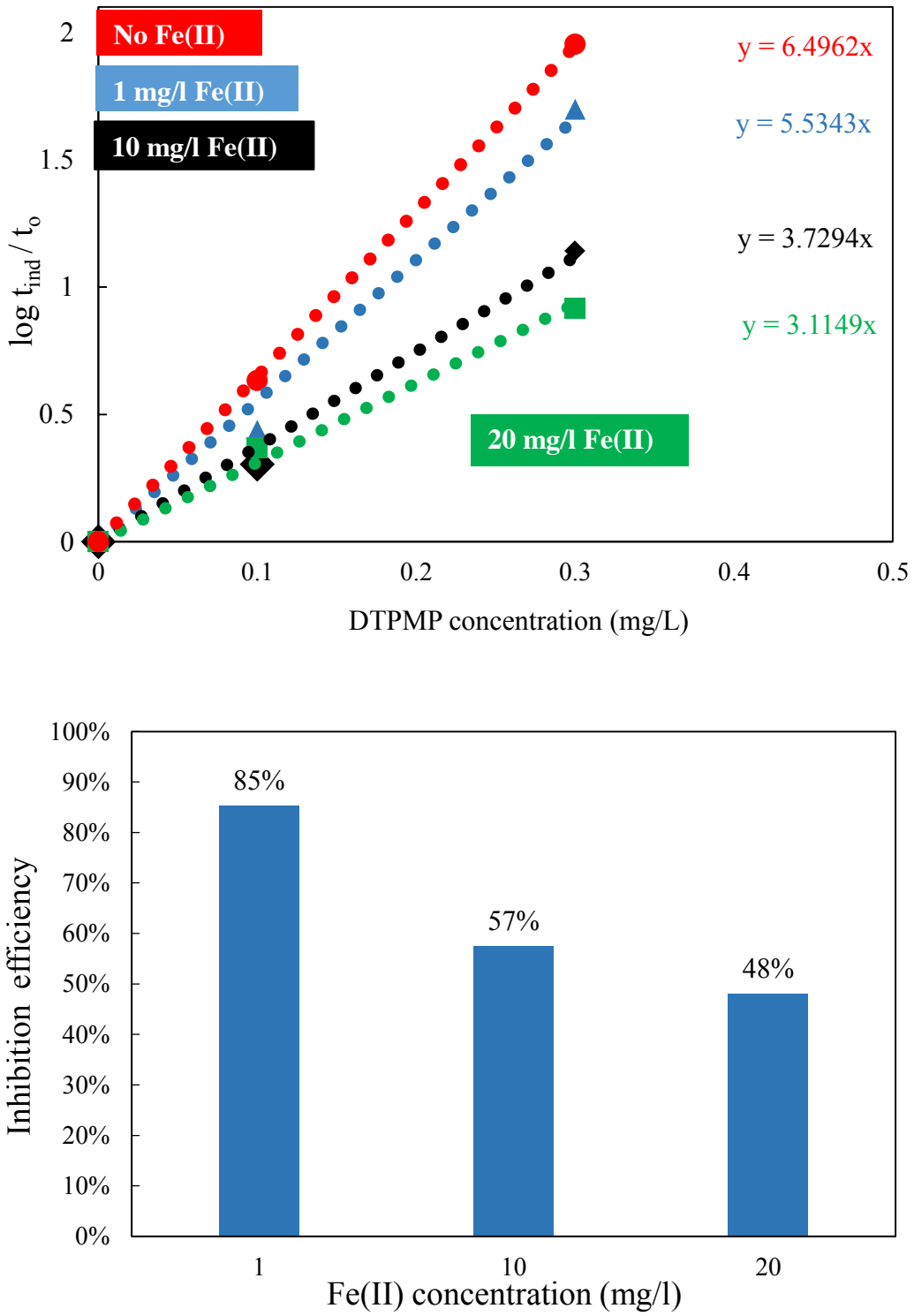

Figure 42. Inhibition efficiency of DTPMP at 25°C and pH 5.5 in the presence of different concentration of Fe(II)

The following equation is used for calculation inhibition efficiency in Figure 42.

$$inhibition\ efficiency =$$

$$\frac{barite\ induction\ time\ (Fe^{2+}\ conc. = b\frac{mg}{L}, inhibitor\ conc. = a\frac{mg}{L})}{barite\ induction\ time\ (inhibitor\ conc.\ a\frac{mg}{L})} * 100\%$$

From Figure 42, we can see that, when Fe(II) concentration increases from 1, 10 to 20 mg/L, DTPMP inhibition efficiency decreases from 85%, 57% to 48%.

5.1.2 Influence of temperature

To investigate Fe(II) impact on DTPMP at different temperature. A set of experiments are conducted at 70°C, no Ca, 1M NaCl, pH=5.5, Barite SI=2.00 in order to compare with results at 25°C in Table 19. Results are listed in Table 20.

Table 20. Influence of Fe(II) on DTPMP performance at 70°C, no Ca, 1M NaCl, pH=5.5, Barite SI=2.00 condition

Exp #	DTPMP (mg/L)	Fe(II) (mg/L)	t_{ind} (s)
1	0	0	15
2	1.22	0	862
3	1.61	0	6345
4	2.00	0	13921
5	1.22	1	202
6	1.22	3	121
7	1.61	1	429
8	2	3	390

From Table 20, we can see at 70°C, no Ca, 1M NaCl, pH=5.5, barite SI=2.00 condition, barite

nucleation induction time is 15s. Addition of 1.22, 1.61 and 2 mg/L DTPMP prolongs barite nucleation induction time to 862s, 6345s and 13921s respectively. When 1 mg/L Fe(II)is in solution, barite nucleation in the presence of 1.22 and 1.61 mg/L DTPMP drops to 202s and 429s compared to 862s and 6345s without Fe(II). When 3 mg/L Fe(II) exists in solution, barite nucleation in the presence of 1.22 and 2 mg/L DTPMP drops to 121s and 390s compared to 862s and 13921s without Fe(II).

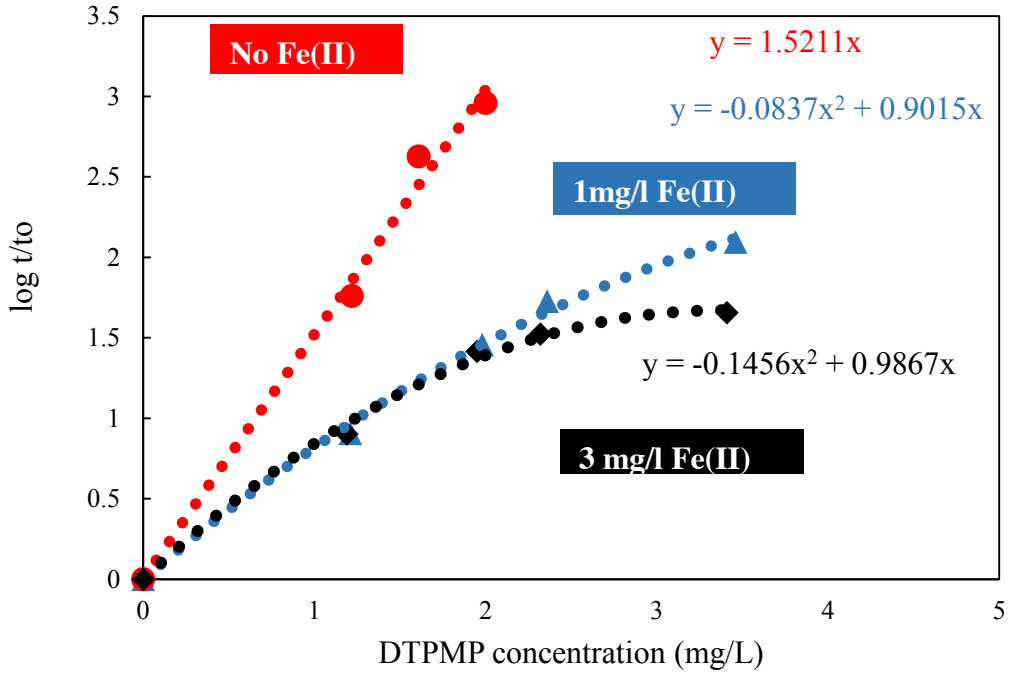

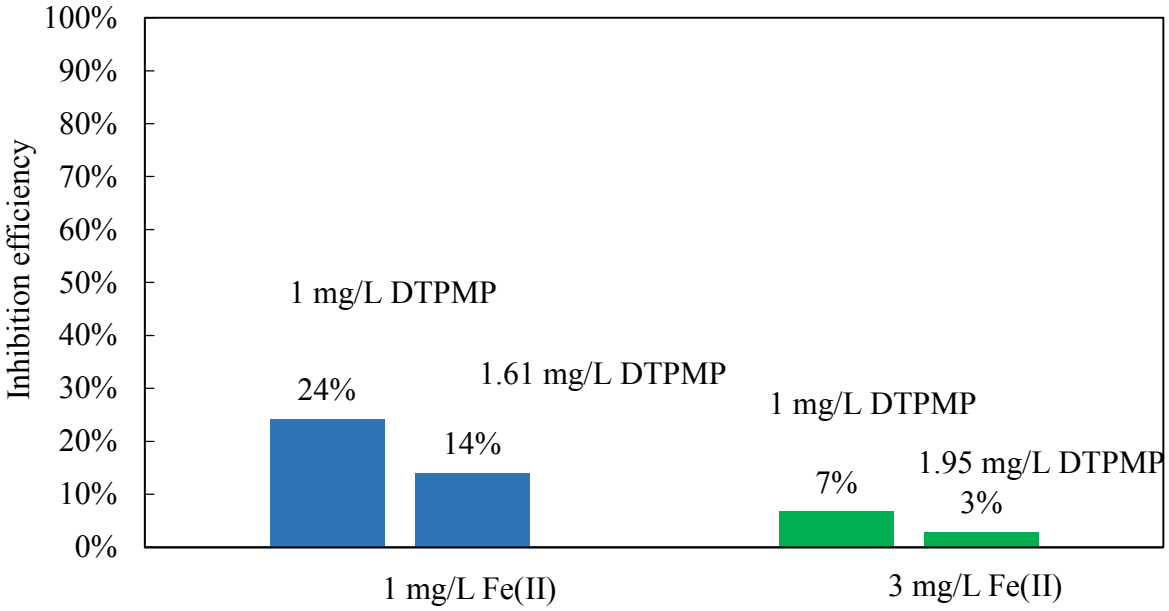

Figure 43. Inhibition efficiency of DTPMP in the presence of different concentration of Fe(II)

From Figure 43, we can see at 1 mg/L Fe(II) decreases the inhibition efficiency of 1 mg/L DTPMP and 1.61 mg/L DTPMP to 24% and 14% respectively. 3 mg/L Fe(II) decrease the inhibition efficiency of 1 mg/L DTPMP and 1.95 mg/L DTPMP to 7% and 3% respectively. The impairment of Fe(II) to DTPMP performance is significant.

5.1.3 Influence of pH

Fe(II) impact on DTPMP at different pH is also investigated. A set of experiments are conducted at 25^{o}C, no Ca, 1M NaCl, pH=6.74, barite SI=2.00condition in order to compare with results at pH 5.5 in Table 20. Results are listed in Table 21.

Table 21. Influence of Fe(II) on DTPMP performance at 25°C, no Ca, 1M NaCl, pH=6.74, barite SI=2.00 condition

Exp #	DTPMP (mg/L)	Fe(II) (mg/L)	t_{ind} (s)
1	0	0	300
2	0.1	0	1700
6	0.3	0	35000
3	0.1	1	731
4	0.1	10	831
5	0.1	20	874
6	0.3	1	2287
7	0.3	10	2028
8	0.3	20	2367

From Table 21, we can see at 25°C, no Ca, 1M NaCl, pH=6.74, barite SI=2.00 condition, barite nucleation induction time is 300s. Addition of 0.1, 0.3 mg/L DTPMP prolongs barite nucleation induction time to 1700s and 35000s respectively. When there are 1, 10 and 20 mg/L Fe(II), barite nucleation time in the presence of 0.1 mg/L DTPMP drops to 731s, 831s and 874s from 1700s. When there are 1, 10, 20 mg/L Fe(II), barite nucleation time in the presence 0.3 mg/L DTPMP decreases from 35000s to 2287s, 2028s, 987s and 2367s respectively.

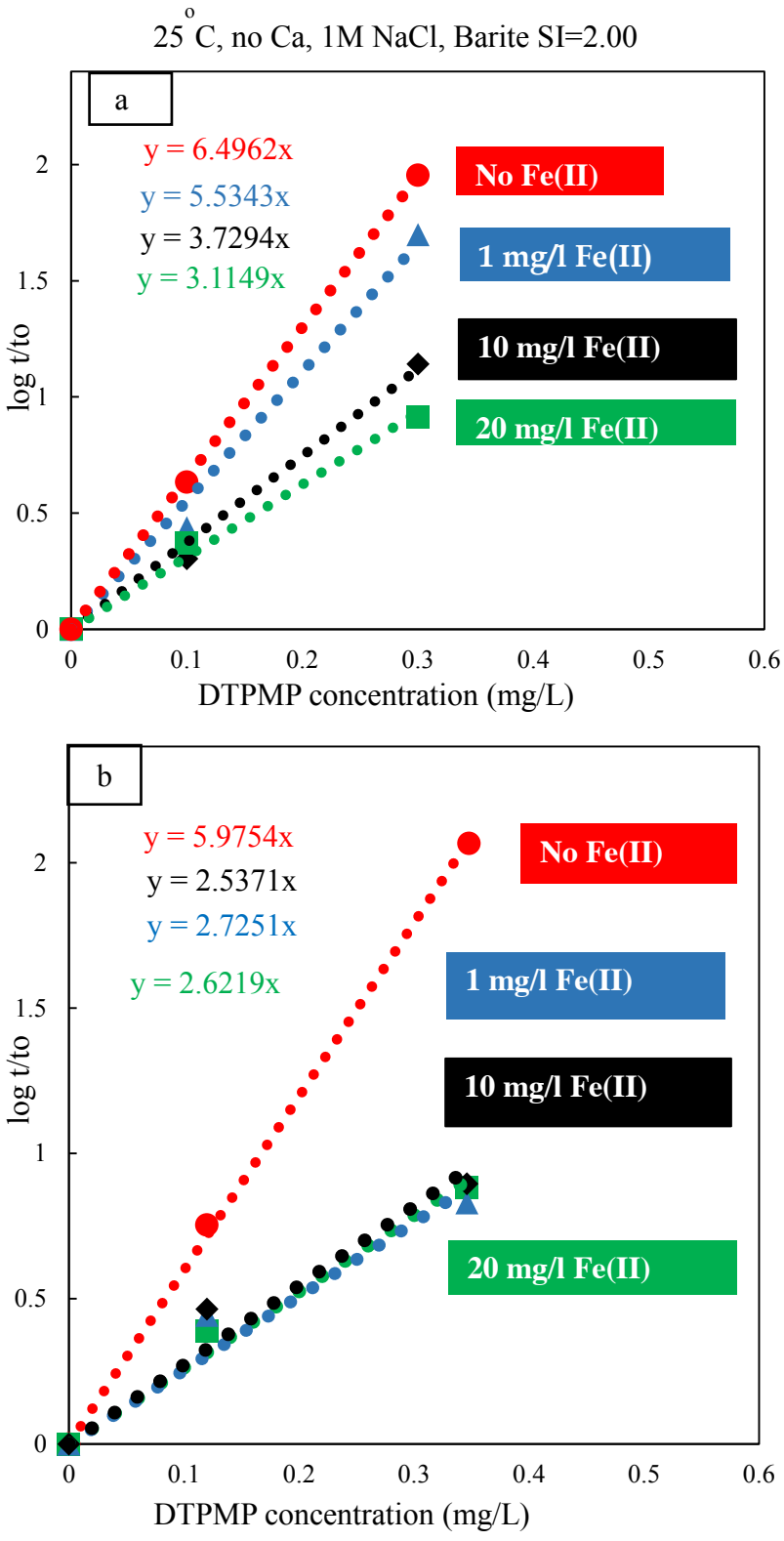
25 °C, no Ca, 1M NaCl, Barite SI=2.00
a
y = 6.4962x
y = 5.5343x
y = 3.7294x
y = 3.1149x
No Fe(II)
1 mg/l Fe(II)
10 mg/l Fe(II)
20 mg/l Fe(II)
log t/to
DTPMP concentration (mg/L)
b
y = 5.9754x
y = 2.5371x
y = 2.7251x
y = 2.6219x
No Fe(II)
1 mg/l Fe(II)
10 mg/l Fe(II)
20 mg/l Fe(II)
log t/to
DTPMP concentration (mg/L)

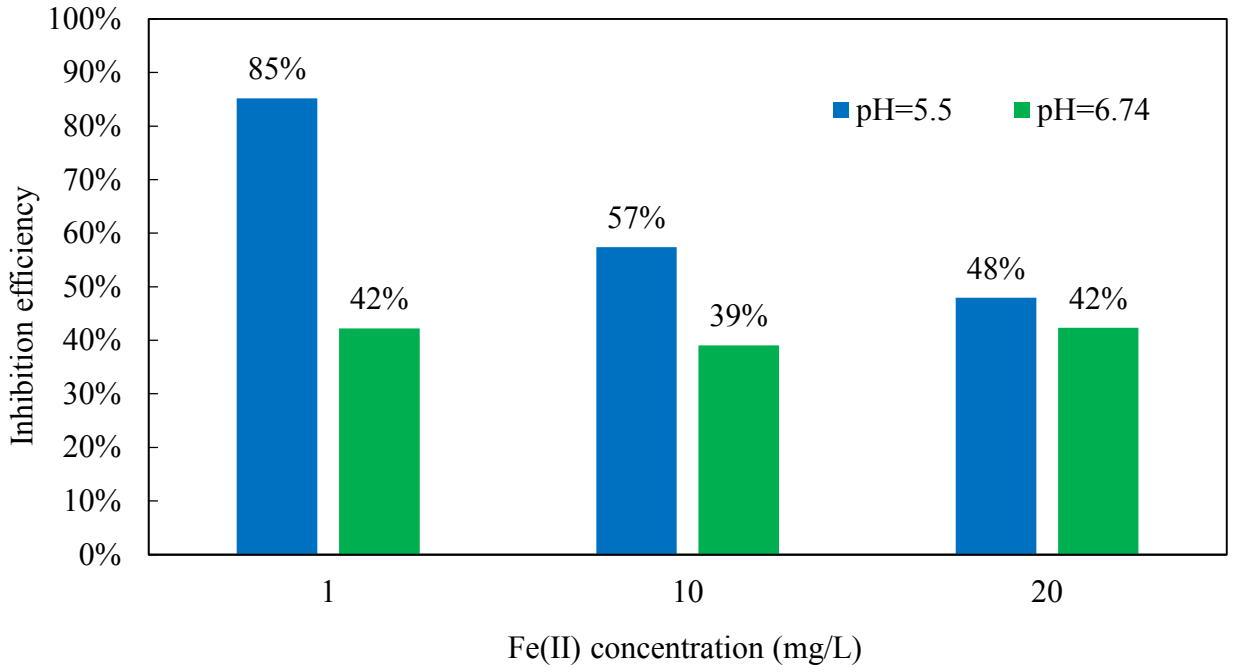

Figure 44. Comparison of DTPMP inhibition efficiency at different pH in the presence of Fe(II)

Figure 44 compares the inhibition efficiency of DTPMP at pH 5.5 and 6.74 condition in the presence of Fe(II). Blue bars represent DTPMP inhibition efficiency at pH 5.5. Red bars represent DTPMP inhibition efficiency at pH 6.74. At pH 6.74, with an increasing Fe(II) concentration of 1, 10 and 20 mg/L, DTPMP inhibition efficiency are 45%, 39% and 42%. At pH 5.5, when Fe(II) concentration increases from 1,10 to 20 mg/L, DTPMP inhibition efficiency decreases from 85%, 57% to 48%. DTPMP retains a higher inhibition efficiency at pH 5.5 than at pH 6.74 in the presence of Fe(II).

5.1.4 Influence of Fe(II) on different scale inhibitors

Fe(II) impact on three different kinds of scale inhibitors—DTPMP, PPCA and PVS, are compared at pH 6.74, 70°C, 4000 mg/l Ca^{2+}, 1M NaCl, Barite SI=2.00 condition. Results are shown in Figure

45 and Figure 46.

pH 6.74, 70°C, 4000 mg/l Ca^{2+}, 1M NaCl, Barite SI=2.00

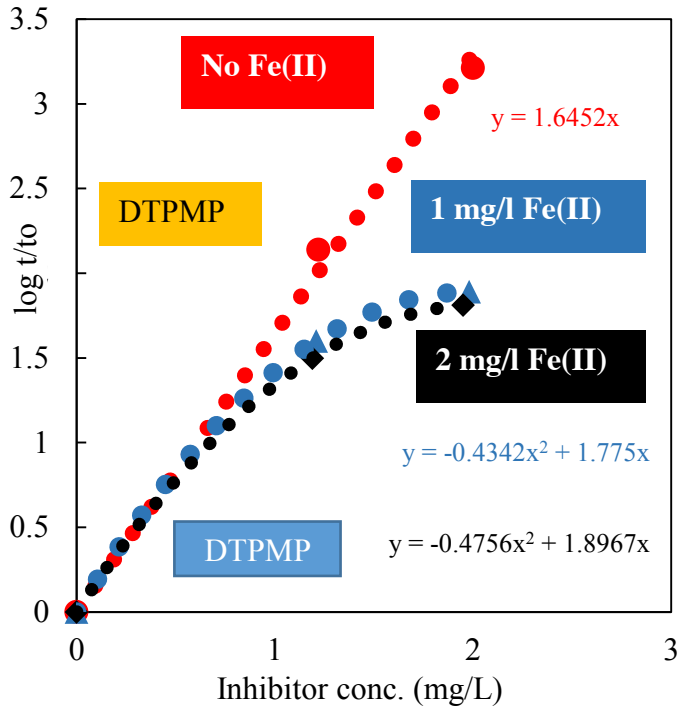

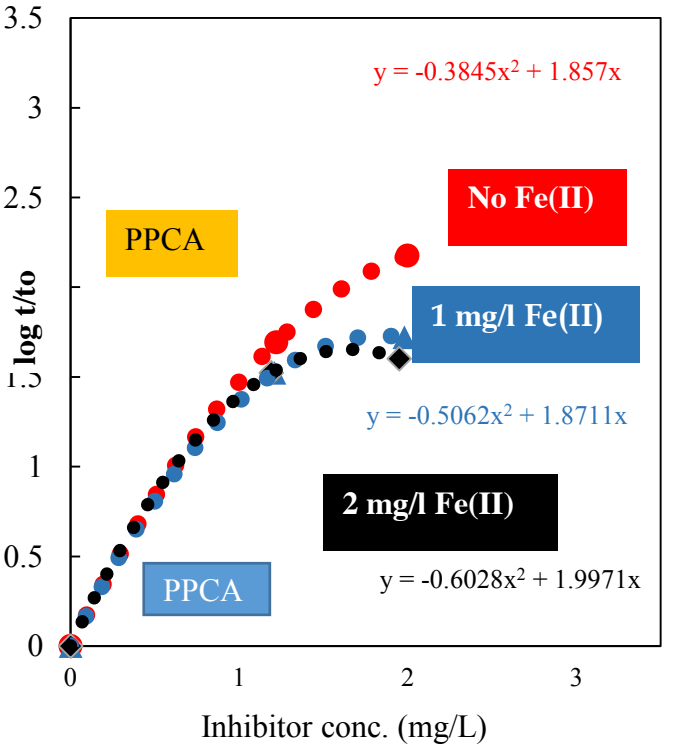

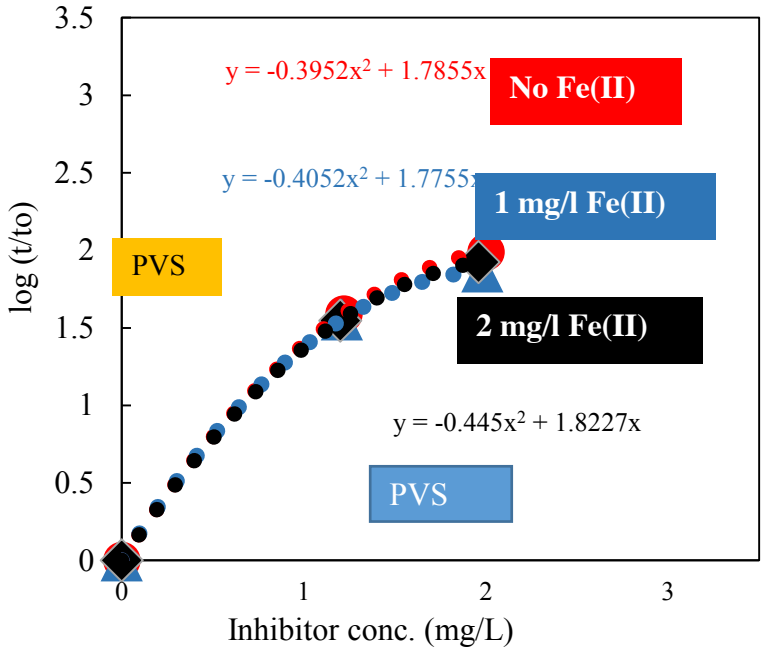

Figure 45. Comparison of the Fe(II) impact on DTPMP, PPCA and PVS.

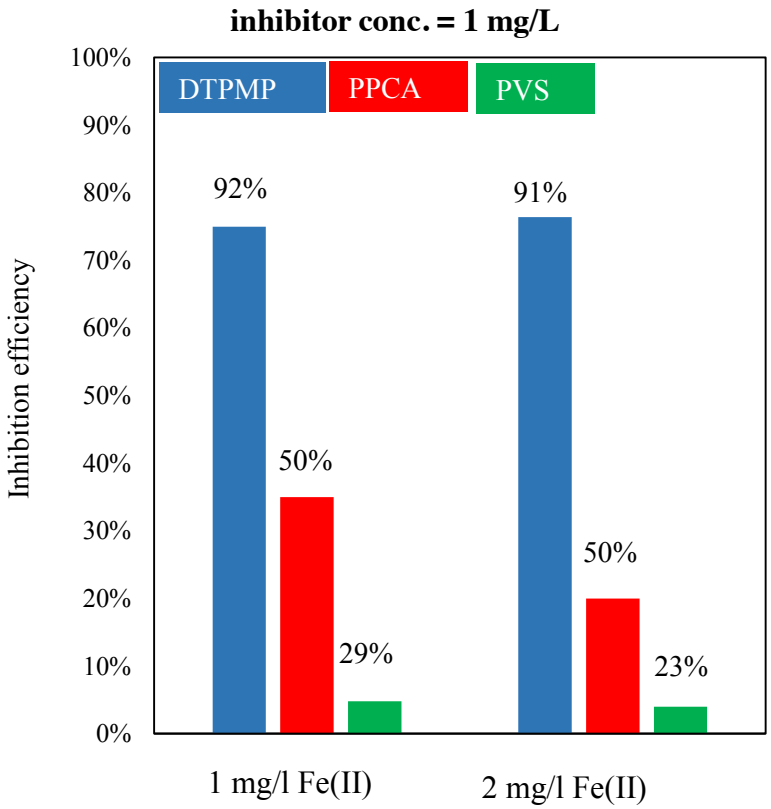

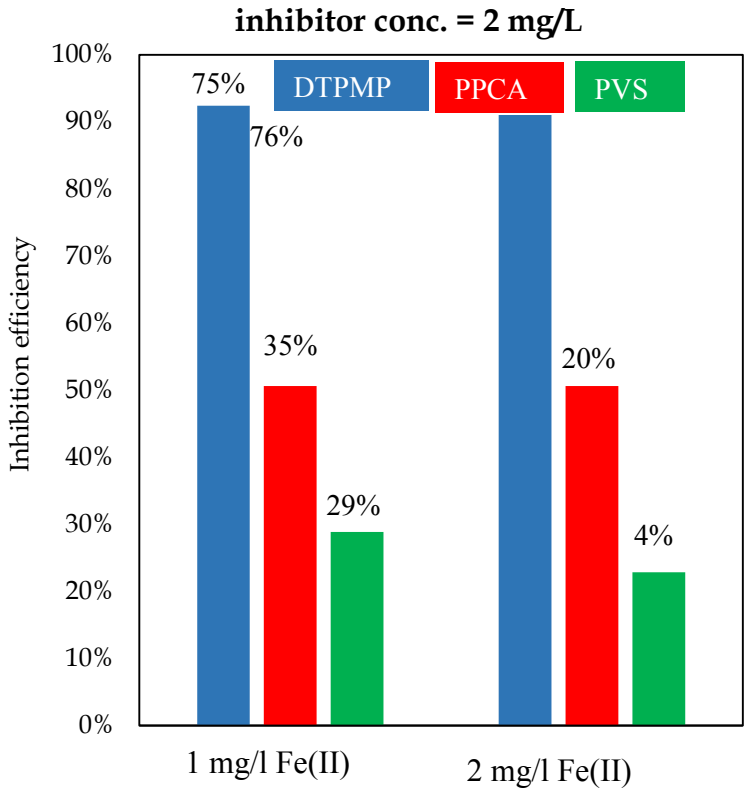

Figure 46. Comparison of inhibition efficiency of different scale inhibitors in the presence of Fe(II).

Interaction between phosphonate, carboxyl, sulfonate groups and transition metal is an important research topic across several academic and industrial areas. Figueira et al. studied iron species bio-sorption by *Sargassum* biomass and found that the complexation of Fe(II)/ Fe(III) with carboxyl and sulfonate groups are important for the uptake of iron species (Figueira et al., 1999). Yepez et al. studied naphthenic acid corrosion and found that carboxylic acids can precipitate with Fe(II) corroded from tubing surface (Yepez et al., 2007). This research topic is also very popular in material science and has wide application in gas storage, catalysis and separations. It was found that the coordination of sulfonate anions with transition metal is relatively weak compared to phosphonates (Shimizu et al., 2009). The coordination of sulfonate anions to transition metal is too weak to compete with water, ammonium and amines (Forbes et al., 2009). But carboxyl groups

are readily to bind transition metal cations (Deeth et al., 2008). Phosphonates, due to their multi-dentate nature, are stronger than carboxylate complex and form insoluble precipitates with transition metal cations (Chandrasekhar et al., 2011). These observations are consistent with the Fe(II) tolerance level observed in this research.

5.1.5 The application of organic chelating agents on reversing Fe(II) effect on scale inhibitors

Citric acid has been tested for its ability to reverse Fe(II) effect on DTPMP. Experiments were done at 70^{o}C, 1M NaCl, Barite SI=2.00 and pH=6.74. Experimental results are shown in Figure 47. In the absence of DTPMP and Fe(II), barite nucleation induction time is 20s. In the presence of 1.92mg/L DTPMP, barite nucleation induction time increases from 20s to 183min. The addition of 1.54 mg/L Fe(II) will decrease 1.92mg/L DTPMP inhibition time from 183min to 16min. When adding increasing amounts of citric acid to the solution with 1.92mg/L DTPMP and 1.54 mg/L Fe(II), DTPMP inhibition ability for barite gradually recovers. When 28.85 mg/L citrate (molar ratio of Fe(II) : citrate = 1:5) is added to solution with 1.15mg/L DTPMP and 1.54 mg/L Fe(II), DTPMP inhibition time is 191 min and the impact of Fe(II) is fully reversed. This result is similar to those of Shen (Shen et al., 2011).

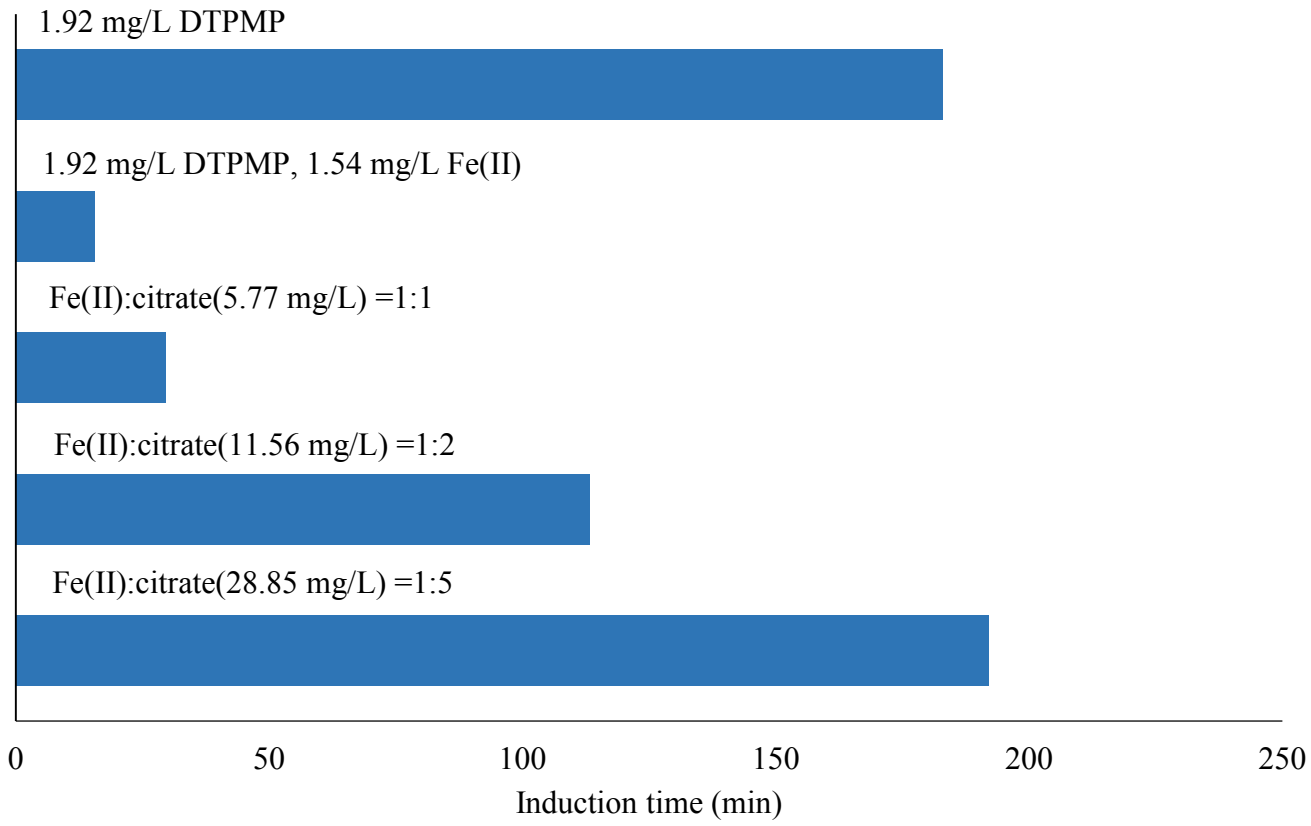

Figure 47. Citric acid reverses Fe(II) effect on DTPMP at 70°C, 1M NaCl, Barite SI=2.00,pH=6.74 condition

EDTA has also been tested for its ability to reverse Fe(II) detrimental effect on DTPMP. EDTA was added into Fe(II) stock solution (concentration of Fe(II)= 100 mg/L by dissolving $(NH_4)_2Fe(SO_4)_2$ in 1M NaCl brine buffered by PIPEs) at molar ratio of EDTA : Fe(III) = 1:1. EDTA is known to enhance the Fe(II) oxidation kinetics dramatically (Jones A. et al. 2015). The stock solution is constantly purged by high-purity Argon and protected by reducing agent hydroxylamine hydrochloride. Measured dissolved oxygen in the stock solution is measured to be below 5 ppb. However, the Fe(II) in the solution is still oxidized within 30 min. Whether this is due to trace amounts of oxygen or due to spontaneous oxidation of water is not known. Apparatus that can achieve a better deoxygenation performance needs to be applied to continue the

investigation on EDTA ability to reverse Fe(II) effect.

5.1.6 Comparison of Fe(III) and Fe(II) impact on scale inhibitors

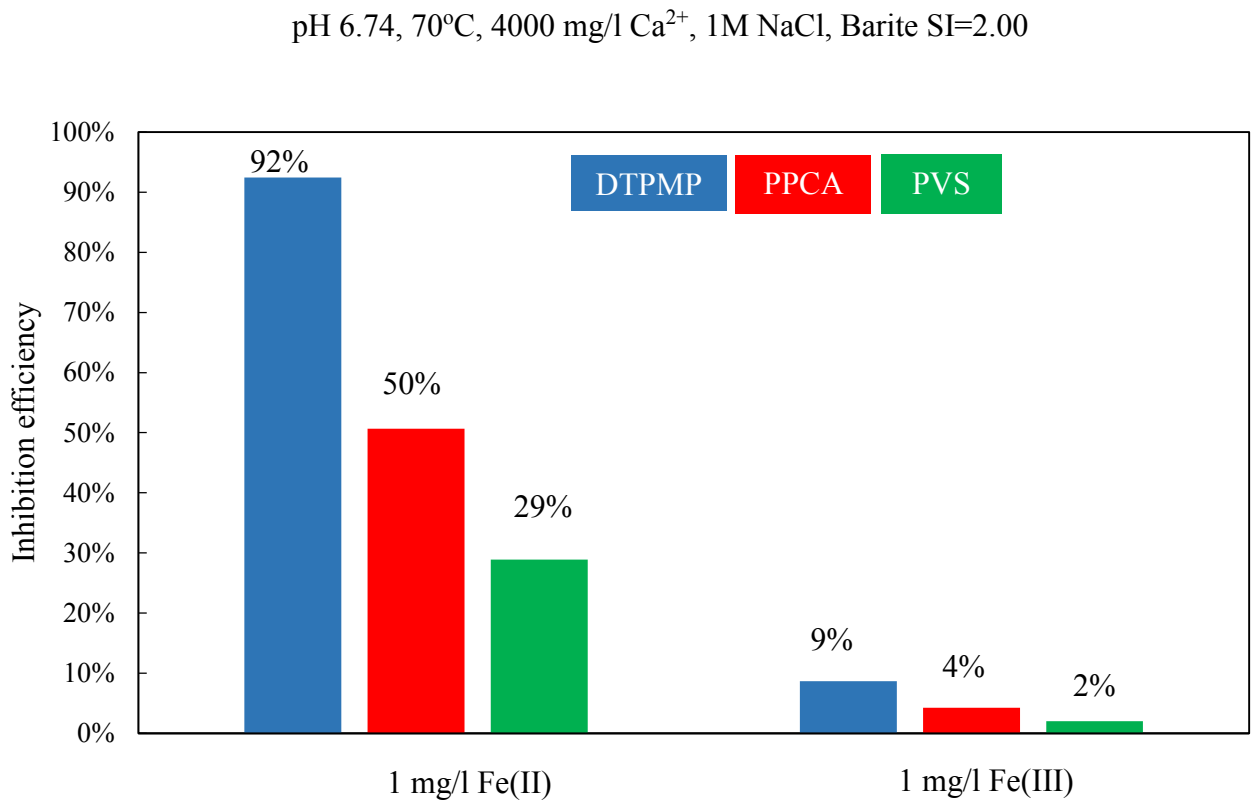

Figure 48. Comparison of different effects of Fe(II) and Fe(III) on DTPMP, PPCA and PVS.

From Figure 48, we can see Fe(III) appears to have more impact on inhibitor performance than Fe(II). The order of Fe(III) tolerance ability of three scale inhibitors is the same as that of their Fe(II) tolerance ability. A small percentage of Fe(II) oxidized to Fe(III) can also cause impairment of scale inhibitor performance especially at higher temperature and pH due to accelerated Fe(II) oxidation rate.

5.2 Experimental data of Fe(II) impact on scale inhibitor using the improved apparatus

The anoxic laser apparatus described in chapter 3 is used to test Fe(II) impact on scale inhibitors. The impact of Fe(II) on scale inhibitors is investigated at 70°C, pH 6.74 and 400 mg/L Ca^{2+} condition.

Table 22. Scale inhibitors tested in this research

Inhibitor no.	Active chemicals
1	DTPMP, Phosphonates (single structure non-polymeric)
2	NTMP, Phosphonates (single structure non-polymeric)
3	PPCA, Polymer with carboxylate acid
4	polymer with 2-propenoic acid
5	P-MAC, Phosphorous incorporated maleic polymer
6	Polymer with sodium 2-propane-1-sulfonate
7	Polymeric non-phosphorous based
8	Polymeric non-phosphorous based
9	PVS, Poly(vinyl sulfonic acid) sodium salt
10	Phosphonates (blend of different structures, non-polymeric)

Table 22 shows the active function groups of the scale inhibitor tested. 1 and 2 have very similar structure, both phosphonates and non-polymeric. 1 is DTPMP and 2 is NTMP. Similarly, 10 is also a non-polymeric phosphonates. However, 10 is a blend of phosphonates with different structures, some are very different from 1 and 2. The rest of the scale inhibitors are all polymeric

scale inhibitors with different function groups as shown in the table.

Table 23. Experimental results of Fe(II) impact on scale inhibitors

Inhibitor no.	Inhibitor conc. (mg/L)	Fe conc. (mg/L)	Induction time (s)	Result
No inhibitor	0	0	20	
10	0.6	0	617	
	0.6	17	743	No effect
1	0.6	0	696	
	0.6	17	50	Impairment
2	1	0	1495	
	1	17	50	Impairment
9	1.92	0	449	
	1.92	1	436	No effect
	1.92	17	484	No effect
	1.92	26	414	No effect
	1.92	50	452	No effect
3	0.5	0	317	
	0.5	17	392	No effect
	0.5	50	416	No effect
4	1	0	1224	
	1	17	1216	No effect
5	1	0	426	
	1	50	468	No effect
6	1.92	0	307	
	1.92	50	436	No effect
7	1.92	0	536	
	1.92	50	628	No effect
8	1.92	0	307	
	1.92	50	387	No effect

Table 23 shows the experimental results of Fe (II) on different scale inhibitors. All the inhibitors

are tested at 1M NaCl, pH 6.7, 400 mg/L Ca^{2+}, barite SI=2.00 and 70ºC condition. The highest Fe (II) testing conc. is 50 mg/L and the lowest is 1 mg/L. Without Fe(II), the induction time of C1 at 0.6 mg/L is 696s, C3 at 1mg/L is 1495s. In the presence of 17 mg/L Fe(II), the induction time of both scale inhibitors both drop significantly to 50s. The induction time of other scale inhibitors tested are not significantly influenced by the presence of Fe(II).

5.3 Discussion

The reason behind Fe(II) effect on phosphonates scale inhibitors is very likely to be the precipitation of Fe(II) with phosphonate functional groups. Previous research found the Fe(II)-NTMP precipitate to be extremely insoluble (Friedfeld, He, and Tomson 1998). Since NTMP and DTPMP have very similar structure, DTPMP is also likely to form sparingly soluble precipitate with Fe(II). The dependence of solubility product of ferrous NTMP with temperature and ionic strength has following relationship: pK_{sp}: $pK_{sp} = 39.54 - 6.14\, I^{0.5} + 2.181 - 1315/T$ (Friedfeld, He, and Tomson 1998). $K_{sp} = (Fe^{2+})^{2.5}(H^{+})(Phn^{6-})$. The precipitate has a formula of $Fe_{2.5}$HNTMP. In 70ºC, 1M NaCl solution, pKsp of $Fe_{2.5}$HNTMP is $10^{-31.75}$. The solubility of $Fe_{2.5}$HNTMP at experimental condition can be calculated as Fe(II) = 0.005 mg/l and NTMP = 0.011 mg/l. The Fe(II) and inhibitor solubility concentration are one or two magnitude lower than concentrations used in this research. Therefore, it's possible that Fe(II) and DTPMP forms sparingly soluble precipitate and impair the inhibition efficiency.

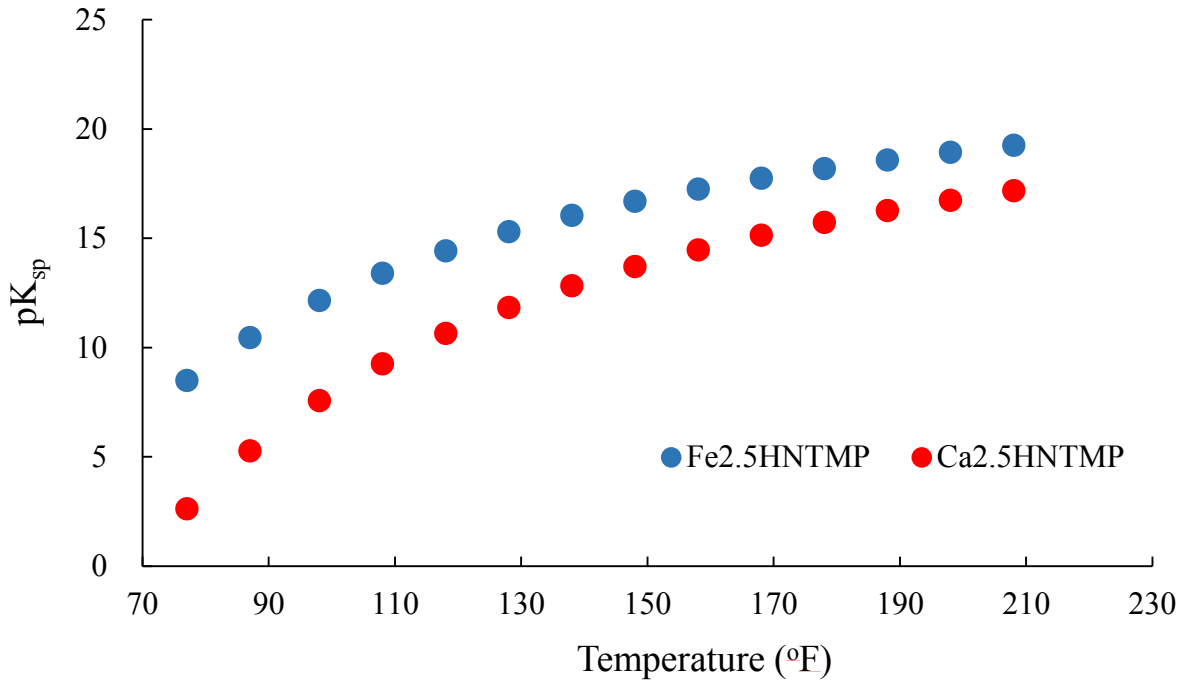

Figure 49. Comparison of solubility product of Fe and Ca-NTMP precipitate

Due to different binding ability with different function groups, Fe(II) might influence different inhibitor performance at different extents. It was found that the coordination of sulfonate anions with transition metal is relatively weak compared to phosphonates (Shimizu et al., 2009). The coordination of sulfonate anions to transition metal is too weak to compete with water, ammonium and amines (Forbes et al., 2009). Carboxyl groups readily bind to transition metal cations (Deeth et al., 2008). Phosphonates, due to their multi-dentate nature, are stronger than carboxylate complex and form insoluble precipitates with transition metal cations (Chandrasekhar et al., 2011). Experimental results are consistent with the reported binding strength between transition metals and phosphonates, carboxylates and sulfonates reported in literature.

Chapter 6. Summary and future work

6.1 Summary

This research focuses on investigating the effect of Fe(III) and Fe(II) on mineral scale inhibitors for barium sulfate nucleation. Several accomplishments have been achieved so far.:

(1) A laser nucleation detection apparatus has been remodeled to adapt to anoxic experimental condition This apparatus and experimental method is able to maintain good reducing environment for Fe(II) and enable us to investigate the effect of Fe(II) on the performance of mineral scale inhibitors without the interference of Fe(III)

(2) Most scale inhibitors have good tolerance for Fe(II). Only some phosphonates-based scale inhibitors (DTPMP and NTMP) were found to be significantly impaired by Fe(II). This result is consistent with previous research in our group that Fe(II) can form insoluble precipitate with phosphonates and t that Fe(II) with other inhibitor function groups have a weaker complexation stability constant with Fe(II) than phosphonates. The significance of this part of work is that it contributes to a better understanding of Fe(II) effect on scale inhibitor since overestimation and underestimation of its effect might lead to treatment failure.

(3) Fe(III) was found to have a significant impact on all mineral scale inhibitors tested even at low concentrations. However, the mechanism of this detrimental effect has been investigated. This research utilized analytical ultracentrifuge to investigate the mechanism of Fe(III) effect. Experimental results show that the mechanism of Fe(III) effect on scale inhibitors is the adsorption

of scale inhibitor onto ferric hydroxide particle surface. If the scale inhibitors were added in excess of the adsorption ability of ferric hydroxide particles, there will be some scale inhibitors left in the solution. These remaining scale inhibitors can still provide inhibition ability for barite.

(4) EDTA and citric acid are very common organic chelating agents used in oilfield for Fe control. Therefore, they were used to reverse the detrimental effect of Fe(III) on scale inhibitors. Both chelating agents were found to be able to reverse the negative impact. Citric acid was found to work better than EDTA despite the fact that EDTA is a much stronger chelating agent than citric acid. They work by different mechanism. EDTA works by direct chelation of Fe(III) while citric acid works by adsorption onto ferric hydroxide particle surface.

6.2 Future work

Future work for this research include:

(1) Fe(II) effect on scale inhibitors can be at a higher temperature and higher Fe(II) concentration since in oilfield condition, Fe(II) concentration and temperature can be much higher. It might be useful to test highest Fe(II) tolerance concentration for common inhibitor which can provide some guideline when applying scale inhibitors in production process.

(2) This research only tested two kinds of organic chelating agents to reverse the effect of Fe(II). Other more effective chelating agents such as DTPA, PDTA can also be tested for their ability to revere the effect of Fe(II) and Fe(III) on scale inhibition.

(3) $CaCO_3$ is another common precipitate in oilfield. The effect of Fe(II) on scale inhibitors for $CaCO_3$ can also be investigated. Besides its interaction with scale inhibitors, Fe(II) can integrate into $CaCO_3$ lattice and change $CaCO_3$ nucleation kinetics. Therefore, the overall effect might be more complicated than in barium sulfate system.

Chapter 7. Reference

Alsaiari, H. A., S. Yean, M. B. Tomson and A. T. Kan (2008). Iron Calcium Carbonate: Precipitation Interaction. SPE International Oilfield Scale Conference, Society of Petroleum Engineers.

Amjad, Zahid, and Konstantinos D. Demadis 2015 Mineral Scales and Deposits: Scientific and Technological Approaches. Elsevier.

Bengtsson, G., S. Fronæus and L. Bengtsson-Kloo (2002). "The kinetics and mechanism of oxidation of hydroxylamine by iron (III)." Journal of the Chemical Society, Dalton Transactions(12): 2548-2552.

Barthorpe, T. 1993. The Impairment of Scale Inhibitor Function by Commonly Used Organic Anions. Paper SPE-25158-MS presented at SPE International Symposium on Oilfield Chemistry

Coleman, J., G. Graham, S. Dyer, P. Hill and K. Sorbie (1999). Iron Release Following Scale Inhibitor Application and Mineral Dissolution in a North Alaskan Reservoir–Some Field Implications. SPE International Symposium on Oilfield Scale, Aberdeen, UK.

Cornel, R. and U. Shwertmann (1991). "Iron oxides in the laboratory. Preparation and characterization." VCH Editions, Weinhein, Germany.

Cornell, R. and P. Schindler (1980). "Infrared study of the adsorption of hydroxycarboxylic acids onα-FeOOH and amorphous Fe (III) hydroxide." Colloid and Polymer Science258(10): 1171-1175.

Crabtree, M., D. Eslinger, P. Fletcher, M. Miller, A. Johnson and G. King (1999). "Fighting scale—removal and prevention." Oilfield Review11(3): 30-45.

Cushner, M., W. Melchior and J. Przybylinski (1990). "Effect of iron (II) on the performance of calcium carbonate inhibitors." Materials performance29(1): 49-52.

Chandrasekhar, Vadapalli, Tapas Senapati, Atanu Dey, and Sakiat Hossain 2011 Molecular Transition-Metal Phosphonates 40(20): 5394–5418.

Cornell, R. M., and U. Schwertmann1979 Influence of Organic Anions on the Crystallization of Ferrihydrite. Clays and Clay Minerals 27(6): 402–410.

Cornell, Rochelle M., and Udo Schwertmann 2003 The Iron Oxides: Structure, Properties, Reactions, Occurrences and Uses. John Wiley & Sons.

Chandrasekhar, V., Senapati, T., Dey, A., and Hossain, S. 2011. Molecular transition-metal phosphonates. Dalton Transactions, 40(20), 5394-5418.

Contreras, E., Tomson, M. B., Yan, C., Guraieb, P., Tomson, R. C., and Huang, J. 2014. Solubility Study of Magnetite under Extreme High Pressure and High Temperature. Paper OTC-25216-MS presented in Offshore Technology Conference, 05-08 May, Houston, Texas.

Deer, W. HOWIE RA and ZUSSMAN J.(1966) An Introduction to the Rock Forming Minerals, Addison Wesley longman limited, Harlow, England.

Donald, L. (1997). Aqueous environmental geochemistry, Upper Saddle River, NJ: Prentice Hall.

Deeth, Robert J.2008 General Molecular Mechanics Method for Transition Metal Carboxylates and Its Application to the Multiple Coordination Modes in Mono- and Dinuclear Mn(II) Complexes. Inorganic Chemistry 47(15): 6711–6725.

Ewing, B. C., A. S. Pabley, and R. E. Callaway 1983 A Synergistic Chelation System for Acidizing in the Presence of High Iron Concentrations. In . Society of Petroleum Engineers. https://www.onepetro.org/conference-paper/SPE-11795-MS, accessed January 23, 2017.

Fink, J. (2011). Petroleum engineer's guide to oil field chemicals and fluids, Gulf Professional Publishing.

Friedfeld, S. J., S. He and M. B. Tomson (1998). "The temperature and ionic strength dependence of the solubility product constant of ferrous phosphonate." Langmuir14(13): 3698-3703.

Forbes, Tori Z., and Slavi C. Sevov 2009 Metal-Organic Frameworks with Direct Transition Metal-Sulfonate Interactions and Charge-Assisted Hydrogen Bonds. Inorganic Chemistry 48(14): 6873–6878.

Furia, Thomas E.1973 CRC Handbook of Food Additives, Second Edition. CRC Press.

Fink, J.2011. Petroleum engineer's guide to oil field chemicals and fluids. Gulf Professional Publishing.

Fan, C., Kan, A. T., Zhang, P., and Tomson, M. B. 2011. Barite Nucleation and Inhibition at 0 to 200oC with and without thermodynamic hydrate inhibitors. SPE Journal, 16(02), 440-450.

Figueira, M. M., Volesky, B., and Mathieu, H. J. 1999. Instrumental analysis study of iron species biosorption by Sargassum biomass. Environmental science & technology, 33(11), 1840-1846.

Gaffney, S., E. Jackson and A. Lyons (1988). The Effect of lron (II) on the Barium Sulphate Scale Inhibition Performance of Diethylenetriaminepentamethylene Phosphonic Acid (DETPMA). Symposium on Chemicals in the Oil Industry, London, England.

Greenberg, J. and M. Tomson (1992). "Precipitation and dissolution kinetics and equilibria of aqueous ferrous carbonate vs temperature." Applied Geochemistry7(2): 185-190.

Guerra, K., K. Dahm and S. Dundorf (2011). Oil and gas produced water management and

beneficial use in the Western United States, US Department of the Interior, Bureau of Reclamation.

Herzog, R. E., Q. Shi, J. N. Patil and J. L. Katz (1989). "Magnetic water treatment: the effect of iron on calcium carbonate nucleation and growth." Langmuir5(3): 861-867.

Kan, A. and M. Tomson (2012). "Scale prediction for oil and gas production." Spe Journal17(02): 362-378.

Hall, B. E., and W. R. Dill 1988 Iron Control Additives for Limestone and Sandstone Acidizing of Sweet and Sour Wells. In . Society of Petroleum Engineers. https://www.onepetro.org/conference-paper/SPE-17157-MS, accessed January 23, 2017.

Hill, P. I., G. M. Graham, S. J. Dyer, and J. Coleman 2000 Iron Release Following Mineral Dissolution Following Scale Inhibitor Application In a North Alaskan Reservoir. In . Society of Petroleum Engineers. https://www.onepetro.org/conference-paper/SPE-58727-MS, accessed January 22, 2017.

He, S., Oddo, J. E., and Tomson, M. B. 1994. The inhibition of gypsum and barite nucleation in NaCl brines at temperatures from 25 to 90oC. Applied Geochemistry, 9(5), 561-567.

Johnson, R. L., Anschutz, A. J.,Smolen, J. M., Simcik, M. F., and Penn, R. L. 2007. The adsorption of perfluorooctane sulfonate onto sand, clay, and iron oxide surfaces. Journal of Chemical & Engineering Data, 52(4), 1165-1170.

Kan, A. T., G. Fu and M. B. Tomson (2002). "Effect of methanol on carbonate equilibrium and calcite solubility in a gas/methanol/water/salt mixed system." Langmuir18(25): 9713-9725.

Kan, A. T., G. Fu and M. B. Tomson (2003). "Effect of methanol and ethylene glycol on sulfates and halite scale formation." Industrial & engineering chemistry research42(11): 2399-2408.

Kelland, M. A. (2014). Production chemicals for the oil and gas industry, CRC press.

Kelland, Malcolm A. 2011 Effect of Various Cations on the Formation of Calcium Carbonate and Barium

Kelland, M. A. 2011. Effect of various cations on the formation of calcium carbonate and barium sulfate scale with and without scale inhibitors. Industrial & Engineering Chemistry Research, 50(9), 5852-5861.

Lasaga, A. C. (2014). Kinetic theory in the earth sciences, Princeton University Press.

Liu, Y., A. T. Kan, C. Yan, F. Wang, L. Wang and M. B. Tomson (2014). An Assay Method for the Detection of all Scale Inhibitors at Extremely low Concentration. SPE International Oilfield Scale Conference and Exhibition, Society of Petroleum Engineers.

Lu, H., A. T. Kan and M. B. Tomson (2010). "Effects of Monoethylene Glycol on Carbonate Equilibrium and Calcite Solubility in Gas/Monoethylene Glycol/NaCl/Water Mixed Systems." Spe Journal15(03): 714-725.

Mullin, J. W. (2001). Crystallization, Butterworth-Heinemann.

Liu, Ya, Amy T. Kan, Chao Yan, et al.2014 An Assay Method for the Detection of All Scale Inhibitors at Extremely Low Concentration. In . Society of Petroleum Engineers. https://www.onepetro.org/conference-paper/SPE-169762-MS, accessed January 23, 2017.

Lindegren, M. 2009. Aqueous surface chemistry of Goethite: adsorption and desorption reactions involving phosphate and carboxylic acids. (Doctoral dissertation, Umeå University)

Liu, Y., Zhang, F., Kan, A. T., Tomson, M. B., Yan, C., and Tomson, R. 2014. Systematic Study of Barite Nucleation and Inhibition with Various Polymeric Scale Inhibitors by Novel Laser Apparatus. Paper SPE-169787-MS presented at SPE International Oilfield Scale Conference.

Mullin, J. W.2001 Crystallization. Butterworth-Heinemann.

Meyer, J. L., and Thomas Jr, W. C. 1982. Trace metal-citric acid complexes as inhibitors of calcification and crystal growth. II. Effects of Fe (III), Cr (III) and Al (III) complexes on calcium oxalate crystal growth. The Journal of urology, 128(6), 1376-1378.

Nowack, B., and Stone, A. 1999. The influence of metal ions on the adsorption of phosphonates onto goethite. Environmental science & technology, 33(20), 3627-3633.

Nowack, Bernd, and Alan T. Stone 1999 The Influence of Metal Ions on the Adsorption of Phosphonates onto Goethite. Environmental Science & Technology 33(20): 3627–3633.

Paykani, A., and Mardan, H. Methods of controlling ferric hydroxide precipitation results from corrosion in acidizing treatments.

Shen, D., D. Shcolnik, W. H. Steiner, D. G. Horstmann, G. N. Taylor and M. Brown (2011). Evaluation of Scale Inhibitors in Marcellus Waters Containing High Levels of Dissolved Iron. SPE International Symposium on Oilfield Chemistry, Society of Petroleum Engineers.

Stoppelenburg, L. and M. Yuan (2000). The Performance of Barium Sulfate inhibitors in iron containing waters in both aerated and anaerobic systems. CORROSION 2000, NACE International.

Stumm, W. (1992). "Chemistry of the Solid-Water Interface: Process at the Mineral-Water and Particle-Water Interface in Natural Systems." John Wily & Sons, New York347.

Stumm, W. and J. J. Morgan (2012). Aquatic chemistry: chemical equilibria and rates in natural waters, John Wiley & Sons.Sulfate Scale with and without Scale Inhibitors. Industrial & Engineering Chemistry Research 50(9): 5852–5861.2014 Production Chemicals for the Oil

and Gas Industry, Second Edition. CRC Press.

S.H, Gaffney, Jackson E., and Lyons, A.1988 The Effect of Lron (II) on the Barium Sulphate Scale Inhibition Performance of Diethylenetriaminepentamethylene Phosphonic Acid (DETPMA). In . London, England.

Shen, Dong, David Shcolnik, Randall Perkins, Grahame Taylor, and Mike Brown 2012 Evaluation of Scale Inhibitors in Marcellus High-Iron Waters. Oil and Gas Facilities 1(05): 34–42.

Shimizu, George K. H., Ramanathan Vaidhyanathan, and Jared M. Taylor 2009 Phosphonate and Sulfonate Metal Organic Frameworks 38(5): 1430–1449.

Stumm, Werner, Laura Sigg, and Barbara Sulzberger 1992 Chemistry of the Solid-Water Interface: Processes at the Mineral-Water and Particle-Water Interface in Natural Systems. Wiley.

Shen, D., Shcolnik, D., Steiner, W. H., Horstmann, D. G., Taylor, G. N., and Brown, M. 2011, January. Evaluation of Scale Inhibitors in Marcellus Waters Containing High Levels of Dissolved Iron presented in SPE International Symposium on Oilfield Chemistry.

Shimizu, G., Vaidhyanathan, R., and Taylor, M. 2009. Phosphonate and sulfonate metal organic frameworks. Chemical Society Reviews, 38(5), 1430-1449.

Stoppelenburg, L., and Yuan, M. 2000. (Yan, Kan et al. 2014)CORROSION 2000.

Tang, C., S. Thompson, J. Parker, A. Lennie, F. Azough and K. Kato (2009). "The ikaite-to-vaterite transformation: new evidence from diffraction and imaging." Journal of Applied Crystallography42(2): 225-233.

Tomson, M., G. Fu, M. Watson and A. Kan (2002). Mechanisms of mineral scale inhibition. International Symposium on Oilfield Scale, Society of Petroleum Engineers.

Tomson, M. B., A. T. Kan, G. Fu and M. Al-Thubaiti (2004). A Molecular Theory of Mineral Scale Inhibition. CORROSION 2004, NACE International.

Taylor, K. C., and H. A. Nasr-El-Din 1999 A Systematic Study of Iron Control Chemicals - Part 2. In . Society of Petroleum Engineers. https://www.onepetro.org/conference-paper/SPE-50772-MS, accessed January 23, 2017.

Taylor, K. C., H. A. Nasr-El-Din, and M. J. Al-Alawi 1999 Systematic Study of Iron Control Chemicals Used During Well Stimulation. SPE Journal 4(01): 19–24.

Tomson, M. B., G. Fu, M. A. Watson, and A. T. Kan 2002 Mechanisms Of Mineral Scale Inhibition. In . Society of Petroleum Engineers. https://www.onepetro.org/conference-paper/SPE-74656-MS, accessed January 22, 2017.

Wang, W.-S., L. Zhen, C.-Y. Xu and W.-Z. Shao (2011). "Synthesis and formation process of SrSO 4 sisal-like hierarchical structures at room temperature." CrystEngComm13(2): 620-625.

Yan, C., A. Kan, F. Zhang, Y. Liu, R. C. Tomson and M. Tomson (2014). "Systematic Study of Barite Nucleation and Inhibition With Various Polymeric Scale Inhibitors by Novel Laser Apparatus." SPE Journal.

Yan, Chao, Amy T. Kan, Fangfu Zhang, et al. 2015 Systematic Study of Barite Nucleation and Inhibition With Various Polymeric Scale Inhibitors by Novel Laser Apparatus. SPE Journal 20(03): 642–651.

Yean, J. 2008. Arsenic removal using iron oxides: Application of magnetite nanoparticles and iron salts (Doctoral dissertation, Rice University).

Yépez, O. 2007. On the chemical reaction between carboxylic acids and iron, including the special case of naphthenic acid. Fuel, 86(7), 1162-1168.

Zhang, N. 2010. Influence of citrate ligands on ferric hydroxide nucleation at low molar ratios: Application for arsenic removal (Doctoral dissertation, Rice University).

Curriculum Vitae

Zhang (April) Zhang

(832) 499-1092 •Zhang.Zhang@rice.edu•1406 Richmond Avenue, Apt 232• Houston, TX 77006

EDUCATION

Doctor of Philosophy expected in May 2016……..……....Rice University, Houston, TX
Department of Environmental Engineering, with a concentration on petroleum chemistry, GPA 4.07/4.33

Master of Science……..……...Rice University, Houston, TX
Thesis title: "Solid solution formation kinetics---A preliminary study for $CaCO_3$/$BaCO_3$ and $BaSO_4$/$SrSO_4$ system"

Bachelor of Science, Emphasis in Chemistry……..... Nankai University, Tianjin, China
Thesis title: "Study on design of new passive samplers and their application in water contaminant monitoring"

Courses: Petroleum phase behavior and flow assurance, Multiphase flow in pipes, Colloidal and interfacial phenomena, Classical and statistics thermodynamics, Environmental Chemistry, Fate and transport of contaminants, Atmospheric processes, Environmental biotechnology

RESEARCH EXPERIENCE

Rice University, *Houston, Texas*

Dr. Mason Tomson's research group

Study mineral scale deposition on steel tubing in aerobic and anaerobic conditions..... Aug. 2011-Aug. 2013

- Applied plug flow reactors to simulate mineral scale deposition process on the oilfield pipeline, including $CaCO_3$scale and $CaCO_3$/$BaCO_3$, $CaCO_3$/$FeCO_3$ mixed scale. Measured deposition rate and explored influence of different tubing materials and temperatures.
- Presented results at *Brine Chemistry Consortium (BCC)*in Dec. 2012 and 2013 for operation, service, and chemical companies, including Shell, Chevron, Conoco Phillips, BP, Statoil,

Schlumberger, Halliburton, etc.

- Upgraded the plug flow reactor apparatus to study deposition kinetics of Ferrous Sulfide mineral scale with a group co-worker; co-authored a publication in the journal of Society of Petroleum Engineers, *featured as the cover article of Journal of Petroleum Technology, September, 2014*

Fe(II) and Fe(III) impact on scale inhibitor performance at temperatures from 77 to 200^{o}F……..... Aug. 2013 – now

- Remodeled laser nucleation detection apparatus to adapt it for anoxic conditions, explored how conditions such as Fe/inhibitor molar ratio, temperature, ionic strength, pH can enhance or diminish this influence
- Presented results at *Brine Chemistry Consortium (BCC)*in Dec. 2014 for operation, service, and chemical companies, including Shell, Chevron, Conoco Phillips, BP, Statoil, Schlumberger, Halliburton, etc.
- Abstracted accepted for poster session at 2015 SPE International Symposium on Oilfield Chemistry, Woodlands, Texas.

SKILLS

Technical: Scanning electron microscope (SEM), Energy dispersed X-ray Analysis (EDAX), inductively coupled plasma mass spectrometry (ICP-MS), inductively coupled plasma atomic emission spectroscopy (ICP-OES), Malvern Zen 3600 Zetasizer

Software: SSP (ScaleSoftPizter), PVTsim, Visual Basic Application, MATLAB, C++, Visual MINTEQ, Groundwater vistas (GMV)

COMMUNITY SERVICE

President of National Association of Corrosion Engineers (NACE) Rice Student Chapter, Rice University

President of student club “Flywest” which helps undergraduate students to achieve their dream of studying abroad, China

Social work with Canada Fuhui Charity Foundation in Liangshan, Sichuan Province, China

PUBLICATIONS

Z Zhang, F Zhang, QL Wang, N Bhandari, F Yan, Y Liu, Z Dai, L Wang. Ferrous Iron Impact on Phosphonate and Polymeric Scale Inhibitors at Temperature Ranging from 25 to 70° C. *SPE-173770-MS*.

Z. Zhang, Ya Liu, Zhang Zhang, Ya Liu, Zhaoyi Dai, Narayan Bhandari, Fangfu Zhang, Fei Yan, Gordon Ruan, Hamad Alsaiari, Yi-Tsung Lu, Guannan Deng, Amy Kan, Mason Tomson. Impact of Fe(III)/Fe(II) on scale inhibition. *SPE-1779905-MS*

Q Wang, **Z Zhang**, AT Kan, MB Tomson. Kinetics and Inhibition of Ferrous Sulfide Nucleation and Precipitation. *SPE-169748-MS*.

L Wang, AT Kan, **Z Zhang**, F Yan, Y Liu, Z Dai, MB Tomson. Field Method for Determination of Bicarbonate Alkalinity. *SPE-169758-MS*.

F Yan, F Zhang, N Bhandari, Y Liu, L Wang, Z Dai, **Z Zhang**, V Bolanos. Interaction between Scale Inhibitors and Shale and Sandstone Formations. *SPE-173769-MS*

N Bhandari, AT Kan, F Zhang, Z Dai, F Yan, Y Liu, **Z Zhang**, V Bolanos. The Effect of Pressure and TDS on Barite Scaling Kinetics. *SPE-173790-MS*

AT Kan, Z Dai, F Zhang, N Bhandari, F Yan, **Z Zhang**, Y Liu, MB Tomson. Scale Prediction and Control at Ultra HTHP. *SPE-173803-MS*.

Wang L., **Zhang Z**., Zhang X Z. Removal of perfluorinated compounds by waste water treatment plants. Acta Scientiae Circumstantiae, 31(7): 1363-1368